1-1-2011

The fourier spectral element method for vibration analysis of general dynamic structures

Xuefeng Zhang
Wayne State University,

THE FOURIER SPECTRAL ELEMENT METHOD FOR VIBRATION ANALYSIS OF GENERAL DYNAMIC STRUCTURES

by

XUEFENG ZHANG

DISSERTATION

Submitted to the Graduate School

of Wayne State University,

Detroit, Michigan

in partial fulfillment of the requirements

for the degree of

DOCTOR OF PHILOSOPHY

2012

MAJOR: MECHANICAL ENGINEERING

Approved by:

Advisor Date

DEDICATION

Dedicate to my parents

Xiqing Zhang and Yuying Li

ACKNOWLEDGEMENTS

I would like to thank my advisor, Dr. Wen Li, for supporting me over the years, and for his inspiring ideas and patient guidance. His constructive feedback, criticism, and moral support have been a great source of inspiration to me academically and in my personal development.

I am also grateful to my co-advisor Dr. Sean Wu, Dr. Dinu Taraza, Dr. Fatih Celiker for their helpful discussion. Their help in preparing the dissertation is greatly appreciated. Special thanks are given to Dr. Sean Wu for his encouragement and support. I learned a lot in his three excellent courses.

I would also like to thank Dr. Jian Wang for his help in preparing the test. Special thanks are given to my research partner Dr. Hongan Xu, Logesh Kumar Natarajan for their help and valuable discussion. Both of them are the unforgotten ingredients in my student life at Wayne State University.

Finally, I want to express my sincere thanks to my wife, Cuifen Yan, for her love, sacrifice, and taking care of our lovely daughter, Melinda Zhang.

TABLE OF CONTENTS

LIST OF TABLES

LIST OF FIGURES

Chapter I Introduction

1.1 Background

With the advance of modern technology, many types of modern machineries, such as air conditioners, vehicles, aircrafts, computers, etc., are created to help people living better. However, the automated machineries inevitably create vibrations in their working process. The vibration can further cause annoying noise, and even structural fatigue or failure. Thus, understanding the vibration characteristics of a structure is of vital importance to improve the quality of the product.

A dynamic structure shows distinctively different characters at different frequency range. At low frequency range, all the structural components are strongly coupled and the response is typically dominated by a small number of lower-order modes. The Finite Element Method (FEM) has become a powerful tool in modeling the low frequency vibration [Reddy, 2006]. A structure may have complex geometry, varying material properties, and subject to complex boundary or loading conditions. In FEM, a structure is first discretized into a large number of small elements, and the governing equation is approximated on each element with some interpolation functions; all the element equations are assembled under the continuity condition among the boundaries; the system equation is then solved with the actual boundary condition of the whole system. Although several commercialized FEM software have successfully served the vibration analysis in the industry, the analyzed frequency is limited to a few hundred Hertz even with millions of elements on the most advanced computer server. It is widely believed that this low frequency limit is primarily due to the insufficient computing power. However, there are other intrinsic reasons that prevent its use in the high frequency range [Langley, 2004]. The FEM is introduced to account for the complex geometric forms, material properties, surface loads, and complex boundary conditions. At high frequency, when these requirements are already met, refining the element size to catch the tiny wave length inevitably spread the numerical “round-off” error. Although increasing the order of the interpolation functions provides a way to improve the results, current FEM is only restricted to low frequency analysis [Li, 2007].

At high frequencies, the response spectra tend to become smooth without strong modal showings, and deterministic method is not practical any more. Since the structural components are weakly coupled, the internal energy level is a more viable parameter. Over the past half century, Statistical Energy Analysis (SEA) has emerged as a dominant method [Lyon, 1962, 1995] in analyzing high frequency vibration, in which a system is divided into a set of subsystems according to their geometric forms, dynamic material properties, as well as their contained mode (wave) types. The basic principle is that a subsystem should contain a group of “similar” energy storage modes (waves), which receives, dissipate, and transmit energy in a simple “heat conduction” form. The energy flow between the neighboring systems is assumed proportional to the difference of their modal energy level by a constant Coupling Loss Factor (CLF). The final system equation is governed by the power balance and energy conservation principle. The calculation is normally fast since very few unknown variables are used in the SEA analysis. The calculation error is also controlled by the powerful energy conservation principle. The calculated internal energy level could also be directly related to some energy parameters, such as Sound Pressure Level. However, the SEA method is still limited to high frequency analysis for the following reasons [Fahy, 1994; Burroughs, 1997; Hopkins, 2003; Park, 2004]:

(1) All the modes in the analyzed frequency band are assumed to have equal modal energy, thus a high modal overlap factor is required; otherwise the coupling loss factor is strongly dictated by modal behavior.

(2) The CLF is assumed to be a constant and only correlate to the physically connected neighbor subsystems. Then SEA method only applies for weakly coupled system. Under strong coupling condition, the indirect coupling loss factors may not be zero [Hopkins, 2002].

(3) The internal damping in the subsystem cannot be too high such that the averaged internal energy level becomes a non-suitable variable.

(4) SEA does not work well for periodic systems, in which a “wave filtering” effect happens.

Furthermore, the only variable in SEA is the averaged energy level, thus no detailed information, such as displacement, stress, strain, is available. The basic assumption in the SEA made it an easy and quick method in analyzing the high frequency vibration; but the same assumptions also made it only suit for high frequency range. When the modal overlap factor is small and modal coupling is strong, SEA method cannot be directly used since the CLF becomes both frequency and space dependent.

Between the low frequency and high frequency range, there is a well-known unsolved medium frequency gap. In the medium frequency range, a dynamic structure exhibits mixed coherent global and incoherent local motions (Langley & Bremner, 1999; Shorter & Langley, 2005). The response spectra are typically highly irregular and very sensitive to the geometric details, material properties, and boundary conditions. A small perturbation change in the structural detail can cause large change in frequency and phase responses. Because the dominant excitation frequency bands usually fall in the medium frequency range for many vibration and noise problems, the medium frequency analysis have both analytical and practical importance. The fact is that the medium frequency range is not clearly defined since the response spectra pattern are more correlated to modal order than frequency range. In some sense, it is accepted that the mid-frequency range is where the conventional deterministic methods such as FEM are not appropriate, yet the SEA assumptions are not applicable. In this critical frequency range, no mature prediction technique is available at the moment, although a vast amount of research efforts can be found in the literature searching for a solution of this unsolved problem (Desmet, 2002; Pierre, 2003).

The first approach in these efforts is to push the upper frequency limit of FEA method so that the mid-frequency problem can be partially or fully covered (Zienkiewicz, 2000; Fries and Belytschko, 2010). The first method in this approach is to improve the computation efficiency of the current FEA method. The most efficient solver in the actual industry computation of large scale problem is the Lanczos method, which is normally used in standard normal mode analysis since its fast and accurate performance. The computation efficiency can also be greatly improved by using sub-structuring method such as Component Mode Synthesis (CMS). Review papers on Sub-structuring methods are reported (Craig, 1977; Klerk, 2008). The Automated Multi-level Synthesis (AMLS) method developed by Bennighof (2004) is widely used in current FEA computation acceleration. AMLS automatically divide the stiffness and mass matrices into tree-like structure, and the lowest level component is solved by using Craig-Bampton CMS method with fixed boundary condition. The other method in pushing the upper frequency limit of FEA is to improve its convergence rate. Such techniques include adaptive meshing (h-method), multi-scale technique, and using high order element (p-method). While many methods are developed for solving the mid-frequency problem, these methods are either directly target to or closely related with the p-method. Discontinuous enrich method (DEM) developed by Farhat (2003) enrich the standard polynomial field within each finite element by a non-conforming field that contains free-space solutions of the homogeneous partial differential equation to be solved. Similar idea that enriches the finite element by using harmonic functions can be found in crack analysis (Housavi, 2011). The Partition of Unity method, which is developed by Babuška (1997), is also used in solving mid frequency vibration problem (Bel, 2005). Desmet (1998) developed a method called wave based method (WBM), which uses the exact solution of homogeneous Helmholtz equation as the approximation solution. Since the governing equation is satisfied by each of the approximation function, the final system equation is solved by only enforcing boundary and continuity conditions using a weighted residual formulation. Ladeveze (1999) developed a method called variational theory of complex rays (VTCR), in which the solution is decomposed as a combination of interior rays, edge rays, and corner rays that satisfy the governing equation. So the final equation is also solved by enforcing the boundary and interface continuity condition by using a variational formulation. VTCR and WBM methods are closely related, and both belong to the Trefftz method.

The second approach in solving the mid frequency problem is to push the lower limit of the SEA method by relaxing some of its stringent requirements, for example, the coupling between systems can be strong, there can be only a few modes in some subsystems, there is only moderate uncertainty in subsystems, or the excitation can be correlated or localized (SEA assume rain-on-the-roof excitation), etc. Several methods have been developed to extend SEA method to medium frequency range based on the belief that the SEA method is still valid if the CLFs can be somehow determined more accurately. The first method is to obtain the exact displacement and force solution using modal superposition method, called Dynamic Stiffness Method [Park, 2004]. The second method is to obtain the exact displacement and force solution using Green's function, called Receptance Method [Shankar, 1995]. The third method is to calculate the CLF using wave scattering theory at the subsystem junctions, called Mobility Power Flow Method [Troshin & Sanderson, 1998] or Spectral Element Method [Igawa, et al., 2004]. In all these methods, the solution of the boundary value problem for each subsystem (element) must make the value at its boundaries compatible with its neighboring subsystem (element). The extent and efficiency of how this task is solved is a vital criterion in deciding the usefulness and success of the method.

The third approach in conquering the mid frequency problem is a hybrid method which combines both the FEA and SEA concepts. The Energy Finite Element Analysis (EFEA) method is a direct combination of the element idea of FEA and energy concept of SEA (Yan, et al., 2000; Zhao & Vlahopoulos, 2004). Since the field energy variable used the same rule as heat transfer law, available thermal FEA software can be directly adopted in EFEA analysis. But the natural differences between thermal problem and vibration problem make this method less attractive in real applications. In fact, complex structure may have some components exhibiting high-frequency behavior while others showing low-frequency behavior. A hybrid deterministic-statistical method known as Fuzzy Structure Theory (Soize, 1993; Shorter and Langley, 2005) was developed, in which a system is divided into a master FEA structure and slave fuzzy structures described by SEA method. The coupling between the FEA and SEA components are described by a diffuse field reciprocity relation (Langley and Bremner, 1999; Langley and Cordioli, 2009). Applications of hybrid FEA plus SEA concept in industry can also be found (Cotoni, etc., 2007; Chen, etc., 2011). Another similar method combing the FEA method and analytical impedance is also developed (Mace 2002).

Although plenty of new methods are proposed for mid-frequency analysis, no mature method is available to solve the mid-frequency challenge in the industry vibration analysis. It is believed that analytical approaches hold the key to an effective modeling of complex structure in the middle frequency range. Fourier Spectral Element Method (FSEM), which is more close to the first approach in solving the mid frequency problem, will be introduced in this dissertation. FSEM model of a system has smaller model size and higher convergence rate than FEM model, which make it possible to tackle higher frequency problem before encountering the computation capacity limitation. FSEM method is closely related to DEM, VTCR, and WBM methods. The difference is that FSEM method satisfies both the governing equation and the boundary condition in an exact sense.

1.2 General description of current research approach

Since the analytical solution is not readily available for the vibration of general beams or plates, a variety of series are used to approximate the displacement function. Fourier series based trigonometric functions are one of the best choices because of their orthogonality and completeness, as well as their excellent stability in numerical calculations. Furthermore, vibrations are naturally expressible as waves, which are normally described by trigonometric functions. However, the Fourier series is only complete in a weak sense. Its convergence speed for a non-periodic function is slow within the interval and typically fails to converge at the boundaries, thus limiting the applications of Fourier method to only a few ideal boundary conditions. Then, it is of vital importance to improve the convergence speed of the Fourier series for its practical application in the vibration analysis. The fact is that displacement functions are approximated by simple polynomials in Finite Element Analysis, which is recognized as one of the most useful techniques in modern engineering applications. The applications of FEM method in vibration analysis is limited to low frequency range because high order polynomials are not stable and have round-off errors in numerical calculation. Recognizing the fact that the convergence rate for the Fourier series expansion of a periodic function is directly related to its smoothness, this dissertation makes a concerted effort to accelerate the convergence of the Fourier series. The research approach is based on a modified Fourier series method proposed by Li (2000, 2002). The method will be briefly explained here for the completeness of the dissertation.

Theorem 1 Let $f(x)$ be a continuous function of period 2L and differentiable to the m_{th} order, where $\mathrm{m}-1$ derivatives are continuous and the m_{th} derivative is absolutely integrable. Then the Fourier series of all m derivatives can be obtained by term-by-term differentiation of the Fourier series of $f(x)$, where all the series, except possibly the last, converge to the corresponding derivative. Moreover, the Fourier coefficients of the function $f(x)$ satisfies the relations $lim_{n\to\infty} a_n\lambda_n^m = lim_{n\to\infty} b_n\lambda_n^m = 0$.

Based on the theorem, Li [2000] introduced an auxiliary polynomial function in the displacement function approximation,

$$w(x) = \bar{w}(x) + p(x) \tag{1.1}$$

where $p(x)$ is chosen to account for all the relevant function and derivative discontinuities with the original beam displacement function, and $\bar{w}(x)$ is a continuous “residual” function with at least three continuous derivatives

Mathematically, the displacement function $w(x)$ defined over [0, L] can be viewed as a part of an even function defined over [-L, L], and the Fourier expansion of this even function then only contains the cosine terms. The Fourier cosine series is able to correctly converge to $w(x)$ at any point over [0, L]. However, its derivative $w'(x)$ is an odd function over [-L, L] leading to a jump at the end locations. Thus, its Fourier series expansion will accordingly have a convergence problem due to the discontinuity at the end points. This difficulty can be removed by requiring the auxiliary function $p(x)$ satisfying following conditions

$$p'(0) = w'(0), p'(L) = w'(L), \tag{1.2}$$

Apparently, the cosine series representation of $\overline{w}(x)$ is able to converge correctly to the function itself and its first derivative at every point in the definition domain. Analogously, discontinuities potentially associated with the third-order derivative can be removed by adding two more requirements on the auxiliary function $p(x)$

$$p'''(0) = w'''(0), p'''(L) = w'''(L), \tag{1.4, 1.5}$$

Then the function $w(x)$ has at least three continuous derivatives over the entire definition domain and its fourth derivatives exist, which is the requirement of an admissible beam displacement function.

The superiority of current method is obvious when we compare it with the Differential Quadrature (DQ) method, which is one of the most popular numerical methods for finding a discrete form of solution. In DQ method, the derivative of a function at a given point is expressed as a weighted linear combination of the function values at all the discrete grid points properly distributed over the entire solution domain. Figure 1.1 shows the fifth mode shape function and its first two derivatives of a clamped beam along with the approximated results from both the DQ interpolation scheme and current method. Only the results on the right half of the beam are shown because of the symmetry of the mode. Although the DQ result approximated the beam function itself relatively well, larger discrepancies are observed for the first and especially the second derivative. It is observed that current method converges to the original solution in a much faster speed. The superiority of current method is more visible for high order derivatives.

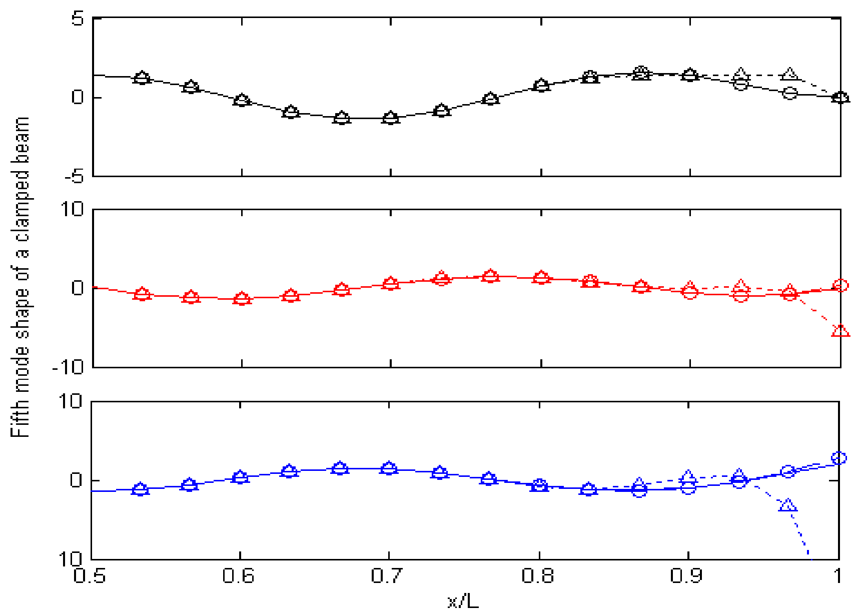

Figure 1.1 A comparison of the DQ interpolation scheme and current FSEM method: Original beam function (black), the first derivative (red), the second derivative (blue); DQ with traditional Legendre interpolation function (triangle); Current method (circle)

Two dimensional vibration functions cannot be directly approximated by the product of two one dimensional functions for the non-separate nature of the two dimensional vibration problems. The displacement function defined over [*0, a; 0, b*] can be viewed as a part of an even function defined over [-*a, a; -b, b*], it is also approximated by

$$w(x, y) = \bar{w}(x, y) + p(x, y) \tag{1.6}$$

the residual function $\bar{w}(x)$ is expressed as a double Fourier cosine series. The auxiliary polynomial function $p(x)$ is such designed that

$$p'(0,y) = w'(0,y),\ p'(a,y) = w'(a,y),\ p'''(0,y) = w'''(0,y),\ p'''(a,y) = w'''(a,y) \quad (1.7\text{-}10)$$

$$p'(x,0) = w'(x,0),\ p'(x,b) = w'(x,b),\ p'''(x,0) = w'''(x,0),\ p'''(x,b) = w'''(x,b). \quad (1.11\text{-}14)$$

then the function $w(x,y)$ in Eq. (1.6) satisfy the required conditions in Theorem 1 on both x and y dimensions, the discontinuity on each edge of the plate is subtracted by one term in $p(x,y)$, and the residual function $\overline{w}(x,y)$ is periodic continuous to the third derivative, i.e. $\overline{w}(x,y) \in C^3(x,y)$.

The form of complementary functions $p(x,y)$ has not been explicitly specified. Actually, any function sufficiently smooth such as polynomials and trigonometric functions can be used. Thus, this idea essentially opens an avenue for systematically defining a complete set of admissible or displacement functions that can be used in the Rayleigh-Ritz methods and universally applied to different boundary conditions for various structural components. The excellent accuracy and convergence of the Fourier series solutions have been repeatedly demonstrated for beams (Li, 2000, 2002; Li & Xu, 2009; and Xu & Li, 2008) and plates (Li, 2004; Li & Daniels, 2002; Du et al., 2007; Li et al., 2009; and Zhang & Li, 2009) under various boundary conditions.

In the Fourier Spectrum Element Method (FSEM) presented in this dissertation, a system is divided into substructures based on its geometric and material characteristics. The governing equation in a typical subsystem is approximated by the improved series, and then the system equation is assembled in an FEM-like process. The vibration of a general 3-D structure composed of triangular plates, rectangular plates, and beams can be solved with high fidelity. FSEM method provides a promising avenue to extend high frequency limit of analytical method.

1.3 Objective and outline

Fourier Spectral Element Method was introduced about a decade ago on the vibration of simple beams with general boundary condition (Li, 2000), and was extended to the vibration of rectangular plates with elastic supports (Li, 2004). The formulation on the vibration of rectangular plates was revised later to enforce computation efficiency (Li, et al., 2009; Zhang & Li, 2009). Similar approach was also adopted on the vibration of beams (Xu, et al., 2010). The objective of this dissertation is to extend the FSEM method on a general 3-D structure composed of arbitrary number of triangular plates, rectangular plates, and beams. Since the matrix size of the FSEM method is substantially smaller than the FEA method, FSEM method has the potential to reduce the calculation time, and tackle the unsolved Mid-frequency problem.

Chapter II reviews several promising methods available in the literature on the vibration of beams with general boundary condition. The strength of each method is also briefly discussed. Then the revised FSEM formulation is introduced on a beam with general boundary condition. A simple example showing its excellent convergence property is also provided.

Chapter III introduces the revised FSEM formulation on a rectangular plate with elastic boundary supports. An exact series solution is first given by using the Weighted Residual Method. Then the variational form of FSEM on rectangular plates with varying elastic boundary supports is obtained by using Rayleigh-Ritz method. Fast convergence of FSEM results is illustrated by comparing them to the convergence of the FEA results as well as those results available in the literature.

Chapter IV introduces a new formulation that extend FSEM concept on the vibration of general triangular plates with elastic supports. FSEM results match well with all the available results in the literature on triangular plates with classical boundary supports, especially interesting are those results on plates with free boundary condition and plates with anisotropic material properties.

Chapter V summarizes all the formulation on triangular plates, rectangular plates, and beams, and introduces the coupling among the three types of elements in a general 3-D space. All formulations are further transformed into a standard unit local coordinates, which enable the storage of one set of matrices for all structures. Finally, the FSEM is benchmarked on four general structure examples with both Lab and FEA results.

Chapter VI conclude this dissertation, and provides some suggested topics to further studies of the FSEM method.

Chapter II Vibration of beams with elastic boundary supports

2.1 Beam vibration description

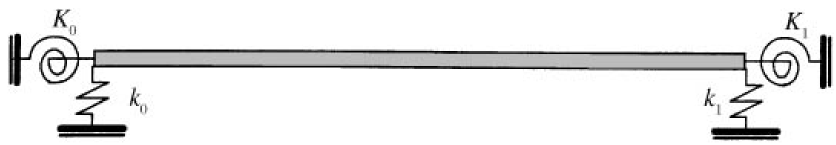

Figure 2.1 A beam elastically restrained at both ends

Consider a uniform Euler-Bernoulli beam as depicted in Figure 2.1. The beam is supported at the two boundary ends with deflectional and rotational elastic springs. The damping, shear deformation, and rotary inertia in the beam are all neglected for simplicity of explanation. The governing differential equation for the vibration of the beam is given as

$$EIw''''(x,t) + \rho A\ddot{w}(x,t) = p(x,t) \tag{2.1}$$

where E, I, ρ A are Elastic modulus, moment of inertia, mass density and cross section area, respectively. $w(x,t)$ is the deflection of the beam. $p(x,t)$is the distributed load on the beam surface. A prime denotes differentiation with respect to position x , and an over dot denotes differentiation with respect to time t.

Assume that the beam is under periodic excitation, i.e. the surface load function $p(x,t) = f(x)e^{iwt}$. The solution of Eq. (2.1) is assumed in the form $w(x,t) = X(x)e^{i\omega t}$, Then the governing differential Eq. (2.1) is simplified as,

$$EIX''''(x) - \omega^2\rho AX(x) = f(x) \tag{2.2}$$

The boundary conditions of the beam can be expressed as,

$$k_0 w(0,t) = -EIw'''(0,t),\ K_0 w'(0,t) = EIw''(0,t) \tag{2.3, 2.4}$$

$$k_L w(L,t) = EIw'''(L,t),\ K_L w'(0,t) = -EIw''(L,t) \tag{2.5, 2.6}$$

where k_0, K_0, k_L, K_L are the translational and rotational constants of the springs. Under the same condition that the beam is under harmonic excitation, the boundary condition could be further simplified as,

$$k_0 X(0) = -EIX'''(0),\ K_0 X'(0) = EIX''(0) \tag{2.7, 2.8}$$

$$k_L X(L) = EIX'''(L),\ K_L X'(L) = -EIX''(L) \tag{2.9, 2.10}$$

Eq. (2.2) and Eq. (2.7-2.10) constitute a forth order linear differential equation with general boundary conditions. This boundary value problem is the starting point of the following discussion. How efficiently this one dimensional problem is solved largely determine the method's applicability in solving high frequency and high dimensional vibration analysis.

2.2 Literature review on the transverse vibration of beams

Many techniques have been developed for the vibration of beams with several constitutional equations, various loading and boundary conditions. It is not the purpose to review all the available methods for beam vibrations. Only some prominent methods designed to solve the boundary value problem presented in Section 2.1 will be reviewed.

2.2.1 Modal Superposition Method

In Modal Superposition Method, the response of a beam under external excitation is assumed as a combination of its natural modes,

$$X(x) = \sum_k D_k\, \phi_k(x) \tag{2.11}$$

where $\phi_k(x)$ is the kth natural mode of the beam, and D_k is the unknown coefficients to be determined by the orthogonality condition of the eigen functions [Rao & Mirza, 1989; Rosa, 1998; Lestari & Hanagud, 2001].

The general expression for ϕ_k is

$$\phi_k(x) = C_1 \sin(\kappa x) + C_2 cos(\kappa x) + C_3 \sinh(\kappa x) + C_4 \cosh(\kappa x) \tag{2.12}$$

where $C_i (i = 1, 2, 3, 4)$are the coefficients to be determined by the boundary conditions.

Substituting Eq. (2.12) in Eq. (2.7-2.10), and writing the result expression in matrix form

$$\mathbf{Bc} = \mathbf{0}. \tag{2.13}$$

where $\boldsymbol{c} = [C_1, C_2, C_3, C_4]$, and $\mathbf{B}$ is a 4×4 matrix.

For Eq. (2.13) to have a nontrivial solution, the coefficient matrix must be singular, i.e.

$$|\mathbf{B}| = 0 \tag{2.14}$$

The only variable in Eq. (2.14) is the frequency ω. All the ωs that satisfy Eq. (2.14) are the natural frequencies of the beam. With a solved frequency ω the corresponding modal coefficients could be further determined by solving Eq. (2.14) with a free parameter among $C_1, C_2, C_3,$ and C_4.

This method can be easily extended to multiple beam vibration analysis [Gurgoze & Erol, 2001; Low, 2003; Naguleswaran, 2003; Maurizi, 2004; Lin, 2008, 2009]. Adding one extra beam to the existing system means adding one extra unknown function,

$$\phi_k(x) = C_1 \sin(\kappa x) + C_2 cos(\kappa x) + C_3 \sinh(\kappa x) + C_4 \cosh(\kappa x) \tag{2.15}$$

Eq. (2.15) has four extra unknown coefficients to be solved. The continuity of the displacement, slope, bending moment, shear forces between the existing system and the added beam compose four extra constraint equations. So adding one extra beam only extends the **B** matrix in Eq. (2.14) by four rows and four columns. The eigen values and eigen functions are solved by the same method as done on the existing system [Lin, 2008, 2009].

The Modal Superposition method is exact in all the frequency range. So it is one of the competitive candidates for high frequency vibration analysis. The disadvantage is that the frequencies have to be determined one by one through numerical searching method. Furthermore, it only suit for simple boundary condition in two dimensional problems. For complex boundary conditions, the “exact” eigen function doesn’t exist.

2.2.2 Receptance Method

Using the Green’s function method [Goel, 1976; Abu-Hilal, 2003], the solution of Eq. (2.2) could also be given as,

$$X(x) = \int_0^L f(\xi) G(x,\xi) d\xi \tag{2.16}$$

where the Green’s function $G(x,\xi)$ is the solution of following equation,

$$X'''' - \kappa X = \delta(x-\xi) \tag{2.17}$$

Eq. (2.17) could be solved by taking the Laplace transform,

$$\hat{X}(s) = \frac{1}{s^4-\kappa^4}\left[e^{-s\xi} + s^3 X(0) + s^2 X'(0) + sX''(0) + X'''(0)\right] \tag{2.18}$$

and the inverse Laplace transform of Eq. (2.18) is found to be

$$G(x,\xi) = \frac{\phi_4(x-\xi)u(x-\xi)}{\kappa^3} + X(0)\phi_1(x) + \frac{X\prime(0)}{\kappa}\phi_2(x) + \frac{X\prime\prime(0)}{\kappa^2}\phi_3(x) + \frac{X\prime\prime\prime(0)}{\kappa^3}\phi_4(x) \quad (2.19)$$

where $u(x-\xi)$ is unit step function, and

$$\phi_1(x) = \frac{1}{2}\big(\cosh(\kappa x) + cos(\kappa x)\big)\,,\ \phi_2(x) = \frac{1}{2}(\sinh(\kappa x) + \sin(\kappa x))\,, \quad (2.20,\ \ 2.21)$$

$$\phi_3(x) = \frac{1}{2}\big(\cosh(\kappa x) - cos(\kappa x)\big)\,,\ \phi_4(x) = \frac{1}{2}(\sinh(\kappa x) - \sin(\kappa x)) \quad (2.22,\ \ 2.23)$$

$X(0)$, $X'(0)$, $X''(0)$, $X'''(0)$ are solved by replacing $x = L$ in Eq. (2.19) and its derivatives. Once the Green's function Eq. (2.19) is obtained, the natural frequencies, mode shapes, and forced response could all be obtained. Detailed discussion and information for various degenerate cases, such as clamped, cantilever, etc, are given by Abu-Hilail [2003]. Green's function method only involves integration over the geometry domain. The slow convergence problem exit in the infinite series summation method is avoided. So it is also one of the promising methods for high frequency analysis.

2.2.3 Discrete Singular Convolution Method

Discrete Singular Convolution (DSC) is introduced by Wei (1999). Singular convolution is defined by the theory of distribution [Wei, 1999]. Let $T(x)$ be a distribution and $\eta(t)$ be an element of the space of test function. A singular convolution is defined as

$$F(t) = (T * \eta)(t) = \int_{-\infty}^{\infty} T(t-x)\eta(x)\,dx \quad (2.24)$$

Her $T(t-x)$ is a singular kernel, and could be chosen as the Direc delta function

$$T(x) = \delta^{(n)}(x)\ (n = 0,1,2,\ldots) \quad (2.25)$$

Since $\delta^{(n)}(x)$ are singular, and can not be directly used in computation. Sequence of approximation $T_\alpha(x) = \sin(\alpha x)/\pi x$ is constructed, and then the Discrete Singular Convolution (DSC) is then defined as

$$F_\alpha(t) = \sum_{k=-M}^{M} T_\alpha(t - x_k)\, f(x_k) \tag{2.26}$$

All the derivatives of $f(x_k)$ are then transferred to the kernel function.

$$f^{(n)}(x) = \sum_{k=-M}^{M} \delta_{\pi/\Delta,\sigma}^{(n)}(x - x_k)\, f(x_k) \tag{2.27}$$

It should be noted that the summation in Eq. (2.27) is symmetric about the evaluated point. Those points near the boundaries must be treated separately. Fictional values are proposed in assisting the DSC computation. For simply supported (clamped) edges, anti-symmetric (symmetric) values about the boundary edge are adopted in the computation [Wei, 2001]. For other more complicated boundary conditions, complicated methods are needed. After all the derivatives and the function itself are substituted into the governing equation, the eigen value, and eigen functions are obtained numerically.

DSC method is categorized as one of the weighted finite difference method with Gaussian regularizer [Boyd, 2006]. Very promising results are reported in the literature [Wei, 2002; Wei et al., 2002; Zhao, et al., 2002], even in the high frequency vibration analysis [Secgin & Sarigul, 2009]. The vital disadvantage is that it only suit for problems with zero deflection along the boundaries; otherwise it lose its high accuracy. Free boundary condition is studied as a special case [Zhao, 2005], but still constitutes a big challenge for DSC method. Another disadvantage is that there is no given method on how to choose the free variable σ. It heavily relies on the experience of the user, and mostly is chosen by trial and error method [Wei & Zhao, 2006, 2007].

2.2.4 Differential Quadrature Method

The Differential Quadrature (DQ) method is proposed by Bellman & Casti [Bellman, et al., 1971, 1972] in the early 1970s. The basic idea in the DQ method is to approximate the derivative of a function as a weighted linear combination of the function values at all the discrete grid points in the whole domain of the spatial coordinate.

$$f'(x_i) \cong \sum_{j=1}^{N} a_{i,j}\, f\left(x_j\right)\ (i = 1, 2, \dots, N) \qquad (2.28)$$

where the discrete grid points $x_i$and the weighting coefficients x_j could be determined in various fashions [Bert & Malik, 1996]. Bellman & Casti chose x_i the roots of the shifted Legendre polynomial of degree N, $P_N^*(x) = P_N(1 - 2x)$. $a_{i,j}$ are determined by letting Eq. (2.28) be exact for the test functions $g_k\ (x) = x^k$, $k = 0, 1,\ \dots, N - 1$. The test functions could also be taken as the following form generalized by Legendre polynomials$g_k\ (x) = \frac{L_N(x)}{(x - x_k) L_N^{(1)}(x)}$, in which $L_N(x)$ and $L_N^{(1)}(x)$ are the N^th order Legendre polynomial and its first derivative. Once the weighting coefficient $a_{i,j}$ is obtained, the high order differential could be easily obtained by repeating the same method. Thus, any partial differential equation can be reduced to a system of linear algebraic equations. Successful solutions are obtained for beam and plate vibration problems under various complex boundary conditions [Bert, et al, 1994; Shu, 1997, 1999, 2000]. Unlike the DSC method, the boundary conditions could be treated as some extra constraint on the weighting coefficient elements in DQ method. It is showed that the DQ method could be cast into high order polynomial interpolation methods [Shu, 2000]. The disadvantages of the DQ method are rooted in the uncertainties or controversy with selecting the test functions and the grid points. Delta-grids are commonly used in approximating the second order derivatives as included in the boundary conditions of a plate problem. However, such grids can potentially lead to an ill-conditioned weighting coefficient matrix [Shu, 2000].

2.2.5 Hierarchical Function Method

Two versions of the finite element method are commonly used in vibration analysis. While h-version finite element regulate the maximum diameter of the element, p-version finite element keep the mesh size fixed and increase the degree of the interpolation functions progressively until the desired accuracy is reached. A particular class of p-version of the finite element method is called Hierarchic Finite Element Method (HFEM), in which the set of p_{max} order interpolation functions constitutes the subset of $p_{max} + 1$ order interpolation function. In HFEM method, four special functions in each direction are designed to account for the boundary conditions; the rest functions are designed to satisfy the condition that their values and their first derivative values on the boundaries are all zero.

Based on Legendre orthogonal polynomials,

$$P_m(\xi) = \frac{1}{m!(-2)^m} \frac{d^m}{d\xi^m}\left[\left(1-\xi^2\right)^2\right] \qquad \xi \in [-1,1] \tag{2.29}$$

Zhu [1985] introduced a set of hierarchic functions by introducing

$$P_m^s(\xi) = \int_{-1}^{\xi} \cdots \int_{-1}^{\xi} P_m(\xi)\, d\xi \cdots d\xi = \sum_{n}^{[m/2]} \frac{(-1)^n}{2^n n!} \frac{(2m-2n-2s-1)!!}{(m-2n)!} \xi^{m-2n} \tag{2.30}$$

Specify s=2 in Zhu's polynomial, Bardell [1991] introduced the following hierarchic function set ,

$$f_r(\xi) \equiv P_{m=r-1}^{s=2} == \sum_{n}^{[(r-1)/2]} \frac{(-1)^n}{2^n n!} \frac{(2r-2n-7)!!}{(r-2n-1)!} \xi^{r-2n-1} \quad r>4 \tag{2.31}$$

along with four function account for the boundary conditions,

$$f_1(\xi) = \tfrac{1}{2} - \tfrac{3}{4}\xi + \tfrac{1}{4}\xi^3, \qquad f_2(\xi) = \tfrac{1}{8} - \tfrac{1}{8}\xi - \tfrac{1}{8}\xi^2 + \tfrac{1}{8}\xi^3 \qquad (2.32,\ 2.33)$$

$$f_3(\xi) = \tfrac{1}{2} + \tfrac{3}{4}\xi - \tfrac{1}{4}\xi^3, \qquad f_2(\xi) = -\tfrac{1}{8} - \tfrac{1}{8}\xi + \tfrac{1}{8}\xi^2 + \tfrac{1}{8}\xi^3 \qquad (2.34,\ 2.35)$$

Analyzed the "round-off" error in Bardell's formulation in high order terms, Beslin & Nicolas [Beslin & Nicolas] introduced another set of hierarchic function set using trigonometric functions,

$$\psi_r(\xi) = \sin(a_r\xi + b_r)\sin(c_r\xi + d_r) \tag{2.36}$$

in which a_r , b_r , c_r d_r are chosen as in following table,

Order	a_r	b_r	c_r	d_r
1	$\pi/4$	$3\pi/4$	$\pi/4$	$3\pi/4$
2	$\pi/4$	$3\pi/4$	$-\pi/2$	$-3\pi/2$
3	$\pi/4$	$-3\pi/4$	$\pi/4$	$-3\pi/4$
4	$\pi/4$	$-3\pi/4$	$\pi/2$	$-3\pi/2$
$r>4$	$(r-4)\pi/2$	$(r-4)\pi/2$	$\pi/2$	$\pi/2$

Very high order modes (up to 850th mode) for simply supported plate are obtained in Beslin's result [1997]. But the accuracy is reduced for free plate. The applicability of the method to other general boundary conditions needs further investigation.

2.2.6 Static Beam Function Method

This method is introduced by Zhou [1996]. The deflection of a beam under static loading satisfy following differential equation,

$$EIw''''(x) = P(x) \tag{2.37}$$

in which $P(x)$ can be expanded into a sine series,

$$P(x) = \sum_{m=1}^{\infty} P_i \sin(m\pi x/L) \tag{2.38}$$

Then the general solution of the beam under static loading is,

$$w(\xi) = C_0 + C_1\xi + C_2\xi^2 + C_3\xi^3 + \sum_{m=1}^{\infty} P_i\,(L/m\pi)^4 \sin(m\pi\xi/L) \tag{2.39}$$

Based on the solution in Eq. (2.39), Zhou introduced a set of function,

$$Y(\xi) = \sum_{i=1}^{\infty} A_i[C_{i0} + C_{i1}\xi + C_{i2}\xi^2 + C_{i3}\xi^3 + \sin(i\pi\xi/L)] \tag{2.40}$$

The coefficients C_{i0}, C_{i1}, C_{i2}, C_{i3} are introduced in each of the basis function to satisfy the boundary conditions.

The method is directly applied in plate vibration in Zhou's work [1996]. Rayleigh-Ritz method is used in the eigen value analysis. Quick convergence is observed in the presented results.

2.2.7 Spectral-Tchebychev Method

Recently, Yagci, et al [Yagci, et al., 2009] presented an interesting method called Spectral-Tchebychev Method. The beam displacement function is approximated by the Tchebychev polynomials,

$$y(\xi) = \sum_{k=0}^{\infty} a_k \mathfrak{J}_k(\xi) \tag{2.41}$$

where $\mathfrak{J}_k(\xi)$ is the k_{th} scaled Tchebychev polynomial.

Then the solution is decomposed into two parts, i.e., $\boldsymbol{y} = \boldsymbol{w} + \boldsymbol{q}$, where $\boldsymbol{w}$ and $\mathbf{q}$ are vectors in the null space and null-perpendicular space of the boundary conditions. The method is used in both linear and non-linear beam vibration analysis, and promising results are reported [Yagci, 2009]. Spectral Tchebychev method used null-Space of the boundary value condition concept, which could also be utilized by other approximation methods.

2.2.8 Fourier Series Method with Stokes Transformation

In Modal Superposition Method, the displacement function is assumed as a linear combination of the eigen functions, then its derivatives are obtained by term-by-term differentiation. Under complex structure or boundary conditions, the displacement could also be approximated by other polynomial or trigonometric functions. However, under what condition the derivative could be moved into the summation bracket and differentiated term-by term will be vital for the correctness of the calculated results. The method is based on following two theorems,

Theorem 2 Let $f(x)$ be a continuous function defined on [0, L] with an absolutely integrable derivative, and let $f(x)$ be expanded in Fourier cosine series

$$f(x) = a_0 + \sum_{m=1}^{\infty} a_m \cos \lambda_m x \qquad 0 < x < L \quad (\lambda_m = m\pi / L) \tag{2.42}$$

then $$f'(x) = -\sum_{m=1}^{\infty} \lambda_m a_m \sin \lambda_m x \tag{2.43}$$

Theorem 3 Let $f(x)$ be a continuous function defined on [0, L] with an absolutely integrable derivative, and let $f(x)$ be expanded in Fourier sine series

$$f(x) = \sum_{m=1}^{\infty} b_m \sin \lambda_m x \qquad 0 < x < L \quad (\lambda_m = m\pi / L) \tag{2.44}$$

then

$$f'(x) = \frac{f(L) - f(0)}{L} + \sum_{m=1}^{\infty} \left(\frac{2}{L} \left[(-1)^m f(L) - f(0) \right] + \lambda_m b_m \right) \cos \lambda_m x \tag{2.45}$$

Theorem 3 is called Stokes Transformation. These theorems tell that while a cosine series can be differentiated term by term, it can be done to sine series only if $f(0) = f(L) = 0$.

The beam displacement function is first approximated by a Fourier sine series [Greif & Mittendorf, 1976; Wang & Lin, 1996; Maurizi & Robledo, 1998].

$$w(x) = \sum_{m=1}^{\infty} A_m \sin \lambda_m x \qquad 0 < x < L \quad (\lambda_m = m\pi / L) \tag{2.46}$$

Then by using the Stokes transformation,

$$w'(x) = \frac{w(L) - w(0)}{L} + \sum_{m=1}^{\infty} \left(\frac{2}{L} \left[(-1)^m w(L) - w(0) \right] + \lambda_m A_m \right) \cos \lambda_m x \tag{2.47}$$

The second derivative is derived by utilizing theorem 2,

$$w''(x) = -\sum_{m=1}^{\infty}\left(\frac{2}{L}\left[(-1)^m w(L) - w(0)\right] + \lambda_m A_m\right)\lambda_m \sin\lambda_m x \tag{2.48}$$

High order derivertives could all be obtained by utilizing a combination the two theories. $w(0)$, $w(L)$, $w''(0)$, and $w''(L)$ are the unknown variables in the boundary conditions, and could be expressed by the coefficients A_m, replace them back into the governing equation, and the natural frequencies and mode shapes could be easily determined by the orthogonal properties of $\sin\lambda_m x$ over the domain [0,L].

The displacement could also be expressed as a Fourier cosine series, and similar procedure and results could be obtained. Also note that the these formula should be treated separately when the four terms $w(0)$, $w(L)$, $w''(0)$, and $w''(L)$ are all zeros. The method is first used in vibration analysis in Rayleigh-Ritz method [Greif & Mittendorf, 1976], and extended into exact analysis method by Wang and Lin [1996], Very promising results are also reported for both beams and plates [Kim & Kim, 2001, 2005; Hurlebaus & Gaul, 2001].

2.3 Transverse vibration of generally supported beams

2.3.1 Analytical function approximation in the beam vibration analysis

The unknown displacement function of a beam is expressed in the following series form,

$$w(x) = \sum_{m=0}^{\infty} A_m \cos(m\pi x/L) + \sum_{j=1}^{4} B_j \sin(j\pi x/L) \tag{2.49}$$

where A_m, B_j are the unknown coefficients to be determined. This series can also be found in Xu's PhD dissertation (Chap. III page 43). The function is a superposition of a Fourier cosine series and an auxiliary polynomial that is used to remove the discontinuities in the original displacement function and its related derivatives. The auxiliary polynomial $p(x)$ is sought as a combination of four sine terms that are orthogonal to the cosine terms in the residual function $\overline{w}(x)$.

2.3.2 Energy equation

Energy equation is recognized as the weak form of the general governing differential equation. It could be obtained by multiply $w(x)$ on both side of the governing Eq. (2.2) and integrate on $[0, L]$.

$$\int_0^L EIw(x)w''''(x)dx - \omega^2 \int_0^L \rho A w^2(x)dx = \int_0^L w(x)p(x)dx \tag{2.50}$$

Use integration by parts twice on the first term, Eq. (2.54) could be further expressed as

$$EIw'''(x)w(x)|_0^L - EIw''(x)w'(x)|_0^L + EI\int_0^L [w''(x)]^2 dx - \omega^2 \int_0^L \rho A w^2(x)dx = \int_0^L w(x)p(x)dx \tag{2.51}$$

the Hamilton Energy equation is easily obtained by utilizing the four boundary condition,

$$H(x) = k_0 w^2(0) + k_L w^2(L) + K_0 {w'}^2(0) + K_L {w'}^2(L) + EI\int_0^L [w''(x)]^2 dx - \omega^2 \int_0^L \rho A w^2(x)dx - \int_0^L w(x)p(x)dx \tag{2.52}$$

Replace $w(x)$ with Eq. (2.49) and utilize the Hamilton principle, which state that the structural motion renders the value of $H(x)$ stationary, i.e.

$$\delta H(x) = 0 \tag{2.53}$$

By equal all the partial derivatives with respect to the unknown coefficients zeros, following equation is derived,

$$(\mathbf{K} - \omega^2\mathbf{M})\mathbf{d} = \mathbf{F} \tag{2.54}$$

Eq. (2.54) form a standard characteristic equation of the beam when $\mathbf{F} = \mathbf{0}.$

2.3.3 Numerical examples

The convergence speed of the current method is first tested on a clamped-clamped beam. This boundary condition is generated by setting both the linear and rotational spring stiffness to infinity, which is represented by a very large number, $1.0 \times 10^{11} EI/L$ and $1.0 \times 10^{11} EI/L^3$, respectively. Table 2.1 shows the first eight lowest frequency parameters, $\mu = L/\pi \cdot \left(\omega\sqrt{\rho A/(EI)}\right)^{1/2}$ with different truncation number (M=4, 5, ⋯, 10) in Equation (2.49). It is seen that the solution converges so fast that just a few terms can lead to an excellent prediction. Based on observation of the excellent convergence speed, the truncation number is set to M=10 in the following calculation.

Table 2.2 lists the first eight lowest frequency parameters $\mu = L/\pi \cdot \left(\omega\sqrt{\rho A/(EI)}\right)^{1/2}$ when the elastic boundary constraints varies from free to clamped boundary condition. By varying the elastic constants used in simulating the boundary conditions in Eq. (2.3-2.6), current method works for a beam with general elastic boundary conditions.

Figure 2.2 give the first eight lowest mode shapes for a cantilevel beam obtained by current method with trucation number M=10 and the exact solution. The classical solution for this case is well known as,

Table 2.1 The first eight lowest frequency parameters $\mu = L/\pi \cdot \left(\omega\sqrt{\rho A/(EI)}\right)^{1/2}$ of a clamped-clamped beam with different truncation number in the approximation series in Equation (2.49).

Mode	M = 4	M = 5	M = 6	M = 7	M = 8	M = 9	M = 10	Exact
1	1.50629	1.50565	1.50565	1.50562	1.50562	1.50562	1.50562	1.50562
2	2.50229	2.50229	2.49993	2.49993	2.49978	2.49978	2.49976	2.49975
3	3.50123	3.50013	3.50013	3.50004	3.50004	3.50002	3.50002	3.50001
4	4.50114	4.50114	4.50034	4.50034	4.50009	4.50009	4.50003	4.5
5	328.610	5.59331	5.59332	5.50024	5.50024	5.50001	5.50004	5.5
6	344.037	344.037	6.60673	6.60671	6.50023	6.50023	6.50003	6.5
7	2340.66	370.007	370.007	7.74446	7.74446	7.50139	7.50148	7.5
8	2619.97	2619.97	382.767	382.767	8.77435	8.77439	8.50164	8.5

Table 2.2 The first eight lowest frequency parameters $\mu = L/\pi \cdot \left(\omega\sqrt{\rho A/(EI)}\right)^{1/2}$ of a beam with the elastic constant coefficient varing from free to clamped boundary condition and truncation number $M = 10$ in Eq. (2.49).

Mode	1	2	3	4	5	6	7	8
k=K=10^{-6} EI/L	0.01197	0.04751	1.50562	2.49976	3.50002	4.50003	5.50027	6.50044
k=K=0.01 EI/L	0.11970	0.23554	1.50697	2.50058	3.50060	4.50049	5.50064	6.50075
k=K=0.1 EI/L	0.21278	0.41675	1.51883	2.50788	3.50580	4.50452	5.50394	6.50354
k=K= EI/L	0.37740	0.71089	1.61165	2.57090	3.55270	4.54188	5.53496	6.53005
k=K=10 EI/L	0.66471	1.04115	1.88023	2.81769	3.77627	4.74474	5.71971	6.69923
k=K=100 EI/L	1.11337	1.48483	2.11641	3.01459	3.98123	4.96376	5.95145	6.94131
k=K=10^{3} EI/L	1.44056	2.20255	2.78815	3.39088	4.17465	5.08477	6.04498	7.02476
k=K=10^{6} EI/L	1.50555	2.49944	3.49916	4.49821	5.49670	6.49454	7.49295	8.48925
Clamped	1.50562	2.49976	3.50002	4.50003	5.50004	6.50003	7.50148	8.50164

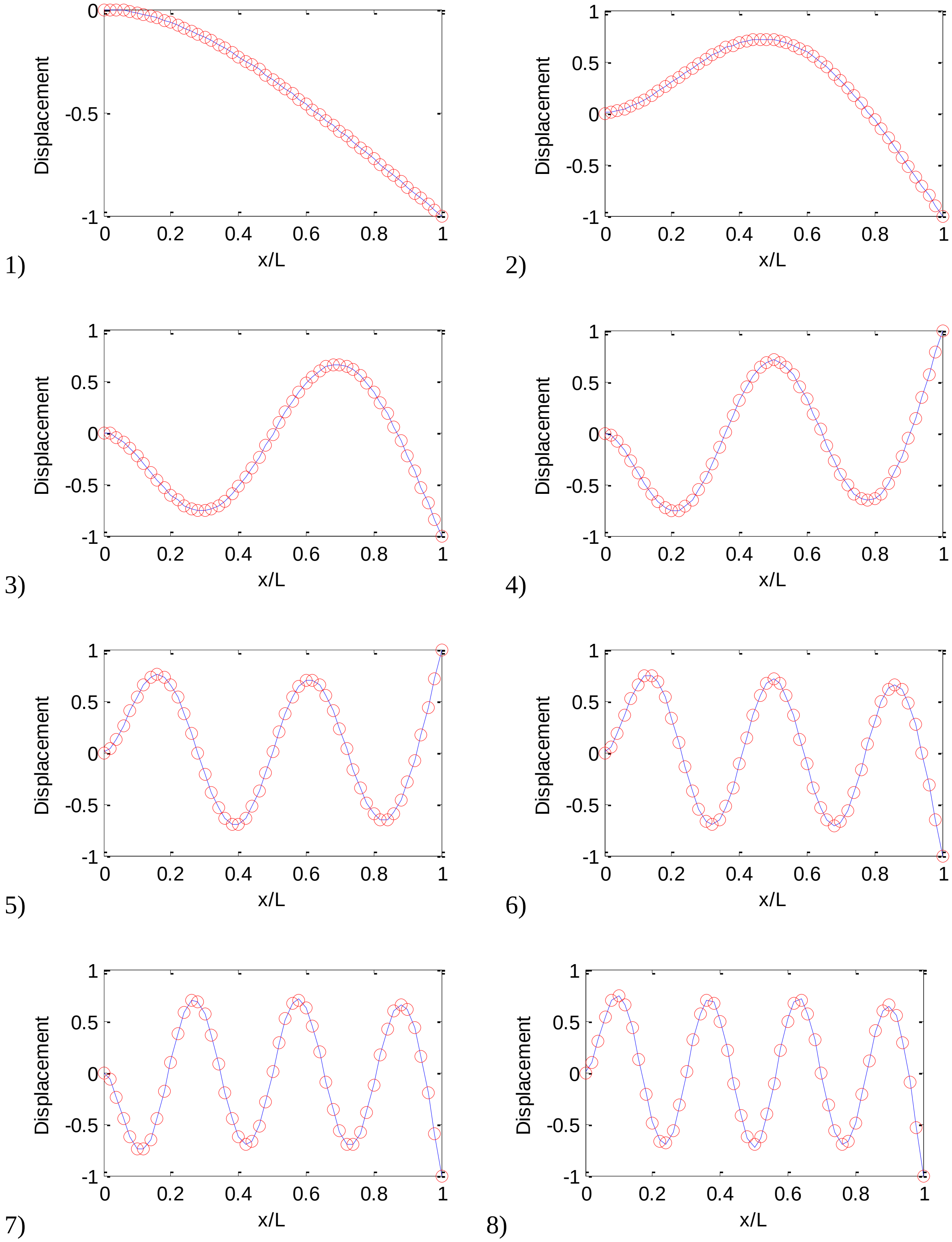

Figure 2.2 The first eight lowest mode shapes for a cantilever beam obtained by current method with truncation number M=10 (blue curves) and by the exact solution equation (red circles).

$$\phi(x) = \cosh(\pi\mu_i x/L) - \cos(\pi\mu_i x/L) - \sigma_i(\sinh(\pi\mu_i x/L) - \sin(\pi\mu_i x/L)) \tag{2.55}$$

where $\sigma_i = [\cosh(\pi\mu_i) + \cos(\pi\mu_i)]/[(\sinh(\pi\mu_i) + \sin(\pi\mu_i))]$. Although only fourteen eigenvalues are calculated with truncation number $M = 10$, it is clear that the listed mode shapes match the exact solution very well. All these results have indicated that the mode shapes can also be accurately obtained by taking only a few terms in the Fourier series.

2.3.4 Discussions and Conclusions

A simple and fast convergent method is presented for the dynamic analysis of a beam with general boundary conditions. The beam displacement is sought as the superposition of a Fourier series and four auxiliary sine functions that is used to remove the discontinuities with the original displacement function and its related derivatives. The modal parameters of the beam can be readily and systematically obtained from solving a standard matrix eigenproblem, instead of the non-linear hyperbolic equations as in the traditional techniques. It has been shown through numerical examples that the natural frequencies and mode shapes can both be accurately calculated for beams with various boundary conditions. The remarkable convergence of the current solution is demonstrated both theoretically and numerically. Extension of the proposed technique to two dimensional structures such as rectangular plates and triangular plates with general boundary conditions will be demonstrated in the following chapters.

Chapter III Transverse vibration of rectangular plates with elastic boundary supports

3.1 Rectangular plate vibration description

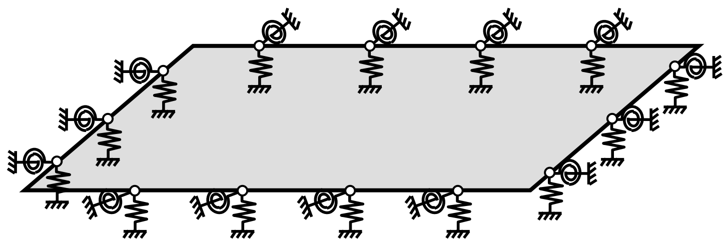

Figure 3.1 A rectangular plate elastically restrained along all the edges

Consider a rectangular plate with its edges elastically restrained against both deflection and rotation as shown in Figure 3.1. It is assumed that the plate vibrates under a harmonic excitation at a given frequency ω. The effects of material damping, rotary inertia, and transverse shear deformations are all neglected. The vibration of the plate is governed by the following differential equation

$$D\nabla^4 \mathrm{w}(x,y) - \rho h \omega^2 w(x,y) = f(x,y) \tag{3.1}$$

where $\nabla^4 = \partial^4/\partial \mathrm{x}^4 + 2\,\partial^4/\partial \mathrm{x}^2\,\partial \mathrm{y}^2 + \partial^4/\partial \mathrm{y}^4$, $w(x,y)$ is the flexural displacement; ω is the angular frequency; D, ρ, and h are the bending rigidity, the mass density and the thickness of the plate, respectively; $f(x,y)$ is the distributed harmonic excitation acting on the plate surface. The frequency term $e^{i\omega t}$ is suppressed on both sides of the Eq. (3.1) for simplicity.

In terms of the flexural displacement, the bending and twisting moments, and the transverse shearing forces can be expressed as

$$M_x = -D\left(\frac{\partial^2 w}{\partial x^2} + \upsilon \frac{\partial^2 w}{\partial y^2}\right), \tag{3.2}$$

$$M_y = -D\left(\frac{\partial^2 w}{\partial y^2} + \upsilon \frac{\partial^2 w}{\partial x^2}\right), \tag{3.3}$$

$$M_{xy} = -D(1-\upsilon)\frac{\partial^2 w}{\partial xy}, \tag{3.4}$$

$$Q_x = -D\frac{\partial}{\partial x}(\Delta w) + \frac{\partial M_{xy}}{\partial y} = -D\left(\frac{\partial^3 w}{\partial x^3} + (2-\upsilon)\frac{\partial^3 w}{\partial y^2 x}\right), \tag{3.5}$$

and

$$Q_y = -D\frac{\partial}{\partial y}(\Delta w) + \frac{\partial M_{xy}}{\partial x} = -D\left(\frac{\partial^3 w}{\partial y^3} + (2-\upsilon)\frac{\partial^3 w}{\partial x^2 y}\right) \tag{3.6}$$

The boundary conditions for an elastically restrained rectangular plate are as follows:

$$k_{x0}(y)w = Q_x,\ K_{x0}(y)\partial w/\partial x = -M_x \qquad \text{at } x = 0 \qquad (3.7,\ 3.\ 8)$$

$$k_{xa}(y)w = -Q_x,\ K_{xa}(y)\partial w/\partial x = M_x \qquad \text{at } x = a \qquad (3.9, 3.10)$$

$$k_{y0}(x)w = Q_y,\ K_{y0}(x)\partial w/\partial y = -M_y \qquad \text{at } y = 0 \qquad (3.11,\ 3.12)$$

and

$$k_{yb}(x)w = -Q_y,\ K_{yb}(x)\partial w/\partial y = M_y \qquad \text{at } y = b \qquad (3.13, 3.14)$$

where $k_{x0}(y)$, $k_{xa}(y)$, $k_{y0}(x)$, and $k_{yb}(x)$ are four stiffness functions representing the linear springs against deflection, $K_{x0}(y)$, $K_{xa}(y)$, $K_{y0}(x)$, and $K_{yb}(x)$ are four stiffness functions representing the rotary springs against rotation, and Q_x, Q_y, M_x, and M_y are shear forces and bending moments at $x = 0$, $x = a$, $y = 0$, and $y = b$ respectively. It should be noted that the stiffness functions allow the spring stiffness varying along each edge. Eq. (3.7-3.14) represent all possible general elastic edge conditions. All the classical homogeneous boundary conditions can be directly obtained by accordingly setting the spring constants to be extremely large or small.

3.2 Literature review on the transverse vibration of rectangular plates

There is a wealth of literature on the vibrations of rectangular plates with various boundary conditions, but a vast majority of them is focused on the classical boundary conditions representing various combinations of clamped, simply supported or free edges [Leissa, 1993]. While a number of studies have been devoted to the vibrations of plates with uniform elastic restraints along an edge [Carmichael, 1959; Laura, et al., 1974, 1977, 1978, 1979; Li, 2002, 2004], only few references can be found dealing with non-uniform elastic restraints [Leissa, et al., 1979; Laura & Gutierrez, 1994; Shu & Wang 1999, Zhao & Wei, 2002]. Due to the non-separatable nature of the plate vibration governing equation, exact solutions are only available for plates which are simply supported (or guided) along at least one pair of opposite edges. Accordingly, a variety of approximate or numerical solution techniques have been employed to solve plate problems under different boundary conditions, which include, but are not limited to, Rayleigh-Ritz procedures, finite strip method [Cheung, 1971], superposition method [Gorman, 1980], Differential Quadrature method (DQ) [Shu, 1997], and Discrete Singular Convolution method (DSC) [Wei, et al., 1997]. Variational Method, such as Rayleigh-Ritz, is another widely used technique for obtaining an approximate solution for the plate vibration. When the Rayleigh-Ritz method is employed in solving plate problems, the displacement function is often expressed in terms of characteristic functions obtained for beams with similar boundary conditions [Warburton, 1954; Leissa, 1973; Dickinson & Li, 1982; Warburton, 1979; 1984]. Although the characteristic functions are well known in the form of trigonometric and hyperbolic functions, they are explicitly dependent upon the boundary conditions. Furthermore, the characteristic function is generally unavailable for beams with complex boundary conditions. Instead of the beam functions, one can also use other forms of admissible functions such as simple or orthogonal polynomials, trigonometric functions and their combinations [Cupial, 1997; Bhat, 1985; Dickinson & Di-Blasio, 1986; Laura & Grossi, 1981; Zhao, 195, 1996; Beslin & Nicolas, 1997]. When the admissible functions do not form a complete set, the accuracy and convergence of the corresponding solution cannot be easily estimated. A well-known problem with use of complete (orthogonal) polynomials is that the higher order polynomials tend to become numerically unstable due to the computer round-off errors. This numerical difficulty can be avoided by using the trigonometric functions [Cupial, 1997] or the combinations of trigonometric functions and lower order polynomials [Laura, 1997; Zhao, 1996]. Although it has become a "standard" practice to express the plate displacement function as the series expansion of the beam functions (whether they are in the form of trigonometric functions, hyperbolic functions, polynomials or their combinations), there is no guarantee mathematically that such a representation will actually converge to the true solution because of the difference between the beam and plate boundary conditions. While the limitation of such a mathematical treatment is not readily assessed, its practical implication becomes immediately clear when a non-uniform boundary condition is specified along an edge. More explicitly, a similar boundary condition cannot be readily chosen for the purpose of determining the appropriate beam functions.

Based on the linearity of the plate vibration problems, a systematic superposition method is proposed by Gorman for solving plate problems under various boundary conditions [Gorman, 1997, 2000, 2003]. In the superposition method a general boundary condition is decomposed into a number of "simple" boundary conditions for which analytical solutions exist or can be easily derived. This technique, however, requires a good understanding and skillful decomposition of the original problems. For more complex boundary conditions when the elastic coefficients are actually function of the coordinate, the superposition method does not work. Moreover, the decomposition of the boundary condition itself creates fictional jump discontinuity at the corners of the plate, which create further convergence problem. The displacement at the corner intersection may be forced to zero in the final solution.

Hurlebaus & Gaul [2001] solved the eigenfrequencies of a plate with completely free boundary conditions by using the following displacement function, $W(x,y) = F_{00}/4 + \sum_{m=1}^{\infty} F_{m0}/2 \cos(\lambda_m x) + \sum_{n=1}^{\infty} F_{0n}/2 \cos(\lambda_n y) + \sum_{m=1}^{\infty}\sum_{n=1}^{\infty} F_{mn} \cos(\lambda_m x) \cos(\lambda_n y)$, where $\lambda_m = m\pi/a$ and $\lambda_n = n\pi/b$. Galerkin weighted residual method and integration by parts are utilized in solving the governing equation, which is further written as an integral relation between the boundary slope value and the function value on the boundaries. The author observed that the displacement function can be further simplified as a double Fourier cosine series, $W(x,y) = \sum_{m=0}^{\infty}\sum_{n=0}^{\infty} F_{mn} \cos(\lambda_m x) \cos(\lambda_n y)$. As pointed out by Rosales & Filipich [2003], the convergence might be lost in the direct term-by-term differentials. Although the solution is correct for plate with free boundary condition, this method may not suit for other complex boundary condition.

Filipich & Rosales [2000] developed a method called Whole Element Method, in which the displacement functional is expressed as a double Fourier sine series plus several designed functions,$\phi_{MN}(x,y) = \sum_{i=1}^{M}\sum_{j=1}^{N} A_{ij} \sin(\lambda_i x) \sin\left(\lambda_j y\right) + x\left(a_0 + \sum_{j=1}^{N} A_{0j} \sin\left(\lambda_j y\right)\right) + y(b_0 + \sum_{i=1}^{N} A_{i0} \sin(\lambda_i x)) + A_{00}xy + \sum_{j=1}^{N} b_j \sin\left(\lambda_j y\right) + \sum_{i=1}^{N} a_i \sin(\lambda_i x) + k_0$. This method is also applied to the vibration of plates with internal supports [Escalante, et al., 2004]. It is observed by current author that the function can be represented by the following form, $\phi_{MN}(x,y) = \sum_{i=1}^{M+2}\sum_{j=1}^{N+2} A_{ij}\varphi_i(x)\,\varphi_j(y)$, where $\varphi_1(x) = 1$, $\varphi_2(x) = x$, and $\varphi_i(x) =$

$\sin(\lambda_{i-2}x)$. It is similar to Zhou's static beam function method applied to 2-D vibration, but with only the first two orders of polynomials.

The series solutions derived in refs. [Pilipich & Rosales, 2000; Hurlebaus, 2001] may not be extended to other boundary conditions other than the completely free case. Although these series solutions were claimed to be able to exactly calculate the eigenfrequencies, mode shapes and even the slopes, they may not automatically become an exact solution in the classical sense because a classical solution will have to be sufficiently smooth; that is, the third-order derivatives are continuous, and the fourth- order derivatives exist everywhere on the plate. For example, if the moments and shear forces cannot be assured to be exact throughout the plate and along the edges (when they are not completely free), it may not be possible to ascertain that the eigenfrequencies and mode shapes can be calculated exactly or with any arbitrary precision. These questions or concerns can be circumvented by the proposed solution which is also expressed in the form of series expansions. It is, however, substantially different from the aforementioned series solutions in that it can be differentiated term-by-term to obtain other useful quantities (such as, slopes, moments and shear forces) at any point on the plate, and hence be directly substituted into the governing equation and boundary conditions to solve for the unknown expansion coefficients in an exact manner. This chapter represents an extension of the solution method previously developed for analyzing vibrations of beams [Li, 2000] and in-plane vibrations [Du, et al., 2007]. In comparison with the solutions for in-plane vibrations, the current method will have to include more supplementary terms to improve the smoothness (and hence the rate of convergence) of the displacement function and to account for the potential discontinuities with the higher-order derivatives along the edges when they are periodically extended onto the entire *x*-*y* plane. A set of supplementary functions is provided in the form of trigonometric functions which is essentially unaffected by the differential operations and can avoid the possibility of nullifying a boundary condition. The mathematical and numerical advantages of the current solution method will become obvious from the following discussions.

3.3 Displacement function selection

The displacement function will be sought in the form of series expansions as:

$$w(x,y)=\sum_{m=0}^{\infty}\sum_{n=0}^{\infty}A_{mn}\cos(\lambda_{am}x)\cos(\lambda_{bn}y)+\sum_{l=1}^{4}\left[\xi_b^l(y)\sum_{m=0}^{\infty}c_m^l\cos(\lambda_{am}x)+\xi_a^l(x)\sum_{n=0}^{\infty}d_n^l\cos(n\pi y)\right] \tag{3.15}$$

where $\lambda_{am}=m\pi/a$, $\lambda_{bn}=n\pi/b$, and $\xi_a^l(x)$ (or $\xi_b^l(y)$) represent a set of closed-form sufficiently smooth functions defined over [0, a] (or [0, b]). The term "sufficiently smooth" implies that the third order derivatives of these functions exist and are continuous at any point on the plate. Such requirements can be readily satisfied by simple polynomials [Li, 2002]. Theoretically, there are an infinite number of these supplementary functions. However, one needs to ensure that the selected functions will not nullify any of the boundary conditions. As mentioned earlier, these functions are introduced specifically to take care of the possible discontinuities with the first and third derivatives at each edge. In the subsequent solution phase, however, the expansion coefficients will have to be directly solved from the governing equations and the boundary conditions. Thus, the selected supplementary functions should not interfere with this process in any way. To better understand it, let's consider, for example, the boundary condition, Eq. (3.8). If the supplementary functions and their second derivatives (with respect to x) all vanish at x=0, then this boundary condition will be mathematically nullified for K_{x0}=0. In other words, the resulting coefficient matrix will become singular for K_{x0}=0. Similar situations can occur at other edges. With this in mind, the supplementary functions will be here chosen in the form of trigonometric functions which are essentially unaffected by differential operations:

$$\xi_a^1(x) = \frac{9a}{4\pi} sin\left(\frac{\pi x}{2a}\right) - \frac{a}{12\pi} sin\left(\frac{3\pi x}{2a}\right), \xi_a^2(x) = -\frac{9a}{4\pi} cos\left(\frac{\pi x}{2a}\right) - \frac{a}{12\pi} cos\left(\frac{3\pi x}{2a}\right), \qquad (3.16,\ 3.17)$$

$$\xi_a^3(x) = \frac{a^3}{\pi^3} sin\left(\frac{\pi x}{2a}\right) - \frac{a^3}{3\pi^3} sin\left(\frac{3\pi x}{2a}\right), \xi_a^4(x) = -\frac{a^3}{\pi^3} cos\left(\frac{\pi x}{2a}\right) - \frac{a^3}{3\pi^3} cos\left(\frac{3\pi x}{2a}\right) \qquad (3.18,\ 3.19)$$

It is easy to verify that $\xi_a^{1'}(0) = \xi_a^{2'}(a) = \xi_a^{3'''}(0) = \xi_a^{4''''}(a) = 1$, and all other first and third derivatives are identically zero at the edges. These conditions are not necessary, but make it easier to understand the meanings of the 1-D Fourier series expansions: each of them represents either the first or the third derivative of the displacement function at one of the edges. By doing such, the 2-D series will be “forced” to represent a residual displacement function which has, at least, three continuous derivatives in both *x* and *y* directions.

It can be proven mathematically that (Theorem 1)the series expansion given in Eq. (3.15) is able to expand and uniformly converge to *any* function $f(x, y) \in C^3$ for $\forall(x, y) \in D$: ([0, *a*;0, *b*]). Also, this series can be simply differentiated, through term-by-term, to obtain the uniformly convergent series expansions for up to the fourth-order derivatives. Mathematically, an exact displacement (or classical) solution is a *particular* function $w(x, y) \in C^3$ for $\forall(x, y) \in D$ which satisfies the governing equation at *every* field point and the boundary conditions at *every* boundary point. Thus, the remaining task for seeking an exact displacement solution will simply involve finding a set of expansion coefficients to ensure the governing equation and the boundary conditions to be satisfied by the current series solution *exactly on a point-wise basis*.

When a plate problem is amenable to the separation of variables, an exact solution is usually expressed as a series expansion where *each* term will simultaneously satisfy the *homogeneous* governing equation and the boundary conditions. However, in determining the response to an applied load, it should not matter whether the governing equation or a boundary condition is satisfied *individually* by each term or *globally* by the whole series. Take a simply supported plate as an example. A sine function will be able to exactly satisfy the characteristic equation and the boundary conditions at each edge. Then the exact solution is often understood as a simple Fourier series which may also be interpreted as a modal expansion. To calculate the vibrational response, however, the governing equation will usually include two more terms to account for the damping effect and the loading condition, and the solution (the expansion coefficients) are solved by equating the like terms on both sides (of course, it must be explicitly assumed that the forcing function can also be expanded into a sine series). In other words, the governing equation is actually satisfied globally by the series, rather than individually by each term. Since in real calculations a series solution will have to be truncated somewhere according to a pre-determined error bound, an *exact* solution really implies that the results can be obtained to *any desired degree of accuracy*. This characterization equally applies to the current solution as described below. The only procedural difference between the classical solution and the proposed one is that the boundary conditions are automatically satisfied by each term, and the expansion coefficients are only required to satisfy the governing equation; in comparison, the expansion coefficients in the current solution will have to explicitly satisfy both the governing equation and the boundary conditions. This distinction will probably have no mathematical significance in regard to the convergence and accuracy of the solution, although a pre-satisfaction of the boundary conditions or governing equation by each of the expansion terms may result in a reduction of the computing effort.

3.4 Exact Method

3.4.1 Theoretical Formulation

In what follows, our attention will be directed to solving the unknown expansion coefficients by letting the assumed solution satisfy both the governing equation and the boundary conditions. Substituting the displacement expression, Eq. (3.15), into the boundary condition, Eq. (3.7), results in

$$k_{x0}\left(\sum_{m=0}^{\infty}\sum_{n=0}^{\infty} A_{mn}\cos(\lambda_{bn}y)\right) + \sum_{l=1}^{4}\left[\xi_b^l(y)\sum_{m=0}^{\infty} c_m^l + \xi_a^l(0)\sum_{n=0}^{\infty} d_n^l\cos(\lambda_{bn}y)\right] =$$

$$-D\left[(2-\upsilon)\sum_{n=0}^{\infty}(-\lambda_{bn}^2)d_n^1\cos(\lambda_{bn}y) + \sum_{n=0}^{\infty} d_n^3\cos(\lambda_{bn}y)\right] \qquad (3.20)$$

It is seen that all the term in the above equation, except for the second one, are in the form of cosine series expansion in *y* direction. So it is natural to also expand $\xi_b^l(y)$ into a cosine series, i.e. $\xi_b^l(y) = \sum_{n=0}^{\infty}\beta_n^l\cos(\lambda_{bn}y)$. By equating the coefficients for the like terms on both sides, the following equations can be derived

$$\frac{k_{x0}}{D}\sum_{l=1}^{4}\left[\beta_n^l\sum_{m=0}^{\infty} c_m^l + \xi_a^l(0)d_n^l\right] + (2-\upsilon)(-\lambda_{bn}^2)d_n^1 + d_n^3 = -\frac{k_{x0}}{D}\sum_{m=0}^{\infty} A_{mn}$$

$$(n = 0, 1, \ldots, \infty,\ x = 0) \qquad (3.21)$$

Three similar equations can be directly obtained from Eqs. (3.9-3.14),

$$\sum_{l=1}^{4}\sum_{m=0}^{\infty}\left[-\lambda_{am}^2\beta_n^l + \upsilon\bar{\beta}_n^l\right]c_m^l + \sum_{l=1}^{4}\left[\xi_a^{l\,\prime\prime}(0) - \upsilon\lambda_{bn}^2\xi_a^l(0)\right]d_n^l - \frac{K_{x0}}{D}d_n^1 = \sum_{m=0}^{\infty}\left[\lambda_{am}^2 +\right.$$

$$\left.\upsilon\lambda_{bn}^2\right]A_{mn}\ (n = 0, 1, \ldots, \infty,\ x = 0) \qquad (3.22)$$

$$\frac{k_{xa}}{D}\sum_{l=1}^{4}\left[\beta_n^l\sum_{m=0}^{\infty}(-1)^m c_m^l + \xi_a^l(a)d_n^l\right] + (2-\upsilon)\lambda_{bn}^2 d_n^2 - d_n^4 = \frac{k_{xa}}{D}\sum_{m=0}^{\infty}(-1)^{m+1}A_{mn}$$

$$(n = 0, 1, \ldots, \infty,\ x = a) \qquad (3.23)$$

And

$$\sum_{l=1}^{4}\sum_{m=0}^{\infty}(-1)^m\left[\upsilon\bar{\beta}_n^l-\lambda_{am}^2\beta_n^l\right]c_m^l+\sum_{l=1}^{4}[\xi_a^l{}''(a)-\upsilon\lambda_{bn}^2\xi_a^l(a)]d_n^l+\frac{K_{xa}}{D}d_n^2=$$

$$\sum_{m=0}^{\infty}(-1)^m[\lambda_{am}^2+\upsilon\lambda_{bn}^2]A_{mn}\ (n=0,1,\dots,\infty,\ x=a) \tag{3.24}$$

where $\xi_b^l{}''(y)=\sum_{n=0}^{\infty}\bar{\beta}_n^l\cos(\lambda_{bn}y)$.

These equations indicate that the unknown coefficients in the 2-D and 1-D series expansions are not independent; they have to explicitly comply with the constraint conditions, Eqs. (3.21-3.24). Four more constraint equations corresponding to the boundary conditions at the remaining two edges can be readily written out by replacing the variables m, β_n^l, $\bar{\beta}_n^l$, a and x, with n, α_m^l, $\bar{\alpha}_m^l$, b and y, respectively. It now becomes clear that satisfying these constraint equations by the expansion coefficients is equivalent to an *exact* satisfaction of all the boundary conditions (by the displacement function) *on a point-wise basis*.

The constraint equations can be rewritten in a matrix form as,

$$\mathbf{Hp}=\mathbf{Qa} \tag{3.25}$$

where $\mathbf{p}=[c_1^1,c_2^1,\dots,c_M^1,c_1^2,c_2^2,\dots,c_M^2,\dots c_1^4,c_2^4,\dots,c_M^4,d_1^1,d_2^1,\dots,d_N^1,d_1^2,d_2^2,\dots,d_N^2,\dots d_1^4,d_2^4,\dots,d_N^4]^{\mathrm{T}}$, and $\mathbf{a}=[A_{01},A_{11},\dots,A_{M1},A_{02},A_{12},\dots,A_{M2},\dots A_{0N},A_{1N},\dots,A_{MN}]^{\mathrm{T}}$. In Eq. (3.25), it is assumed that all the series expansions are truncated to $m=M$ and $n=N$ to facilitate numerical implementation.

Eq. (3.25) represents a set of $4(M+N)$ equations against a total of $4(M+N)+M\times N$ unknown expansion coefficients. Thus, additional $M\times N$ equations will have to be provided to solve for the expansion coefficients. By substituting Eq. (3.15) into the governing differential equation get

$$\sum_{m=0}^{\infty}\sum_{n=0}^{\infty}(\lambda_{am}^4+\lambda_{bn}^4+2\lambda_{am}^2\lambda_{bn}^2)A_{mn}\cos(\lambda_{am}x)\cos(\lambda_{bn}y)+\sum_{l=1}^{4}\Big[\sum_{m=0}^{\infty}\Big(\lambda_{am}^4\xi_b^l(y)-2\lambda_{am}^2\xi_b^{l\,\prime\prime}(y)+\xi_b^{l\,(4)}(y)\Big)c_m^l\cos(\lambda_{am}x)+\xi_a^l(x)\sum_{n=0}^{\infty}\Big(\lambda_{bn}^4\xi_a^l(x)-2\lambda_{bn}^2\xi_a^{l\,\prime\prime}(x)+\xi_a^{l\,(4)}(x)\Big)d_n^l\cos(\lambda_{bn}y)\Big]-\frac{\rho h\omega}{D}\Big[\sum_{m=0}^{\infty}\sum_{n=0}^{\infty}A_{mn}\cos(\lambda_{am}x)\cos(\lambda_{bn}y)+\sum_{l=1}^{4}\big[\xi_b^l(y)\sum_{m=0}^{\infty}c_m^l\cos(\lambda_{am}x)+\xi_a^l(x)\sum_{n=0}^{\infty}d_n^l\cos(n\pi y)\big]\Big]=0 \tag{3.26}$$

Again, after all the non-cosine functions in the above equation are expanded into cosine series, $\xi_b^{l\,(4)}(y)=\sum_{n=0}^{\infty}\bar{\bar{\beta}}_n^l\cos(\lambda_{bn}y)$, the following equations can be obtained by comparing the like terms on both sides

$$(\lambda_{am}^4+\lambda_{bn}^4+2\lambda_{am}^2\lambda_{bn}^2)A_{mn}+\sum_{l=1}^{4}\big[\big(\lambda_{am}^4\beta_n^l-2\lambda_{am}^2\bar{\beta}_n^l+\bar{\bar{\beta}}_n^l\big)c_m^l+(\alpha_m^l\lambda_{bn}^4-2\lambda_{bn}^2\bar{\alpha}_m^l+\bar{\bar{\alpha}}_m^l)d_n^l\big]-\frac{\rho h\omega^2}{D}[A_{mn}+\sum_{l=1}^{4}[\beta_n^l c_m^l+\alpha_m^l d_n^l]]=0 \tag{3.27}$$

where $m=0,1,\dots,M-1$, and $n=0,1,\dots,N-1$. It can be further written in a matrix form as

$$\big(\tilde{\mathbf{K}}\mathbf{a}+\mathbf{B}\mathbf{p}\big)-\frac{\rho h\omega^2}{D}\big(\tilde{\mathbf{M}}\mathbf{a}+\mathbf{F}\mathbf{p}\big)=\mathbf{0} \tag{3.28}$$

Equations. (3.25) and (3.28) cannot be directly combined to form a characteristic equation about the coefficient vectors **a** and **p** because the assembled mass matrix will become singular. By following the approach traditionally used for determining an eigenvalue, one may first solve Eq. (3.28) for **a** in terms of **p**. Substituting the result into the boundary conditions, Eq. (3.25), will lead to a set of homogeneous equations. The eigenvalues can then be obtained as the roots of a nonlinear function which is defined as the determinant of the coefficient matrix. Such an approach is numerically not preferable because of the well known difficulties and concerns associated with solving a highly nonlinear equation. Instead, Eq. (3.25) will be here used to eliminate the vector **p** from Eq. (3.28), resulting in

$$\left[\mathbf{K} - \frac{\rho h \omega^2}{D}\mathbf{M}\right]\boldsymbol{a} = \mathbf{0} \tag{3.29}$$

where $\mathbf{K} = \widetilde{\mathbf{K}} + \mathbf{B}\mathbf{H}^{-1}\mathbf{Q}$, and $\mathbf{M} = \widetilde{\mathbf{M}} + \mathbf{F}\mathbf{H}^{-1}\mathbf{Q}$

Equation (3.29) represents a standard characteristic equation from which all the eigenpairs can be determined. Once the eigenvector **a** is determined for a given eigenvalue, the corresponding vector **p** can be calculated directly using Eq. (3.25). Subsequently, the mode shapes can be constructed by substituting **a** and **p** into Eq. (3.15). Detailed formulation can be found in a recently published paper (Li, etc, 2009)

Although this study is focused on free vibrations of an elastically restrained plate, the forced vibration can also be determined by simply adding a load vector to the right side of Eq. (3.29). It should be noted that the elements of the load vector represent the Fourier coefficients of the forcing function when it is expanded into a cosine series over the plate area.

3.4.2 Numerical Results

Several examples involving various boundary conditions will be given to show the superiority of current method. First, consider a C-S-S-F plate, in which C, S, F represent clamped, simply supported, and free edges, respectively. A clamped edge can be viewed as a special case when the stiffness constants for the (translational and rotational) springs become infinitely large (which is represented by a very large number, 5.0×10^7, in the actual calculations). The free-edge condition is easily created by setting the stiffness constants for both springs equal to zero. The displacement expansion is truncated to $M = N = 20$ in all the subsequent calculations. The frequency parameters $\Omega = \omega a^2\sqrt{\rho h/D}$ are listed in Tables 3.1.

The above examples are presented as the special cases of elastically restrained plates. It is shown that the frequency parameters for the classical homogeneous boundary conditions can be accurately determined by modifying the stiffness of the restraining springs. It should be emphasized that unlike most existing techniques, the current method offers a unified solution for a variety of boundary conditions including all the classical cases, and the modification of boundary conditions from one case to another is as simple as changing the material properties or the plate dimensions.

Table 3.1. Frequency parameters $\Omega = \omega a^2\sqrt{\rho h/D}$ for C-S-S-F rectangular plate with different aspect ratios (* Li, 2004; † FEM with 300×300 elements).

r=a/b	$\Omega = \omega a^2\sqrt{\rho h/D}$					
	1	2	3	4	5	6
1.0	16.785	31.115	51.392	64.016	67.549	101.21
	16.87 *	31.14	51.64	64.03	67.64	101.2
	16.790†	31.110	51.393	64.017	67.534	101.10
1.5	18.463	50.409	53.453	88.682	107.65	126.05
2.0	20.577	56.265	77.316	110.69	117.24	175.77
	22.997	59.705	111.90	114.54	153.06	188.54
2.5	23.07 *	59.97	111.9	115.1	153.1	189.6
	23.003 †	59.723	111.90	114.58	153.06	188.60
3.0	25.628	63.672	119.11	154.20	193.38	196.24
3.5	28.399	68.063	124.31	199.00	204.21	246.85
4.0	31.274	72.795	130.07	205.32	261.95	299.44

Next, consider a square plate elastically supported along all of its edges. The stiffnesses for the transverse and rotational restraints are chosen as $ka^3/D = 100$ and $Ka/D = 1000$, respectively. The frequency parameters are shown in Table 3.2 for plates with different aspect ratios from 1 to 4. Thus far, our attention has been focused on the frequency parameters for different boundary conditions and aspect ratios. As a matter of fact, the eigenpairs (eigenfrequencies and eigenvectors) are simultaneously obtained from the characteristic equation, Eq. (3.32). For a given eigenfrequency, the corresponding eigenvector actually contains the expansion coefficients, A_{mn}. In order to determine the mode

Table 3.2. Frequency parameters $\Omega = \omega a^2\sqrt{\rho h/D}$ for a square plate with $ka^3/D = 100$ and $Ka/D = 1000$ at $x = 0, a$ and $y = 0, b$, respectively († FEM with 300×300 elements).

	$\Omega = \omega a^2\sqrt{\rho h/D}$					
r=a/b	1	2	3	4	5	6
1.0	17.509	25.292	25.292	33.893	46.285	46.856
1.5	20.718	27.455	35.433	44.712	47.694	69.282
2.0	23.217	29.346	48.772	50.239	60.024	86.096
2.5	25.374	31.069	49.812	70.381	80.411	93.651
3.0	27.322	32.675	50.822	94.186	95.857	105.98
3.5	29.123	34.192	51.807	94.717	126.54	136.68
4.0	30.809	35.639	52.770	95.243	161.35	162.31

shape, the expansion coefficients for the 1-D Fourier series expansions also need to be calculated using Eq. (3.28). Once all the expansion coefficients are known, the mode shapes can be simply obtained from Eq. (3.15) in an analytical form. For example, plotted in Figure 3.2 are the mode shapes that correspond to the six frequencies given in the first row of Table 3.2. Because the stiffnesses of the restraining springs are sufficiently large, the characteristics of the rigid body motions are effectively eliminated. Although one can still see the traces of the modes for a completely clamped plate, the edges and corners now become quite alive in the current case.

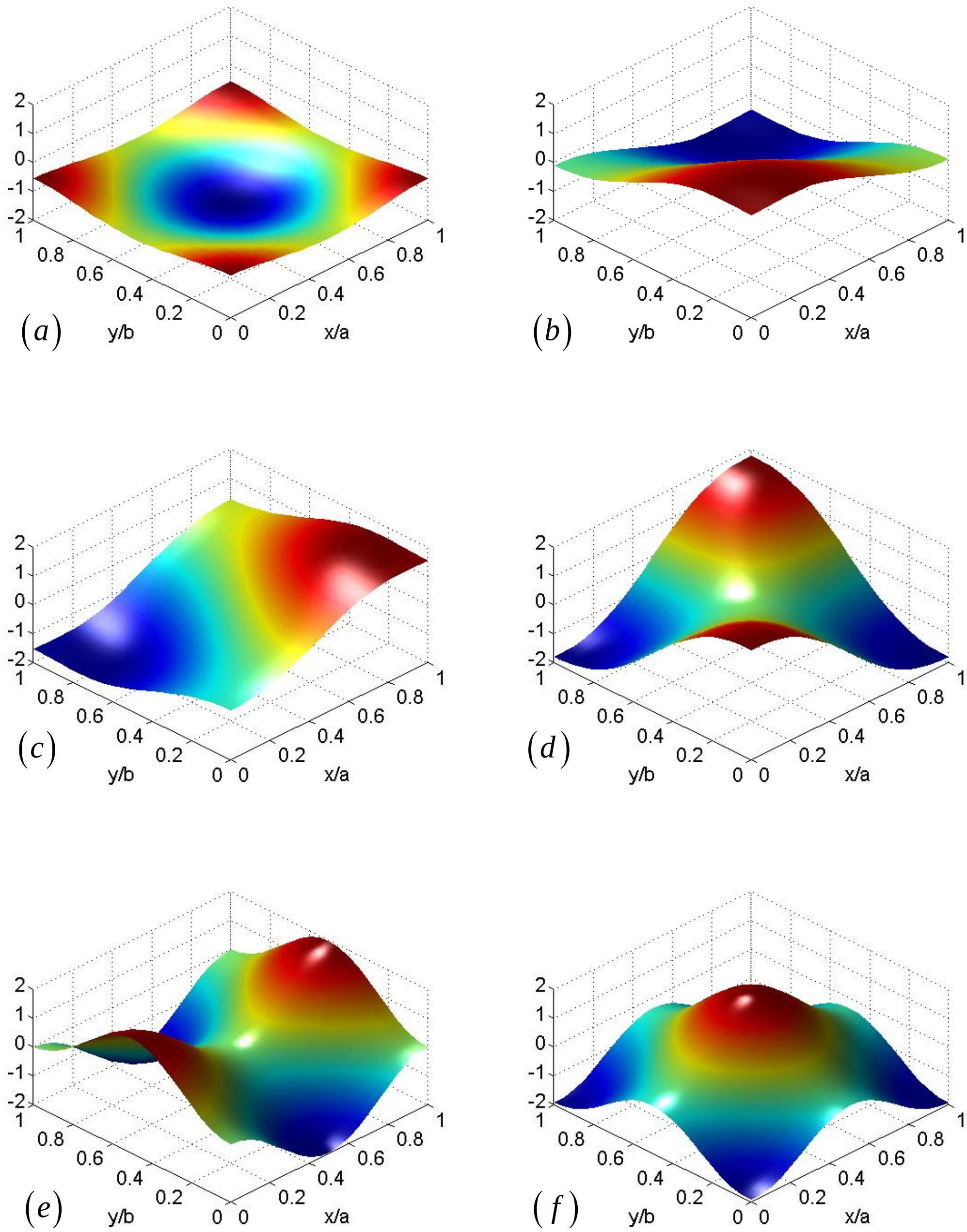

Figure 3.2. The (a) first, (b) second, (c) third, (d) fourth, (e) fifth, and (f) sixth mode shapes of a square plate with $ka^3/D = 100$ and $Ka/D = 1000$ at all four edges.

3.5 Variational Method

3.5.1 Theoretical Formulation

Rayleigh-Ritz method is used in finding an approximate solution from the Hamilton's equation

$$H(w) = T(w) - V(w) + W(w) \tag{3.30}$$

where $T(w)$ is the total kinetic energy, $V(w)$ is the total potential energy, and $W(w)$ is the input work by the excitation force $f(x, y)$.

For a purely bending plate, the total potential energy can be expressed as

$$V(w) = \frac{D}{2}\int_0^a \int_0^b \left[\left(\frac{\partial^2 w}{\partial x^2}\right)^2 + \left(\frac{\partial^2 w}{\partial y^2}\right)^2 + 2\mu \frac{\partial^2 w}{\partial x^2}\frac{\partial^2 w}{\partial y^2} + 2(1-\mu)\left(\frac{\partial^2 w}{\partial x \partial y}\right)^2\right] dxdy + \frac{1}{2}\int_0^b \left(k_{x0}w^2 + K_{x0}\left(\frac{\partial w}{\partial x}\right)^2\right)_{x=0} dy + \frac{1}{2}\int_0^b \left(k_{x1}w^2 + K_{x1}\left(\frac{\partial w}{\partial x}\right)^2\right)_{x=a} dy + \frac{1}{2}\int_0^a \left(k_{y0}w^2 + K_{y0}\left(\frac{\partial w}{\partial y}\right)^2\right)_{y=0} dx + \frac{1}{2}\int_0^a \left(k_{y1}w^2 + K_{y1}\left(\frac{\partial w}{\partial y}\right)^2\right)_{y=b} dx \tag{3.31}$$

the total kinetic energy is calculated from

$$T(w) = \frac{1}{2}\int_0^a \int_0^b \rho h \left(\frac{\partial w}{\partial t}\right)^2 dxdy \tag{3.32}$$

and the external work is calculated from

$$W(w) = \int_0^a \int_0^b f(x, y) w(x, y) dxdy \tag{3.33}$$

In Eq. (3.31), the first integral represents the strain energy due to the bending of the plate and the rest integrals represent the potential energies stored in the springs.

Hamilton' principle states that the true displacement field $w(x, y)$ of the plate renders the value of $H(w)$ stationary. The motion of the plate subject to Eqs. (3.1, 3.7-3.14) is found from the extremalization of the Hamiltonian of the plate over the chosen displacement function space.

$$\delta H(w) = 0 \tag{3.34}$$

Equations. (3.1, 3.7-3.14) can be derived by substituting Eqs. (3.30-3.33) into Eq. (3.34) and integrating by parts.

In Hamilton's principle, it is critical to choose an appropriate admissible function space in which the true displacement function exits. How efficient the method is depends on how fewer coefficients are needed to faithfully represent the true displacement function. When the admissible functions form a complete set, the Rayleigh-Ritz solution converges to the analytical solution obtained in strong form. In this study, the admissible function for the displacement is expressed as Eq. (3.15).

In what follows, our attention is directed to solving the Hamilton's Eq. (3.34). The displacement expression Eq. (3.34) is substituted into Eqs. (3.30-3.33) in determining the generalized coordinates (namely, the Fourier expansion coefficients). In the process, however, the stiffness functions and all other non-cosine terms have to be first expanded into Fourier cosine series, for instance, $k_{x0}(y) = \sum_{l=0}^{\infty} \tilde{k}_{x0,l} \cos(\lambda_{bl} y)$, $\xi_b^l(y) = \sum_{n=0}^{\infty} \tilde{\beta}_n^l \cos(\lambda_{bn} y)$.

The equations formed by taking partial derivative to A_{mn}were summarized as,

$$\sum_{m'=0}^{\infty} \sum_{n'=0}^{\infty} K_{mn,m'n'}^{11} A_{m'n'} + \sum_{j=1}^{4} \left[\sum_{m'=0}^{\infty} K_{mn,jm'}^{12} c_{m'}^{j} + \sum_{n'=0}^{\infty} K_{mn,jn'}^{13} d_{n'}^{j} \right] -$$
$$\rho h \omega^2 \Delta_m \Delta_n \left[A_{mn} + \sum_{j=1}^{4} \left[\tilde{\beta}_n^j c_m^j + \tilde{\alpha}_m^j d_{n'}^j \right] \right] = f_{mn} \tag{3.35}$$

Taking partial derivative respect to c_m^i (i=1, 2, 3, 4) results in,

$$\sum_{m'=0}^{\infty}\sum_{n'=0}^{\infty}K_{im,m'n'}^{21}A_{m'n'}+\sum_{j=1}^{4}\left[\sum_{m'=0}^{\infty}K_{im,jm'}^{22}c_{m'}^{j}+\sum_{n'=0}^{\infty}K_{im,jn'}^{23}d_{n'}^{j}\right]-$$

$$\rho h\omega^{2}\Delta_{m}\left[\sum_{n'=0}^{\infty}\left(A_{mn'}+\sum_{j=1}^{4}\left[\tilde{\alpha}_{m}^{j}d_{n'}^{j}\right]\right)\tilde{\beta}_{n}^{i}+\sum_{j=1}^{4}\left[\beta_{i,j}^{0,0}c_{m}^{j}\right]\right]=f_{am}^{i} \tag{3.36}$$

Taking partial derivative respect to d_n^j (i=1, 2, 3, 4) results in,

$$\sum_{m'=0}^{\infty}\sum_{n'=0}^{\infty}K_{in,m'n'}^{31}A_{m'n'}+\sum_{j=1}^{4}\left[\sum_{m'=0}^{\infty}K_{in,jm'}^{32}c_{m'}^{j}+\sum_{n'=0}^{\infty}K_{in,jn'}^{33}d_{n'}^{j}\right]-$$

$$\rho h\omega^{2}\Delta_{n}\left[\sum_{m'=0}^{\infty}\left(A_{mn'}+\sum_{j=1}^{4}\left[\tilde{\beta}_{n}^{j}c_{m'}^{j}\right]\right)\tilde{\alpha}_{m'}^{i}+\sum_{j=1}^{4}\left[\alpha_{i,j}^{0,0}d_{n}^{j}\right]\right]=f_{bn}^{i} \tag{3.37}$$

The series in Eqs. (3.35-3.37) are truncated to predetermined number M and N in x and y direction respectively, and are further written in matrix form,

$$\begin{bmatrix}K_{mn,m'n'}^{11} & K_{mn,jm'}^{12} & K_{mn,jn'}^{13}\\ K_{im,m'n'}^{21} & K_{im,jm'}^{22} & K_{im,jn'}^{23}\\ K_{in,m'n'}^{31} & K_{in,jm'}^{32} & K_{in,jn'}^{33}\end{bmatrix}\begin{bmatrix}A_{mn}\\ c_{m}^{i}\\ d_{n}^{i}\end{bmatrix}-\rho h\omega^{2}\begin{bmatrix}M_{mn,m'n'}^{11} & M_{mn,jm'}^{12} & M_{mn,jn'}^{13}\\ M_{im,m'n'}^{21} & M_{im,jm'}^{22} & M_{im,jn'}^{23}\\ M_{in,m'n'}^{31} & M_{in,jm'}^{32} & M_{in,jn'}^{33}\end{bmatrix}\begin{bmatrix}A_{mn}\\ c_{m}^{i}\\ d_{n}^{i}\end{bmatrix}=$$

$$\begin{bmatrix}f_{mn}\\ f_{am}^{i}\\ f_{bn}^{i}\end{bmatrix} \tag{3.38}$$

The full expression of the K^{ij}, M^{ij}, f_{mn}, f_{am}^i, f_{bn}^i in Eq. (3.38) and α_m^i, b_n^i, α_m^i, β_n^i, $\tilde{\alpha}_m^i$, $\tilde{\beta}_n^i$,$\alpha_{i,j}^{0,0}$, $\beta_{i,j}^{0,0}$ in Eqs. (3.35-3.37) are given in a recently published paper (Zhang & Li, 2009). A summarized version of the formulation can also be found in another recently published paper by the authors (Zhang & Li, 2010). Equation (3.38) is further written as

$$(\mathbf{K}-\rho h\omega^{2}\mathbf{M})\mathbf{a}=\mathbf{f} \tag{3.39}$$

where $\mathbf{a}=[A_{mn}\quad c_m^i\quad d_n^i]^T$ and$f=[f_{mn}\quad f_{am}^i\quad f_{bn}^i]^T$

For a given force, $\mathbf{f}\neq 0$, the response of plate can be directly solved from Eq. (3.39). When $\mathbf{f}=0$, Eq. (3.39) represents a standard matrix characteristic equation from which all the eigenpairs can be determined by solving a standard matrix eigenvalue problem. Once the generalized coordinates, **a**, is determined, the corresponding mode shape or displacement field can be constructed by substituting **a** into Eq. (3.15).

3.5.2 Numerical Results

Several examples involving plates with nonuniform elastic restraints are given in this section. First, let's consider a problem previously investigated by several researchers [Leissa, et al, 1979; Laura & Gutierrez, 1994; Shu & Wang, 1999; Zhao & Wei, 2002]. As shown in Figure 3.3, this problem involves a simply supported plate with rotational restraints of parabolically varying stiffness along two opposite edges (SESE). This is a special case of the general boundary condition Eqs. (3.7-3,14), when the stiffness functions are set to: $k_{x0}(y) = k_{xa}(y) = \infty$, $k_{y0}(x) = k_{yb}(x) = \infty$, and $K_{x0}(y) = K_{xa}(y) = 0$, and $K_{y0}(x) = K_{yb}(x) = K_c(1-x)D/a$.

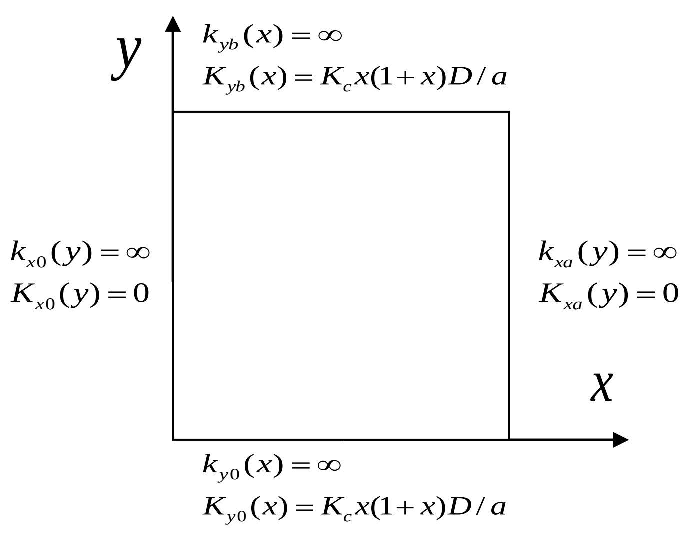

Figure 3.3 A simply supported plate with rotational springs of parabolically varying stiffness along two opposite edges, where K_c is a constant.

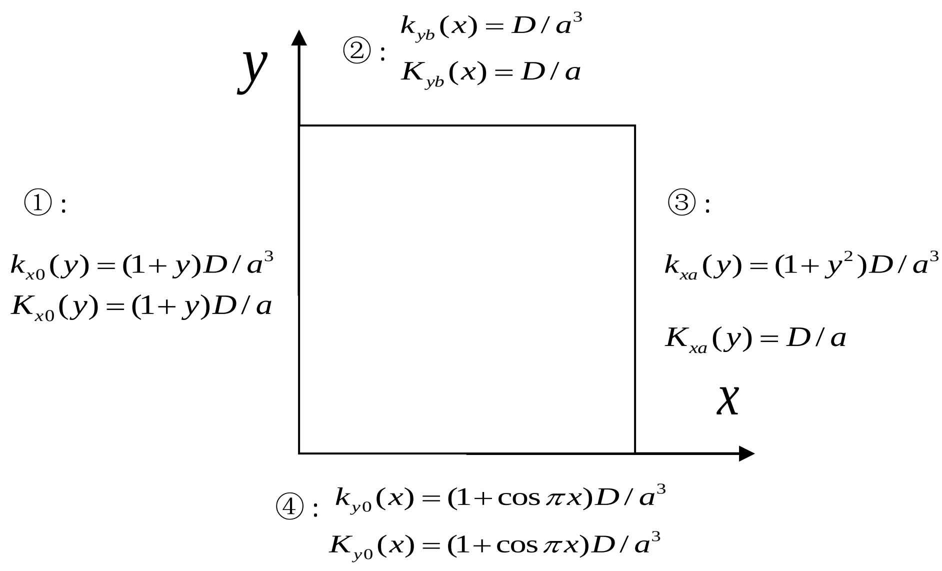

Figure 3.4. A rectangular plate with varying elastic edge supports including linear, parabolic, and harmonic functions.

where K_c is a constant. Another "classical" case is referred to as CECE where the two simply supported edges become fully clamped, namely, $K_{x0}(y) = K_{xa}(y) = \infty$

The fundamental frequencies calculated using various methods are shown in Table 3.3 for the SESE and CECE cases, respectively. It is noted that the current results compare well with those previously obtained from other different techniques. As mentioned earlier, the series expansion, Eq. (3.39), will has to be truncated in numerical calculations. It is chosen as $M = N = 10$ in all the subsequent calculations.

Although nonuniform restraints against rotations are allowed in the above examples, the transverse displacement is fully restrained along each edge. In many practical applications, however, both the translational and rotational restraints may have to be considered as elastic and their stiffnesses can vary from point to point on an edge. While the restraining of transverse displacement along each edge may be needed in the previous studies for whatever reasons, it is definitely unnecessary for the current method. When the displacement is not identically equal to zero along each edge, the frequency parameter, $\Omega = \omega a^2 \sqrt{\rho h / D}$, become dependent upon Poisson's ratio. For the simplicity, Poisson's ratio will be set as $\nu = 0.3$ in the following calculations.

TABLE 3.3. Frequency parameters $\Omega = \omega a^2 \sqrt{\rho h / D}$ for (a) SESE: Simply supported plate with rotational springs of parabolically varying stiffness along two opposite edges (b) CECE: Setup (a) with two simply supported edges clamped (a, Leissa, et al, 1979; b, Laura & Gutierrez, 1994; c, Shu & Wang, 1999; d, Zhao & Wei, 2002)

	SESE						CECE				
λ	K_c	a	b	c	d	current	a	b	c	d	current
0.5	0	12.337	12.34	12.337	12.337	12.349	23.814	23.82	23.816	23.816	23.816
	0.1	12.341	12.34	12.341	12.340	12.354	23.844	23.82	23.818	23.819	23.818
	1	12.372	12.38	12.379	12.362	12.391	23.876	23.85	23.839	23.843	23.839
	10	12.621	12.66	12.666	12.550	12.674	24.136	24.01	23.996	24.019	23.996
	100	13.319	13.37	13.364	13.207	13.366	24.561	24.41	24.393	24.410	24.393
	10^6	13.688	13.7	13.686	13.686	13.686	24.566	24.60	24.578	24.579	24.578
1	0	19.739	19.74	19.734	19.739	19.748	28.951	28.96	28.951	28.952	28.951
	0.1	19.757	19.76	19.761	19.764	19.770	28.969	28.98	28.966	28.970	28.966
	1	19.915	19.95	19.951	19.985	19.960	28.219	29.12	29.102	29.128	29.103
	10	21.235	21.49	21.487	21.701	21.493	32.179	30.24	30.222	30.383	30.222
	100	25.799	26.13	26.147	26.356	26.149	35.379	33.82	33.796	33.960	33.795
	10^6	28.951	28.98	28.951	28.951	28.950	35.992	36.01	35.985	35.987	35.985

In the current method, the stiffness for each restraining spring can be specified as an arbitrary function of spatial coordinates. Specifically, we consider the restraining scheme depicted in Figure 3.4 where the stiffness functions are "arbitrarily" selected as uniform, linear, parabolic and sinusoidal along the edges. As mentioned earlier, each of the stiffness function will be generally represented by a Fourier cosine series expansion. For convenience, the current restraining conditions at $x=0$, $y=b$, $x=a$ and $y=0$ will be labeled as ①, ②, ③ and ④, respectively. The first ten frequency parameters, $\Omega = \omega a^2\sqrt{\rho h/D}$, are presented in Tables 3.4 for plates of different aspect ratios, $r=b/a$, when they are subjected to the restraining condition ①+②+③+④. The FEM solution is shown in Table 3.4 as a reference. In the FEM model, each edge is divided into 100 elements, which is considered adequately fine to capture the spatial variations of these lower order modes. The current results match well with those obtained from the FEM model.

Table 3.4. Frequency parameters $\Omega = \omega a^2\sqrt{\rho h/D}$ for rectangular plates with boundary condition described in Figure 3.4 († Finite Element Method with 100×100 elements).

r=a/b	Ω_1	Ω_2	Ω_3	Ω_4	Ω_5	Ω_6	Ω_7	Ω_8	Ω_9	Ω_{10}
1	2.17	5.14	5.71	15.00	24.17	27.14	37.17	37.53	64.56	65.48
	†2.18	5.09	5.78	14.98	24.17	27.16	37.12	37.50	64.57	65.49
1.5	2.39	5.75	8.78	22.12	25.77	48.46	54.76	63.22	70.21	89.07
2	2.58	5.84	13.24	25.75	29.82	60.68	64.53	94.94	104.3	110.1
2.5	2.76	5.93	18.36	25.73	37.97	64.46	73.60	121.0	122.1	148.0
4	3.23	6.18	25.68	36.85	64.16	64.96	114.7	122.1	175.9	199.6

Thus far, our attention has been focused on the frequency parameters for different boundary conditions and aspect ratios. As a matter of fact, in the current solution the eigenpairs (eigenfrequencies and eigenvectors) are simultaneously obtained from the characteristic equation, Eq. (3.39). For a given eigenfrequency, the corresponding eigenvector actually contains the expansion coefficients, A_{mn}, c_m, and d_n from which the mode shape can be readily calculated from Eq. (3.15) in an analytical form. For example, plotted in Figure 3.5 are the first eight mode shapes for a plate of aspect ratio r = 2 under the boundary condition of ①+②+③+④. For conciseness, the FEM mode shapes will not be presented here; it suffices to say that the modes in Figure 3.5 have all been validated by the FEM model.

3.6 Conclustions

An analytical method has been developed for the vibration analysis of rectangular plates with arbitrary elastic edge restraints of varying stiffness distributions. The displacement function is generally expressed as a standard two-dimensional Fourier cosine series supplemented by several one-dimensional Fourier series expansions that are introduced to ensure the availability and uniform convergence of the series representation for any boundary conditions. Unlike the existing techniques such as DQ and DSC methods, the current method offers a unified solution to a wide class of plate problems and does not require any special procedures or schemes in dealing with different boundary conditions. Both translational and rotational restraints can be generally specified along any edge, and an arbitrary stiffness distribution is universally described in terms of a set of invariants, cosine functions. While this treatment is very useful and effective for a continuously-distributed restraint, it may not be suitable for a discretely or partially restrained edge because of the possible slow convergence or overshoots of the series representation at or near a discontinuity point. This problem, however, can be easily resolved by substituting the given (discontinuous) stiffness functions into Eq. (3.31) directly and carrying out the integrations analytically or numerically. The method was first applied to several “classical” cases which were previously investigated by using various techniques.

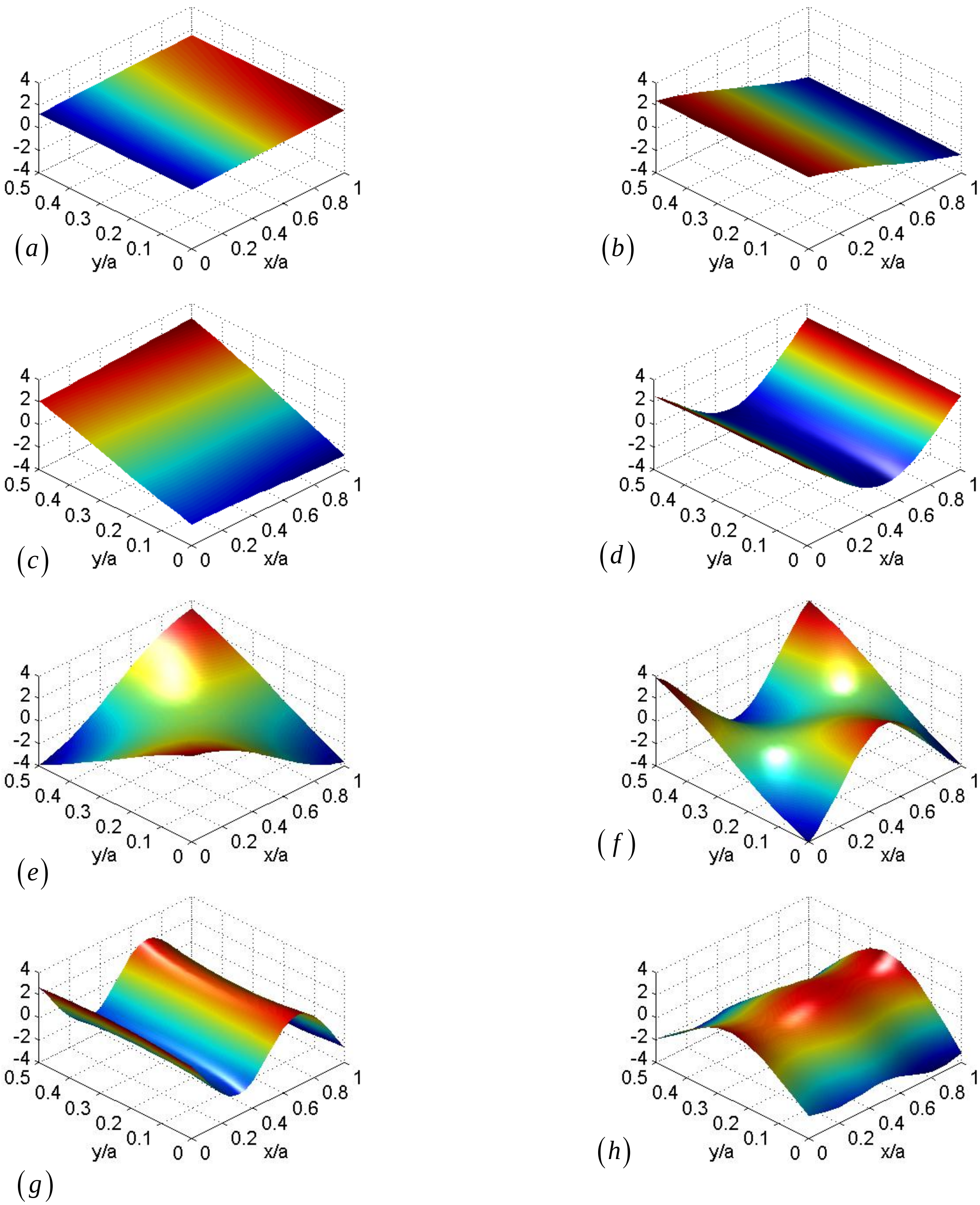

Figure 3.5. The (a) first, (b) second, (c) third, (d) fourth, (e) fifth, (f) sixth, (g) seventh and (h) eighth mode shapes for a plate with aspect ratio $r = 2$ and boundary condition described in Figure 3.4.

It is also used to solve a class of more difficult problems in which the displacement is no longer completely restrained in the translational direction. The accuracy and reliability of the current method are repeatedly demonstrated through all these examples, as evidenced by a good comparison with the existing or FEA results. Finally, it should be mentioned that although the current solution is sought in a weak form from the Rayleigh-Ritz procedure, it is mathematically equivalent to what would be obtained from the strong formulation because the constructed displacement function is sufficiently smooth over the entire solution domain. The adoption of a weak formulation may become far more advantageous when the vibration of a plate structure is attempted.

Chapter IV Vibration of general triangular plates with elastic boundary supports

4.1 Triangular plate vibration description

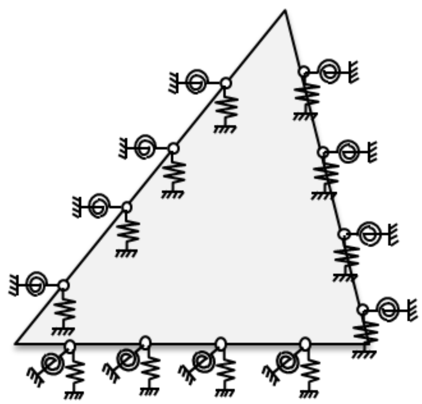

Figure 4.1. A general triangular plate with elastically restrained edges.

Figure 4.1 shows an isotropic triangular plate with its edges elastically restrained against both translation and rotation. The effects of damping, rotational inertia, and transverse shear deformation are all neglected here for simplicity of presentation. The vibration of the plate is governed by the following differential equation

$$\mathrm{D}\nabla^4 w(x,y) - \rho h\omega^2 w(x,y) = f(x,y) \tag{4.1}$$

where $\nabla^4 = \frac{\partial^4}{\partial x^4} + 2\frac{\partial^4}{\partial x^2 \partial y^2} + \frac{\partial^4}{\partial y^4}$; $w(x,y)$ is the flexural displacement; ω is the angular frequency; $f(x,y)$ is the distributed harmonic excitation acting on the plate surface; and D, ρ, and h are the bending rigidity, the mass density, and the thickness of the plate, respectively. The governing equation given here is exactly the same as Eq. (3.1) except that the domain is changed to a triangular region.

The boundary conditions along the elastically restrained edges can be specified as

$$k_i w = Q_i,\ K_i \frac{\partial w}{\partial n} = M_i \qquad (i = 1, 2, 3) \qquad (4.2, 4.3)$$

where k_i (K_i) is the stiffness function of the translational (rotational) elastic restraints on the i^{th} edge, and Q_i, M_i are the shear force and bending moment at the i^{th} edge, respectively. The stiffness for each elastic restraint is also allowed to vary along the edges. Thus, Eqs. (4.2, 4.3) represent a general set of boundary conditions from which any of the classical homogeneous boundary conditions (free, simply supported, clamped and guided) can be simply specified as a special case when the stiffness for each of the elastic restraints is set equal to either zero or infinity.

4.2 Literature review on the transverse vibration of triangular plates

Triangular plates are important structural elements since any polygon plate can be analyzed as a combination of triangular plates. The vibration of triangular plates has been extensively studied in the past years [Leissa, 1993]; however, its solvability is limited because the triangular domain cannot be described by two variables with independent constant bounds. The first quick method is to map the triangular domain onto a rectangular domain by a coordinate transformation [Karunasena et al., 1996, 1997]. Then, the problem can be solved by directly adopting the methods used in analyzing the vibration of rectangular plates. The drawback of this seemingly easy method is that singularity is introduced in the mapping process. Another method is to extend the triangular domain into a quadrilateral domain by adding one extremely thin layer on it, and the problem is solved as a quadrilateral plate with variable thickness [Huang, et al., 2001; Sakiyama, et al.,2003]. This method gives approximate frequency results since the mass and spring matrices are only slightly modified by the extending thin layer. However, care must be taken that the mode shapes adjacent to the extended edge are more distorted than the remaining area. The third method is to map the general triangular domain onto a right angled isosceles domain [Singh & Saxena, 1996; Singh & Hassan, 1998]. This process is more stable since it is normally a linear transformation. The transformed domain is largely simplified, although it is still a triangle.

An analytical solution is not available for the vibration of the triangular plates. A trial series from a certain functional is usually chosen to approximate the solution [Leissa, 1993]. The critical step is to identify which trial functional to use. First of all, the functional must be complete to approximate all the possible mode shapes at different frequencies. Second, the functional must satisfy all the boundary conditions either individually or collectively. Whereas excessive functionals cause slow convergence, incomplete functional leads to solutions with missed frequencies. One of the extensively used methods is to approximate the displacement by the product of a complete series and a given function that satisfies all the geometric boundary conditions, and the product is then used as the trial function in the vibration analysis, The geometric boundary conditions are thus satisfied by each individual function in the series. Since the original functional is diluted, the convergence speed of the solution is accordingly improved. However, the method is complicated to use in real calculations since different boundary conditions are to be satisfied by different functions. It should also be pointed out that the natural boundary conditions are completely ignored in this method. Since the stresses in the plate are obtained by high order derivatives of the mode shapes, which are not calculated with enough accuracy, no meaningful results are reported in the literature. Another method is to choose a polynomial function that satisfies all the geometric boundary conditions, and the remaining functions are generated by the Gram-Schmidt orthogonalization procedure [Bhat, 1987; Lam, et al., 1990; Singh & Chakraverty, 1992]. Once the functional is chosen, the next step is to determine the unknown coefficients in the approximation series. The Weighted residual method and the Rayleigh-Ritz method are both used in the literature. The Rayleigh-Ritz method is more frequently used since it is closely related to the least square method and produces symmetric stiffness and mass matrices.

Furthermore, Leissa and Jaber [1992] used two dimensional simple polynomials as the trial function in studying the vibration of free triangular plates with the Rayleigh-Ritz method, and the best possible frequency solutions are carefully chosen to avoid the ill-conditioning of the matrices. Huang et al. [2005] used a complete series plus some special functions in dealing with the singularities at the corners. Other methods used in analyzing the triangular plate vibration are the Superposition method [Saliba, 1996], the Finite Element method [Haldar & Sengupta, 2003], and the Differential Quadrature method [Chen and Cheung, 1998].

Most of the relevant literature found on the vibration of triangular plates is on plate with classical boundary conditions, which rarely exist in practice. Although boundaries with elastic restraints are more inclusive, little attention has been paid to this research subject. The only paper found in the literature is the research done by Nallim et al. [2005]. The orthogonal polynomials in their trial function are so constructed that the first member of the series satisfies all the geometrical boundary conditions. For an elastically restrained edge, however, the geometric and natural boundary conditions are mixed and cannot be satisfied separately. It is not easy to decide which polynomial in their method to choose for an elastically restrained edge ranging from free to clamped boundary conditions. It is concluded that a more simple and efficient method is still needed for the vibration of triangular plates with elastically restrained edges.

The primary focus of the current chapter is to introduce a trial function that satisfies all the boundary conditions of a triangular plate with elastically restrained edges. Several single series are specially designed and added into an already complete double series. Similar methods have been successfully applied to the vibration analysis of both beams [Li & Daniels, 2002] and rectangular plates [Li, et al., 2009; Zhang & Li, 2009]. It should be stressed that although the functional is denser than a general complete series, the convergence speed is actually improved by the added single series. Furthermore, the same set of functions could be used for all the general boundary conditions, which makes the method very attractive in real applications. Since the boundary conditions are all satisfied and the convergence speed is greatly improved, the high order derivative values including the bending moments and shear forces can be calculated by directly differentiating the obtained displacement solution. The general triangular plate is first mapped onto a right angled isosceles triangular plate. The unknown coefficients in the trial function are determined by the Rayleigh-Ritz method, and the resulting matrices are all analytically evaluated. Some numeral examples are given to test the completeness and convergence speed of the method.

4.3 Variational formulation using the Rayleigh-Ritz method

A variational formulation is used in providing a solution for the current problem. The response of the plate subject to arbitrary forcing function $f(x,y)$ is obtained by extremalizing the Hamiltonian of the plate under a suitable subspace,

$$\delta H(w) = \delta \int_{t_0}^{t_1} \left(T\left(\frac{\partial w}{\partial t}\right) - V(w) + W(w) \right) dt = 0 \tag{4.4}$$

where $T\left(\frac{\partial w}{\partial t}\right)$ is the total kinetic energy, $V(w)$ is the total potential energy, and $W(w)$ is the work done by the excitation force.

For a purely bending plate, the total potential energy can be expressed as

$$V = \frac{D}{2}\iint_{A'}\left[\left(\frac{\partial^2 w}{\partial x'^2}\right)^2 + \left(\frac{\partial^2 w}{\partial y'^2}\right)^2 + 2\mu\frac{\partial^2 w}{\partial x'^2}\frac{\partial^2 w}{\partial y'^2} + 2(1-\mu)\left(\frac{\partial^2 w}{\partial x'\partial y'}\right)^2\right]dx'dy'$$

$$+\frac{1}{2}\sum_{i=1}^{3}\int_0^{l_i}\left(k_i w^2 + K_i\left(\frac{\partial w}{\partial n_i}\right)^2\right)dl_i \tag{4.5}$$

where A' represents the original triangular domain; l_i represents the i^{th} edge, and μ is the Poisson's ratio of the plate material. The first integral represents the strain energy due to the bending of the plate and the rest integrals represent the potential energy stored in the restraining springs.

The total kinetic energy and the external work are calculated from

$$T = \frac{1}{2}\iint_{A'}\rho h\left(\frac{\partial w}{\partial t}\right)^2 dx'dy' \tag{4.6}$$

and

$$W = \iint_{A'} f(x',y')w(x',y')\,dx'dy' \tag{4.7}$$

4.3. Coordinate transformation

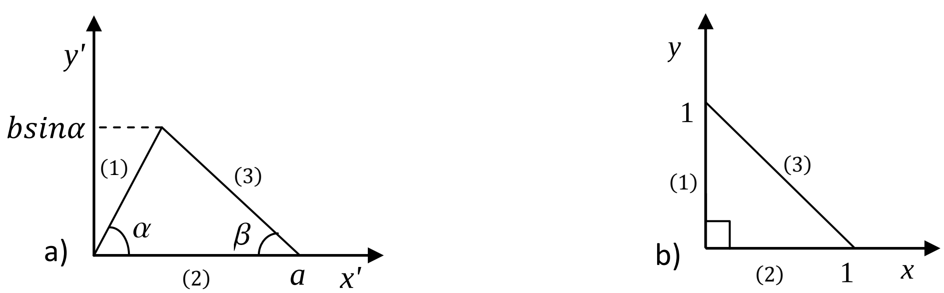

Figure 4.2.A triangular plate before (a) and after (b) coordinator transformation

The geometric information of the triangular plate can be described by the length a and b of two edges and the apex angle α between them. In assisting the integral calculation, the irregular triangular domain (Figure 4.2a) is mapped onto a right-angled isosceles triangular domain (Figure 4.2b) by using the following coordinate transformation,

$$\begin{cases} x' = ax + bycos\alpha \\ y' = bysin\alpha \end{cases} \tag{4.8}$$

Then the relation of the first and second derivatives between the original and transformed coordinates could be written as follows,

$$\begin{bmatrix} \frac{\partial w}{\partial x'} \\ \frac{\partial w}{\partial y'} \end{bmatrix} = \begin{bmatrix} 1/a & 0 \\ -\cot\alpha/a & 1/(bsin\alpha) \end{bmatrix} \begin{bmatrix} \frac{\partial w}{\partial x} \\ \frac{\partial w}{\partial y} \end{bmatrix} \tag{4.9}$$

which is further written as $\mathfrak{D}_\mathbf{1}\mathbf{w}' = \boldsymbol{\mathcal{T}}\mathfrak{D}_\mathbf{1}\mathbf{w}$.

$$\begin{bmatrix} \frac{\partial^2 w}{\partial x'^2} \\ \frac{\partial^2 w}{\partial y'^2} \\ \frac{\partial^2 w}{\partial x' \partial y'} \end{bmatrix} = \begin{bmatrix} 1/a^2 & 0 & 0 \\ \cot^2\alpha/a^2 & 1/(bsin\alpha)^2 & -2\cot\alpha/(absin\alpha) \\ -\cot\alpha/a^2 & 0 & 1/(absin\alpha) \end{bmatrix} \begin{bmatrix} \frac{\partial^2 w}{\partial x^2} \\ \frac{\partial^2 w}{\partial y^2} \\ \frac{\partial^2 w}{\partial x \partial y} \end{bmatrix} \tag{4.10}$$

which is further written as $\mathfrak{D}_\mathbf{2}\mathbf{w}' = \overline{\boldsymbol{\mathcal{T}}}\mathfrak{D}_\mathbf{2}\mathbf{w}$.

$$\frac{\partial w}{\partial n_i} = \mathbf{n}_i \boldsymbol{\mathcal{T}}\mathfrak{D}_\mathbf{1}\mathbf{w} \quad (i = 1, 2, 3) \tag{4.11}$$

where $\mathbf{n}_1 = [-\sin\alpha \quad \cos\alpha]$, $\mathbf{n}_2 = [0 \quad 1]$, and $\mathbf{n}_3 = [\sin\beta \quad \cos\beta]$ are the normal derivatives of the three corresponding edges.

The total potential energy can be further expressed as

$$V = \frac{D}{2}\iint_A \left[\left(\left(\overline{\boldsymbol{\mathcal{T}}}_{\langle 1\rangle}\right)^T \boldsymbol{\mathfrak{D}}_{\mathbf{2}}\mathbf{w}\right)^2 + \left(\left(\overline{\boldsymbol{\mathcal{T}}}_{\langle 2\rangle}\right)^T \boldsymbol{\mathfrak{D}}_{\mathbf{2}}\mathbf{w}\right)^2 + 2\mu\left(\overline{\boldsymbol{\mathcal{T}}}_{\langle 1\rangle}\right)^T \boldsymbol{\mathfrak{D}}_{\mathbf{2}}\mathbf{w}\left(\overline{\boldsymbol{\mathcal{T}}}_{\langle 2\rangle}\right)^T \boldsymbol{\mathfrak{D}}_{\mathbf{2}}\mathbf{w} + 2(1 - \mu)\left(\left(\overline{\boldsymbol{\mathcal{T}}}_{\langle 3\rangle}\right)^T \boldsymbol{\mathfrak{D}}_{\mathbf{2}}\mathbf{w}\right)^2\right] J_0\, dxdy + \frac{1}{2}\int_0^1 (k_1 w^2 + K_1(\mathbf{n}_1\boldsymbol{\mathcal{T}}\boldsymbol{\mathfrak{D}}_{\mathbf{1}}\mathbf{w})^2)|_{x=0} J_1 dx + \frac{1}{2}\int_0^1 (k_2 w^2 + K_2(\mathbf{n}_2\boldsymbol{\mathcal{T}}\boldsymbol{\mathfrak{D}}_{\mathbf{1}}\mathbf{w})^2)|_{y=0} J_2 dy + \frac{1}{2}\int_0^1 (k_3 w^2 + K_3(\mathbf{n}_3\boldsymbol{\mathcal{T}}\boldsymbol{\mathfrak{D}}_{\mathbf{1}}\mathbf{w})^2)|_{x=(1-y)} J_3 dy \tag{4.12}$$

where A represents the transformed right-angled unit isosceles triangular area. $\overline{\boldsymbol{\mathcal{T}}}_{\langle i\rangle}$ is the i_{th} row of the transformation matrix $\overline{\boldsymbol{\mathcal{T}}}$; $J_0 = absin\alpha$ is the Jacobian of the transformation on the area, $J_1 = b,\ J_2 = a$ and $J_3 = \sqrt{a^2 + b^2 - 2abcos\alpha}$ are the Jacobians of the transformations along the three edges.

The total kinetic energy and the external work are further written as

$$T = \frac{1}{2}\iint_A \rho h \left(\frac{\partial w}{\partial t}\right)^2 J_0 dxdy \tag{4.13}$$

and

$$W = \iint_A f(x,y) w(x,y) J_0 dxdy \tag{4.14}$$

Replacing the transformed potential energy Eq. (4.12) into the Hamiltonian Eq. (4.4), one get

$$\delta V = \iint_A (\boldsymbol{\mathfrak{D}}_{\mathbf{2}}\mathbf{w})^{\boldsymbol{T}} \mathbb{T}\delta(\boldsymbol{\mathfrak{D}}_{\mathbf{2}}\mathbf{w}) J_0 dxdy + \int_0^1 \left(k_1 w\delta(w) + K_1 \boldsymbol{\mathfrak{D}}_{\mathbf{1}}\mathbf{w}\mathbb{N}_{\mathbf{1}}\delta(\boldsymbol{\mathfrak{D}}_{\mathbf{1}}\mathbf{w})\right)\Big|_{x=0} J_1 dx + \frac{1}{2}\int_0^1 \left(k_2 w\delta(w) + K_2 \boldsymbol{\mathfrak{D}}_{\mathbf{1}}\mathbf{w}\mathbb{N}_{\mathbf{2}}\delta(\boldsymbol{\mathfrak{D}}_{\mathbf{1}}\mathbf{w})\right)\Big|_{y=0} J_2 dy + \frac{1}{2}\int_0^1 \left(\left(k_3 w\delta(w) + K_3 \boldsymbol{\mathfrak{D}}_{\mathbf{1}}\mathbf{w}\mathbb{N}_{\mathbf{3}}\delta(\boldsymbol{\mathfrak{D}}_{\mathbf{1}}\mathbf{w})\right)\right)\Big|_{x=(1-y)} J_3 dy \tag{4.15}$$

where $\mathbb{T} = \mathrm{D}\left[\left(\boldsymbol{\mathcal{T}}_{\langle 1\rangle}\right)^{\mathrm{T}}\left(\boldsymbol{\mathcal{T}}_{\langle 1\rangle} + \mu\boldsymbol{\mathcal{T}}_{\langle 2\rangle}\right) + \left(\boldsymbol{\mathcal{T}}_{\langle 2\rangle}\right)^{\mathrm{T}}\left(\boldsymbol{\mathcal{T}}_{\langle 2\rangle} + \mu\boldsymbol{\mathcal{T}}_{\langle 1\rangle}\right) + 2(1-\mu)\left(\boldsymbol{\mathcal{T}}_{\langle 3\rangle}\right)^{\mathrm{T}}\boldsymbol{\mathcal{T}}_{\langle 3\rangle}\right]$, and

$\mathbb{N}_i = (\mathbf{n}_i\boldsymbol{\mathcal{T}})^T \mathbf{n}_i\boldsymbol{\mathcal{T}} \quad (i = 1, 2, 3)$.

$$\delta T = \rho h \omega^2 J_0 \iint_A w \delta w \, dxdy \tag{4.16}$$

$$\delta W = J_0 \iint_A f \delta w \, dxdy \tag{4.17}$$

4.4. Displacement function and resultant matrix equation

Since an analytical result is not available, a trial function is used along with the Rayleigh-Ritz method. When the displacement field is periodically extended onto the whole x-y plane, as implied by the Fourier approximation, discontinuities may exist along the edges for the flexibility of the boundaries. To assure uniform convergence of the solution, the discontinuity along each of the edges is transformed to some sets of single Fourier series. The displacement function for the transformed unit right-angled isosceles triangular area is chosen as,

$$w(x,y) = \sum_{m=0}^{\infty} \sum_{n=0}^{\infty} A_{mn} \cos(m\pi x) \cos(n\pi y)$$

$$+ \sum_{j=1}^{2} \xi_j(y) \sum_{m=0}^{\infty} c_{jm} \cos(m\pi x) + \sum_{j=1}^{2} \xi_j(x) \sum_{n=0}^{\infty} d_{jn} \cos(n\pi y)$$

$$+ \sum_{j=1}^{3} (1-x-y)^j \sum_{m=0}^{\infty} e_{jm} \left(\cos(m\pi x) + (-1)^m \cos(m\pi y)\right) \tag{4.18}$$

where

$$\xi_1(x) = \frac{9}{4\pi} sin\left(\frac{\pi x}{2}\right) - \frac{1}{12\pi} sin\left(\frac{3\pi x}{2}\right), \; \xi_2(x) = \frac{1}{\pi^3} sin\left(\frac{\pi x}{2}\right) - \frac{1}{3\pi^3} sin\left(\frac{3\pi x}{2}\right)$$

It is easy to verify that $\xi_1'(0) = \xi_2'''(0) = 1$. Each of the two terms accounts for the potential discontinuity of the original function or its derivatives along one of the edges $x = 0$ (the same for $y = 0$). The third single series $(1-x-y)^j$ is similarly designed for the hypotenuse, i.e. $\frac{\partial^j (1-x-y)^j}{\partial n^j} = 1$. To simplify the formulation, the normal derivative of the series associated with e_{jm} against the hypotenuse is also set to zero. Therefore, the double series only represents a residual displacement function that is continuous and has at least three continuous derivatives over the entire x-y plane. Because the smoother a periodic function is, the faster its Fourier series converges, the current displacement function quickly converges to the analytical vibration solution of a triangular plate with given elastic boundary conditions.

When the displacement function in Eq. (4.18) and its derivatives are substituted into the Energy Eqs. (4.15)-(4.17) and then the Hamiltonian Eq. (4.4), the following system of linear equations is obtained,

$$\begin{bmatrix} \mathbf{K}^{11} & \mathbf{K}^{12} & \mathbf{K}^{13} & \mathbf{K}^{14} \\ \mathbf{K}^{21} & \mathbf{K}^{22} & \mathbf{K}^{23} & \mathbf{K}^{24} \\ \mathbf{K}^{31} & \mathbf{K}^{32} & \mathbf{K}^{33} & \mathbf{K}^{34} \\ \mathbf{K}^{41} & \mathbf{K}^{42} & \mathbf{K}^{43} & \mathbf{K}^{44} \end{bmatrix} \begin{bmatrix} \mathbf{A} \\ \mathbf{c} \\ \mathbf{d} \\ \mathbf{e} \end{bmatrix} - \rho h \omega^2 \begin{bmatrix} \mathbf{M}^{11} & \mathbf{M}^{12} & \mathbf{M}^{13} & \mathbf{M}^{14} \\ \mathbf{M}^{21} & \mathbf{M}^{22} & \mathbf{M}^{23} & \mathbf{M}^{24} \\ \mathbf{M}^{31} & \mathbf{M}^{32} & \mathbf{M}^{33} & \mathbf{M}^{34} \\ \mathbf{M}^{41} & \mathbf{M}^{42} & \mathbf{M}^{43} & \mathbf{M}^{44} \end{bmatrix} \begin{bmatrix} \mathbf{A} \\ \mathbf{c} \\ \mathbf{d} \\ \mathbf{e} \end{bmatrix} = \begin{bmatrix} \boldsymbol{f}_A \\ \boldsymbol{f}_c \\ \boldsymbol{f}_d \\ \boldsymbol{f}_e \end{bmatrix} \tag{4.19}$$

where $\mathbf{A} = [A_{00}, A_{01}, \dots, A_{M1}, A_{10}, \dots, A_{MN}]$, $\mathbf{c} = [c_{10}, c_{11}, \dots, c_{1M}, c_{20}, \dots, c_{2M}]$,

$\mathbf{d} = [d_{10}, d_{11}, \dots, d_{1N}, d_{20}, \dots, d_{2N}]$, and $\mathbf{e} = [e_{10}, e_{11}, \dots, e_{1M}, e_{20}, \dots, e_{3M}]$. More detailed information on $\boldsymbol{K}^{ij}$ and $\boldsymbol{M}^{ij}$ is given in the Appendix and can be found in reference (Zhang & Li, 2011).

Eq. (4.19) could be further written as,

$$\mathbf{K}\widetilde{\mathbf{A}} - \rho h \omega^2 \mathbf{M}\widetilde{\mathbf{A}} = \mathbf{f} \tag{4.20}$$

For a given excitation $\mathbf{f} \neq \mathbf{0}$, all the unknown expansion coefficients in the response function of the plate can be directly solved from Eq. (4.20). By setting $\mathbf{f} = \mathbf{0}$, Eq. (4.20) simply represents a characteristic equation from which all the eigenpairs can be readily determined by solving a standard eigenvalue problem.

4.5 Vibration of anisotropic triangular plates

The vibration formulations of the anisotropic triangular plates are essentially the same as those of the isotropic plates except the potential energy of the plate is expressed as

$$V = \frac{1}{2}\iint_{A'}\left[D_{11}\left(\frac{\partial^2 w}{\partial x'^2}\right)^2 + 2D_{12}\frac{\partial^2 w}{\partial x'^2}\frac{\partial^2 w}{\partial y'^2} + D_{22}\left(\frac{\partial^2 w}{\partial y'^2}\right)^2 + 4\left(D_{16}\frac{\partial^2 w}{\partial x'^2} + D_{26}\frac{\partial^2 w}{\partial y'^2}^2\right)\frac{\partial^2 w}{\partial x'\partial y'} + 4D_{66}\left(\frac{\partial^2 w}{\partial x'\partial y'}\right)^2\right]dx'dy' \tag{4.21}$$

where the rigidities D_{ij}s are given by the following formulations,

$D_{11} = \frac{\mathrm{h}^3}{12}(Q_{11}\cos^4\beta + 2(Q_{12} + 2Q_{66})\sin^2\beta\cos^2\beta + Q_{22}\sin^4\beta)$,

$D_{12} = \frac{\mathrm{h}^3}{12}((Q_{11} + Q_{22} - 4Q_{66})\sin^2\beta\cos^2\beta + Q_{12}(\cos^4\beta + \sin^4\beta))$,

$D_{22} = \frac{\mathrm{h}^3}{12}(Q_{11}\sin^4\beta + 2(Q_{12} + 2Q_{66})\sin^2\beta\cos^2\beta + Q_{22}\cos^4\beta)$,

$D_{16} = \frac{\mathrm{h}^3}{12}((Q_{11} - Q_{12} - 2Q_{66})\cos^3\beta\sin\beta + (Q_{12} - Q_{22} + 2Q_{66})\sin^3\beta\cos\beta)$,

$D_{26} = \frac{\mathrm{h}^3}{12}((Q_{11} - Q_{12} - 2Q_{66})\sin^3\beta\cos\beta + (Q_{12} - Q_{22} + 2Q_{66})\cos^3\beta\sin\beta)$,

$D_{66} = \frac{\mathrm{h}^3}{12}((Q_{11} + Q_{22} - 2Q_{12} - 2Q_{66})\sin^2\beta\cos^2\beta + Q_{66}(\cos^4\beta + \sin^4\beta))$,

$Q_{11} = \mathrm{E}_1/(1 - \nu_{12}\nu_{21})$, $Q_{22} = \mathrm{E}_2/(1 - \nu_{12}\nu_{21})$,

$Q_{12} = \nu_{12}\mathrm{E}_2/(1 - \nu_{12}\nu_{21}) = \nu_{21}\mathrm{E}_1/(1 - \nu_{12}\nu_{21})$, and $Q_{66} = G_{12}$,

where E_1, E_2 are the elastic modulus of the plate in the two principal directions, and β is the angle between the first principal direction and the x-axis of the original coordinate; ν_{12}, ν_{21} are the Poisson's ratios, and G_{12} is the shear modulus.

Almost all the steps used in solving the vibration of isotropic plates are applicable to those of anisotropic plates. The only change is that the $\mathbb{T}$ matrix in Eq. (4.15) is redefined as,

$$\mathbb{T} = \left(\boldsymbol{\mathcal{T}}_{\langle 1\rangle}\right)^{\mathrm{T}}\left(D_{11}\boldsymbol{\mathcal{T}}_{\langle 1\rangle} + D_{12}\boldsymbol{\mathcal{T}}_{\langle 2\rangle} + 2D_{16}\boldsymbol{\mathcal{T}}_{\langle 3\rangle}\right) + \left(\boldsymbol{\mathcal{T}}_{\langle 2\rangle}\right)^{\mathrm{T}}\left(D_{12}\boldsymbol{\mathcal{T}}_{\langle 1\rangle} + D_{22}\boldsymbol{\mathcal{T}}_{\langle 2\rangle} + 2D_{26}\boldsymbol{\mathcal{T}}_{\langle 3\rangle}\right) + 2\left(\boldsymbol{\mathcal{T}}_{\langle 3\rangle}\right)^{\mathrm{T}}\left(D_{16}\boldsymbol{\mathcal{T}}_{\langle 1\rangle} + D_{26}\boldsymbol{\mathcal{T}}_{\langle 2\rangle} + 2D_{66}\boldsymbol{\mathcal{T}}_{\langle 3\rangle}\right) \tag{4.22}$$

4.6 Numerical results and discussions

To test the completeness, convergence speed, and applicability of the described method, the results of some representative triangular plates with various boundary conditions are compared with those available in the literature. The geometry of the plate is completely defined by the length of two neighboring edges (a and b) and the angle α between them. The truncation term in all the series is set as M=N=10. The Poisson's ratio is chosen as $\nu = 0.3$ in all results on isotropic plates. The elastic constants k_i and K_i of the translational and rotational elastic restraints are normalized by the flexible rigidity of the plate material and the length of the corresponding edge, i.e., $k_i {l_i}^3/D = k = const$ and $K_i l_i/D = K = const$. The infinite spring constant in classical boundary conditions is represented by the number 10^8.

4.6.1 Convergence test on a free equilateral triangular plate

Although plenty of results are reported on the triangular plate vibration with other classical boundary conditions, few results are found for plates with free boundary conditions [Leissa & Jaber, 1992], which then stand as an interesting example to test the convergence speed of the current method. Table 4.1 lists the first several non-dimensional parameters $\Omega = \omega a^2\sqrt{\rho h/D}$ of an equilateral triangular plate with free boundary conditions obtained with different truncation numbers in the series. The Poisson's ratio is chosen as $\nu = 0.3$. Most of the results found in the literature fall among the current results with different truncation numbers. Among them those results reported by Leissa and Jaber [1992] are very close to current results with large truncation numbers, and their results are obtained with a series specially designed for triangular plates with free boundary conditions. It is observed that the current results converge at a faster speed. Based on the convergence property of the current method, all the following results are calculated with M=N=10.

Table 4.1. The first seven non-dimensional frequency parameters $\Omega = \omega a^2\sqrt{\rho h/D}$ of a free equilateral plate obtained with different truncation numbers ($\upsilon = 0.3$). (#: Lessia & Jaber, 1992; ##: Liew, 1993; †: Singh & Hassan, 1998; ‡: Nallim, et al., 2005)

M=	4	5	6	7	8	9	10	Ref. #	Ref.##	Ref. †	Ref. ‡
Ω1	34.28	34.28	34.27	34.27	34.27	34.27	34.27	34.27	34.38	34.28	34.285
Ω2	36.07	36.06	36.06	36.06	36.06	36.06	36.06	36.06	36.06	36.28	36.068
Ω3	36.08	36.06	36.06	36.06	36.06	36.06	36.06	36.06	36.16	36.33	36.066
Ω4	84.83	84.69	84.68	84.68	84.68	84.68	84.68	84.68	84.68		
Ω5	84.87	84.70	84.69	84.68	84.68	84.68	84.68	84.68	85.33		
Ω6	92.11	92.01	91.96	91.95	91.95	91.95	91.95	91.95	91.95		
Ω7	117.0	116.3	116.2	116.2	116.2	116.2	116.2				

4.6.2 Vibration of triangular plates with classical boundary conditions

Table 4.2 lists the first three non-dimensional frequency parameters $\Omega = \omega a^2\sqrt{\rho h/D}$ for isosceles triangular plates with ten classical boundary conditions. Three different apex angles are chosen as $\alpha = 60$, 90, and 120. C, S, F are used to represent classical boundary conditions, e.g., SCF means simply supported on edge 1, clamped on edge 2, and free on edge 3. Finite Element results are also included for the cases with $\alpha = 120$ since larger differences are found for some of the high order modes than the cases with $\alpha = 60$ and 90.

Table 4.2. The first three non-dimensional frequency parameters $\Omega = \omega a^2\sqrt{\rho h/D}$ for isosceles triangular plates with three different apex angles and ten classical boundary conditions along with those results found in literature. †: Singh & Hassan, 1998; ‡: Nallim, et al., 2005; * : Bhat, 1987; # : Finite Element Method with 3,000 elements.

α	60			90			120		
Source	Ω1	Ω2	Ω3	Ω1	Ω2	Ω3	Ω1	Ω2	Ω3
CCC	99.023	189.02	189.04	93.790	157.79	194.77	140.16	207.50	267.20
	†99.02	189.01	189.01	93.79	157.79	194.82	140.17	207.83	272.22
	‡99.020	189.01	189.01	93.791	157.83	195.00	#139.90	207.18	266.48
CCS	81.601	164.99	165.32	73.394	131.58	165.00	105.21	165.32	218.75
	†81.601	164.99	165.32	73.395	131.58	165.05	105.26	165.72	223.54
	‡81.601	164.99	165.32	73.397	131.63	165.49	#105.09	165.16	218.35
CCF	40.047	95.872	101.83	29.095	63.567	89.882	34.637	66.495	99.205
	†40.016	95.827	101.79	29.093	63.567	89.866	34.641	66.498	99.863
	‡40.018	95.838	101.80	29.093	63.571	90.133	#34.630	66.490	99.165
SCF	26.562	75.316	84.353	17.967	47.950	73.626	18.924	46.785	75.581
	†26.561	75.314	84.35	17.976	47.949	73.629	18.951	46.791	75.941
	‡26.560	75.313	84.349	17.967	47.950	73.629	#18.905	46.782	75.563
SSC	66.177	142.74	143.48	65.790	121.08	154.45	100.58	158.91	212.23
	†66.177	142.74	143.48	65.791	121.09	154.61	100.77	159.28	219.54
	‡66.177	142.79	143.50				#99.546	157.76	210.43
SSS	52.639	122.82	122.82	49.348	98.696	128.30	71.929	122.82	169.93
	†52.638	122.82	122.82	49.348	98.7	128.43	72.121	123.23	176.39
	‡52.63	122.83	122.84				#71.675	122.77	169.67
FSF	22.646	26.659	69.397	14.561	24.737	42.026	11.365	27.097	41.835
	†22.646	26.659	69.418	14.561	24.738	42.039	11.38	27.175	41.995
	‡22.647	26.659	69.404				#11.362	27.091	41.828

FSS	16.092	57.630	68.330	17.316	51.035	72.966	24.255	59.936	95.038
	†16.092	57.63	68.33	17.316	51.036	72.982	24.327	59.999	95.398
	‡16.092	57.630	68.33				#24.235	59.933	95.007
FCF	8.9205	35.090	38.484	6.1637	23.457	32.663	5.6959	21.477	35.993
	†8.9210	35.095	38.484	6.1670	23.458	32.682	5.7010	21.501	36.269
	*8.9221	35.132	38.505	6.1732	23.414	32.716	5.7171	21.526	37.455
	‡8.9166	35.094	38.483				#5.6899	21.457	35.950
FFF	34.279	36.062	36.062	19.068	29.123	45.397	13.431	25.189	46.086
	†34.284	36.281	36.332	19.077	29.191	45.62	13.434	25.22	46.639
	‡34.281	36.064	36.065				#13.431	25.190	46.090

4.6.3 Vibration of triangular plates with elastically restrained boundary conditions

Table 4.3 lists the first ten non-dimensional frequency parameters $\Omega = \omega a^2\sqrt{\rho h/D}$ for a right-angled isosceles triangular plate with evenly spread elastic boundary constraints. The rotational spring K and linear spring k are varied in such a way that the plate boundary conditions go from FFF to SSS, and to CCC. The infinite number is represented by a very large number, i.e., 10^8. Current results agree well with those found in the literature [Kim, 1990; Leissa & Jaber, 1992] and those calculated with finely meshed Finite Element Method.

Table 4.3. The first ten non-dimensional frequency parameters $\Omega = \omega a^2\sqrt{\rho h/D}$ for an right-angled isosceles triangular plate with evenly spread elastic boundary constraints. K represents rotational spring and k represents linear spring. Infinite number is taken as 10^8. †: Kim & Dickinson, 1990; ‡: Leissa & Jaber, 1992; #: Finite Element Method with 3,359 elements.

	Ω1	Ω2	Ω3	Ω4	Ω5	Ω6	Ω7	Ω8	Ω9	Ω10
FFF	0	0	0	19.068	29.123	45.397	49.475	72.350	84.052	99.939
				†19.080	29.250	46.030	49.650	73.680	85.970	
				‡19 068	29.123	45.398	49.476	72.367	84.091	
$k=10^{-2}$, ,K=0	0.2151	0.3162	0.3221	19.071	29.125	45.399	49.476	72.350	84.053	99.939
$k=10^{-1}$, ,K=0	0.6797	0.9998	1.0184	19.102	29.147	45.414	49.488	72.359	84.062	99.945
k=1,K=0	2.1337	3.1564	3.2182	19.410	29.364	45.567	49.606	61.129	72.449	84.155
k=10, ,K=0	6.3389	9.8189	10.111	22.327	31.439	47.061	50.792	73.348	85.075	100.62
$k=10^{2}$, ,K=0	16.122	27.202	30.064	40.847	46.600	59.707	62.425	82.290	93.674	106.75
	#16.141	27.296	30.400	41.304	47.004	60.444	63.018	83.329	94.027	107.05
$k=10^{3}$, ,K=0	35.803	58.496	69.775	86.908	97.059	114.16	119.54	136.28	146.73	158.15
$k=10^{4}$, ,K=0	47.291	90.916	115.91	145.83	168.77	199.88	203.64	208.81	228.97	259.95
SSS	49.348	98.696	128.30	167.79	197.39	246.74	256.61	286.22	335.57	365.20
	†49.350	98.760	128.40	169.10	200.30	249.80				
$K=10^{-2}$, $k=10^{8}$	49.378	98.726	128.33	167.81	197.42	246.77	256.64	286.25	335.60	365.22
$K=10^{-1}$, $k=10^{8}$	49.646	98.994	128.60	168.08	197.69	247.04	256.91	286.53	335.87	365.49
K=1, $k=10^{8}$	52.131	101.54	131.17	170.67	200.28	249.64	259.52	289.11	338.48	368.10
K=10, $k=10^{8}$	66.626	118.21	148.66	189.10	219.05	269.05	279.16	309.10	358.69	388.73
$K=10^{2}$, $k=10^{8}$	87.448	147.49	182.21	227.47	260.33	315.13	326.20	358.87	411.64	444.30
$K=10^{3}$, $k=10^{8}$	93.029	156.48	193.14	240.73	275.30	332.86	344.34	378.65	433.86	467.89
$K=10^{4}$, $k=10^{8}$	93.691	157.59	194.51	242.42	277.23	335.20	346.75	381.30	436.89	471.15
CCC	93.766	157.71	194.67	242.62	277.46	335.47	347.03	381.62	437.26	471.55
	†93.790	157.80	194.80	243.10	278.20	336.30				

4.6.4 Vibration of anisotropic triangular plates

The method is then applied to an orthotropic right-angled cantilever triangular plate (FCF). The plate is made of carbon/epoxy composite material with the following material properties [Kim & Hong, 1988]: $\mathrm{E}_1 = 229\mathrm{GPa}$, $\mathrm{E}_2 = 13.4\mathrm{GPa}$, $\nu_{12} = 0.315$, and $G_{12} = 5.25\mathrm{GPa}$. $\beta = 90°$ is used to agree with the setup in the ref. [Nallim, et al., 2005]. Table 4.4 listed the first eight non-dimensional frequency parameters $\Omega = \omega a^2\sqrt{\rho h/D_0}$ along with those of Nallim et al [2005], and Kim and Dickinson [1990]. D_0 is defined as $D_0 = \mathrm{E}_1\mathrm{h}^3/12(1-\nu_{12}\nu_{21})$.

Table 4.4. The first eight non-dimensional frequency parameters $\Omega = \omega a^2\sqrt{\rho h/D_0}$ of an orthotropic right-angled cantilever triangular plate (FCF). The plate is made of carbon/epoxy composite material ($\beta = 90°$) with following material properties: $\mathrm{E}_1 = 229\mathrm{GPa}$, $\mathrm{E}_2 = 13.4\mathrm{GPa}$, $\nu_{12} = 0.315$, and $G_{12} = 5.25\mathrm{GPa}$. †: Kim & Dickinson, 1990; ‡: Nallim, et al., 2005.

b/a	Ω1	Ω2	Ω3	Ω4	Ω5	Ω6	Ω7	Ω8
1/3	23.6754	89.4748	130.222	231.597	316.94	441.197	503.05	606.82
	† 23.68	89.47	130.2	231.7	317.1	444.5	-	-
	‡23.6763	89.4695	130.219	231.596	317.051	441.966	506.012	614.757
1/2.5	22.948	81.861	123.651	214.978	295.822	385.13	449.929	546.656
	† 22.95	81.86	123.7	215	296.2	387.7	-	-
	‡22.9486	81.8557	123.648	214.987	295.971	386.676	451.631	556.032
1/2	22.0617	72.3317	117.122	191.578	262.183	325.734	403.386	452.889
	† 22.06	72.34	117.1	191.7	263.2	327.5	-	-
	‡22.0622	72.3326	117.125	191.606	262.589	327.511	404.302	466.37
1/1.5	20.9671	60.6675	110.24	156.043	210.946	292.66	315.431	353.502
	† 20.97	60.67	110.3	156.2	211.8	294	-	-
	‡20.9674	60.6674	110.249	156.097	211.363	295.571	319.255	370.871

1	19.5691	46.9946	97.0025	112.684	157.792	200.499	245.756	279.578
	† 19.57	47	97.12	113.1	158.1	201.1	-	-
	‡19.5694	46.9954	97.141	112.9	159.198	205.563	264.355	294.432
1.5	18.3704	37.0553	68.5394	101.211	108.011	145.966	165.998	200.34
	† 18.37	37.06	68.55	101.6	108.4	147.8	-	-
	‡18.3712	37.0727	68.7113	102.34	114.767	156.485	180.852	235.89
2	17.6458	31.9099	53.549	78.814	99.9765	108.448	138.459	148.446
	† 17.65	31.91	53.59	79.83	100.6	113.7	-	-
	‡17.648	31.9297	54.6002	85.6955	100.443	134.046	147.991	207.21
2.5	17.1539	28.7661	45.0686	63.7816	85.2004	98.2941	109.379	132.775
	† 17.16	28.77	45.22	65.41	93.14	99.14	-	-
	‡17.1571	28.8573	46.7145	69.2801	98.3726	122.602	137.191	192.978
3	16.7939	26.6391	39.6706	54.3677	70.9871	89.5571	96.9944	111.301
	† 16.78	26.65	39.97	56.54	81.82	97.59	-	-
	‡16.8013	26.8304	41.0884	61.3023	97.0716	114.903	131.315	182.076

Comparisons are also made with an anisotropic isosceles triangular plate with evenly spread elastic boundary constraints. The geometric parameters are $\mathrm{a} = 1$, $\mathrm{b} = 1/(2\cos 75°)$, and $\alpha = 75°$. The material properties are chosen to agree with those reported by Nallim et al [2005], i.e. $\mathrm{E}_1 = 207\mathrm{GPa}$, $\mathrm{E}_2 = 21\mathrm{GPa}$, $\nu_{12} = 0.3$, and $G_{12} = 7\mathrm{GPa}$. The angle β in the current paper is complementary to the one reported in Nallim's paper. Table 4.5 listed the first eight non-dimensional frequency parameters $\Omega = \omega a^2\sqrt{\rho h/D_0}$ for $\beta = 0°,$ and $30°$. It is observed that the current results agree with those in the literature, but the difference increases with the decrease of the elastic constants k and K.

Table 4.5. The first six non-dimensional frequency parameters $\Omega = \omega a^2\sqrt{\rho h/D_0}$ of an anisotropic isosceles triangular plate with evenly spread elastic boundary constraints. The geometric parameters are $\mathrm{a} = 1$, $\mathrm{b} = 1/(2\cos 75°)$, and $\alpha = 75°$. The material properties are $\mathrm{E}_1 = 207\mathrm{GPa}$, $\mathrm{E}_2 = 21\mathrm{GPa}$, $\nu_{12} = 0.3$, and $G_{12} = 7\mathrm{GPa}$. ‡ Nallim, et al., 2005

β=0 °	Ω1	Ω2	Ω3	Ω4	Ω5	Ω6	‡ Ω1	‡ Ω2	‡ Ω3
K		$k=10^8$							
0	18.203	28.616	40.571	54.235	57.578	69.667	18.242	29.157	43.264
1	20.468	30.880	42.910	56.640	60.330	72.129	20.196	31.230	45.584
10	27.257	38.582	51.433	65.884	69.556	82.091	27.371	39.669	56.794
50	33.752	46.619	60.964	76.871	80.615	94.866	34.098	48.309	72.146
100	35.532	48.956	63.884	80.433	84.253	99.457	35.899	50.879	77.789
10^8	37.909	52.158	67.996	86.079	89.964	108.50	37.911	53.191	74.466
K		k=100							
0	6.675	9.208	11.794	12.574	15.765	17.166	6.868	9.151	11.866
1	7.172	9.676	13.128	13.631	17.681	18.715	7.154	9.245	11.995
10	7.481	10.210	13.933	17.664	18.605	24.257	7.472	9.513	12.403
50	7.595	10.467	14.324	19.169	19.619	25.133	7.591	9.685	12.684
100	7.619	10.522	14.404	19.298	19.981	25.352	7.615	9.723	12.746
10^8	7.662	10.616	14.540	19.495	20.582	25.657	7.672	9.810	12.856
K		k=50							
0	4.985	7.185	8.811	10.366	12.647	14.521	5.114	6.905	8.610
1	5.425	7.647	10.829	11.147	14.856	16.068	5.324	6.974	9.470
10	5.689	8.175	11.509	15.420	15.694	21.091	5.525	7.215	9.963
50	5.797	8.403	11.869	16.320	17.178	22.166	5.605	7.364	10.226
100	5.819	8.446	11.945	16.465	17.489	22.430	5.621	7.394	10.279
10^8	5.860	8.522	12.068	16.656	17.929	22.760	5.657	7.437	10.346
K		k=10							
0	2.514	4.220	4.629	6.513	8.331	9.602	2.497	3.476	3.967
1	2.887	4.499	6.724	7.384	10.166	11.938	2.577	3.696	5.829
10	3.085	4.864	7.402	10.774	11.604	17.836	2.701	4.580	9.324
50	3.141	5.047	7.846	12.283	12.567	19.387	2.691	4.088	7.111
100	3.150	5.082	7.938	12.571	12.778	19.744	2.698	4.110	7.205
10^8	3.168	5.129	8.045	12.904	13.044	20.224	2.706	4.139	7.318
K		k=1							

0	0.970	1.751	1.783	3.341	5.803	6.957			
1	1.155	1.976	4.260	4.704	8.452	10.593			
10	1.201	2.455	5.548	8.461	10.478	17.110			
50	1.211	2.686	6.208	10.195	11.635	18.797			
100	1.212	2.729	6.338	10.528	11.879	19.180			
10^8	1.215	2.777	6.499	10.929	12.196	19.702			
K		k=0							
0	0.000	0.000	0.000	2.620	5.401	6.650			
1	0.000	1.189	3.892	4.189	8.257	10.448			
10	0.000	1.915	5.327	8.136	10.356	17.031			
50	0.000	2.203	6.024	9.919	11.535	18.734			
100	0.000	2.254	6.159	10.260	11.783	19.119			
10^8	0.000	2.314	6.329	10.674	12.109	19.645			
β=30 °	Ω1	Ω2	Ω3	Ω4	Ω5	Ω6	‡ Ω1	‡ Ω2	‡ Ω3
K		k=10^8							
0	17.909	28.630	40.942	53.348	57.649	69.637	17.922	28.966	43.322
1	19.907	30.839	43.264	55.533	60.001	71.999	19.715	31.013	45.736
10	26.493	38.577	51.987	64.579	69.614	82.029	26.449	39.587	56.504
50	31.546	45.076	59.887	73.510	79.055	92.403	31.752	47.199	67.167
100	32.770	46.745	62.016	76.034	81.751	95.455	33.038	49.166	70.229
10^8	34.302	48.888	64.813	79.456	85.463	99.690	34.315	49.116	67.989
K		k=100							
0	6.794	9.376	12.381	13.132	16.868	18.169	6.872	9.240	11.779
1	7.237	9.845	13.234	14.481	17.947	20.467	7.122	9.349	12.148
10	7.551	10.355	14.130	17.326	19.151	24.125	7.458	9.549	12.565
50	7.652	10.578	14.497	18.397	19.843	25.103	7.581	9.657	12.785
100	7.672	10.627	14.570	18.573	19.993	25.297	7.581	9.657	12.785
10^8	7.703	10.698	14.682	18.849	20.200	25.591	7.639	9.730	12.974
K		k=50							
0	5.066	7.277	9.470	10.536	14.054	15.037	5.130	6.954	8.652
1	5.469	7.739	10.847	11.750	15.007	17.577	5.313	7.044	9.517
10	5.730	8.253	11.610	14.658	15.986	20.984	5.515	7.223	10.066
50	5.830	8.465	11.920	15.664	16.681	22.069	5.591	7.323	10.290
100	5.851	8.506	11.981	15.831	16.836	22.305	5.606	7.344	10.333

10^8	5.882	8.565	12.070	16.086	17.030	22.601	5.627	7.377	10.426
K		k=10							
0	2.533	4.210	4.968	6.497	9.448	9.655	2.505	3.476	3.974
1	2.885	4.503	6.701	7.363	10.113	13.467	2.574	3.701	5.833
10	3.092	4.819	7.319	10.265	11.628	17.626	0.000	0.000	0.000
50	3.155	4.955	7.686	11.441	12.617	19.219	2.644	3.936	6.603
100	3.166	4.980	7.759	11.661	12.836	19.556	2.673	4.023	6.996
10^8	3.181	5.011	7.845	11.947	13.113	19.962	2.681	4.068	7.185
K		k=1							
0	0.968	1.770	1.782	3.253	6.746	7.117			
1	1.149	1.927	4.140	4.901	8.304	12.167			
10	1.199	2.315	5.388	8.423	10.446	16.847			
50	1.210	2.492	5.991	9.813	11.633	18.598			
100	1.212	2.524	6.105	10.081	11.885	18.962			
10^8	1.214	2.559	6.236	10.421	12.204	19.406			
K		k=0							
0	0.000	0.000	0.000	2.490	6.415	6.778			
1	0.000	1.094	3.747	4.486	8.097	12.017			
10	0.000	1.736	5.152	8.176	10.317	16.761			
50	0.000	1.974	5.796	9.603	11.528	18.530			
100	0.000	2.016	5.040	5.916	9.877	11.783			
10^8	0.000	2.062	6.055	10.228	12.101	19.345			

4.6.5 Mode shapes

Once the natural frequencies are obtained, the corresponding eigenvectors quickly determine the mode shapes under the given frequencies. Figure 4.3 gives the first three mode shapes of triangular plates with different geometries and boundary conditions. a1-a6 in Figure 4.3 are the first six modes of a free equilateral triangular plate as described in Section 3.1. b1-b6 in Figure 4.3 are the first six mode shapes of a right-angled isosceles triangular plate with elastic boundary constraints $k = 10$ and $K = 100$ as described in Section 3.3. c1-c6 in Figure 4.3 are the first six mode shapes of an anisotropic plate with $\beta = 30°$ and elastic boundary constraints

$k = 100$ and $K = 50$ as described in Section 3.4. The mode shapes are checked and agree with those available in the literature.

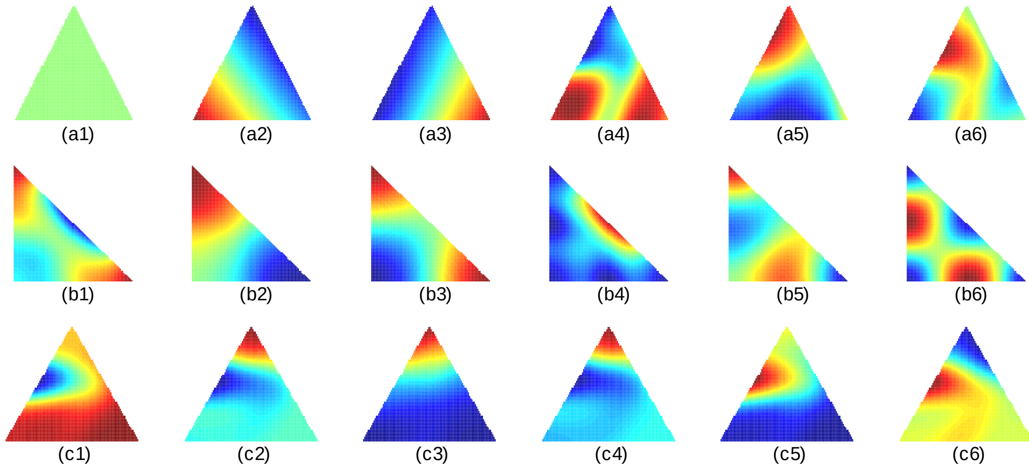

Figure 4.3. The first six mode shapes of a free equilateral triangular plate as described in Section 4.6.1 (a1-a6), a right-angled isosceles triangular plate with elastic boundary constraints $k = 10$ and $K = 100$ as described in Section 4.6.3 (b1-b6), and an anisotropic plate with $\beta = 30°$ and elastic boundary constraints $k = 100$ and $K = 50$ as described in Section 4.6.4 (c1-c6).

4.7 Conclusions

The applicability and convergence of a method in solving the vibration of triangular plates depend largely on how and to what extend the actual displacement can be faithfully represented by the chosen displacement function. A general triangular plate is first mapped onto a right-angled unit isosceles triangular plate. Then a displacement function is introduced that collectively satisfies all the boundary conditions of a triangular plate with elastically restrained edges. Several single series are specially designed and added into the already complete double series in the displacement function. The trial functional is denser than a normal complete series and the convergence speed is improved by the added single series. Furthermore, the same set of functions is used for all the boundary conditions, which makes the method very attractive in real applications. Since the boundary conditions are all satisfied and the convergence speed is improved, the high order derivative values including the bending moments and the shear forces can be directly calculated by differentiating the obtained displacement solution. The unknown coefficients in the trial functions are determined by the Rayleigh-Ritz method, and the resulting matrix elements are all analytically evaluated. Numerical examples are tested on general isotropic and anisotropic triangular plates with a variety of classical and elastic boundary conditions. The completeness of the current method as well as its fast convergence are verified by all the collected results.

The current method should also be applicable to plates with other more complicated geometries and material properties, such as plates with variable thickness, plates with shear deformation and rotary inertia effects, etc.

Chapter V Vibration of build-up structure composed of triangular plates, rectangular plates, and beams

5.1 Structure vibration description

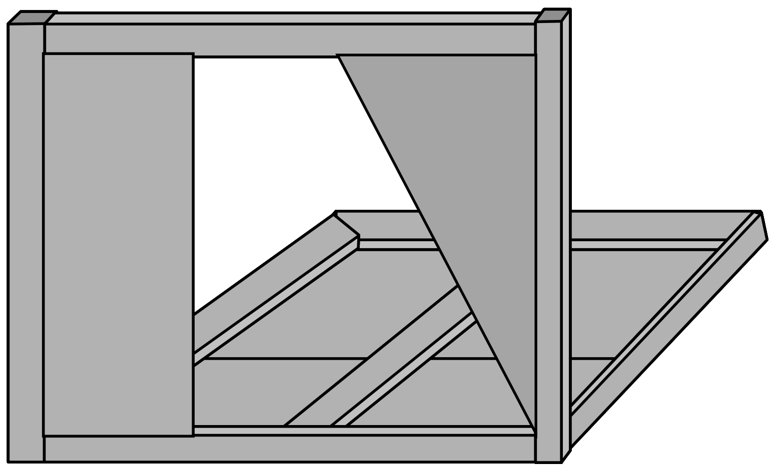

Figure 5.1 A general structure composed of triangular plates, rectangular plates and beams

Studied in this chapter are complex industrial structures consist of an arbitrary number of triangular plates, rectangular plates, and beams (Figure 5.1). The coupling among the plates and beams are modeled by a combination of linear and rotational springs, which can account for any coupling ranging from free to rigid connection. While the coupling location between a beam and plate can be on the boundary or interior of the plate, two plates are only coupled along their edges, The same apply to two beams, which are only coupled at their end points to ensure fast convergence of the solution.

5.2 Literature review

With increasing customer demands and stricter fuel efficiency regulation, the auto industry generated a steadily increasing interest in optimizing the mechanical structure of and thus reducing the weight of the vehicle. Noise and vibration attributes of the vehicle make up one of the major part of the heavy investment. The natural frequencies of the vehicle shift toward higher frequency range when the vehicle becomes more roomy and lighter. An accurate and computation efficient algorism in mid-frequency noise and vibration prediction is still in need despite the stride improvement of FEA method and modern computation power.

A structure shows different characteristics at three different frequency ranges. At low frequencies, where only a few modes dominate the response of a structure, deterministic FEA method is the golden tool for vibration analysis. But as the frequency increase, the element size has to be reduced to capture the small wave length. Furthermore, the structure is more sensitive to structure variations such as material property variation, manufacture tolerance, modeling approximation, etc. At high frequencies, where the model density is so high that only statistically averaged response is possible, SEA method is the appropriate tool to use. However, there is still a wide mid-frequency range that is more sensitive to human ear and strongly correlated with the product quality. In this frequency range, the computational requirement is prohibitively large for FEA method, while the basic assumption of the SEA method is not yet fulfilled. Furthermore, complex structure may have some components exhibit high-frequency behavior while others show low-frequency behavior. At this critical frequency range, no mature prediction technique is available at the moment although a vast amount of research efforts can be found in the literature searching for a solution of this unsolved problem (Desmet, 2002; Piere, 2003). The first approach in these efforts is to push the upper frequency limit of FEA method so that the mid-frequency problem can be partially or fully covered (Zienkiewicz, 2000; Fries and Belytschko, 2010). The first method in this approach is to improve the computation efficiency of the current FEA method. The most efficient solver is chosen in the actual industry computation of large scale problem, Lanczos method is normally used in standard normal mode analysis since its fast and accurate performance. The computation efficiency can also be greatly improved by using sub-structuring method such as Component Mode Synthesis (CMS). Review papers on Sub-structuring methods can be found in the literature (Craig, 1977; Klerk, 2008). Following the old principle of “divide and conquer”, an expensive large problem is replaced by solving a combination of several (or many) smaller problems. Since the computation time decrease exponentially with the decrease of matrix size, CMS can potentially save the computation time by magnitude of order while keep a relatively good accuracy. Different approaches exist in CMS method on how the components are connected. The component boundary condition can be chosen as free, fixed, or a mixed boundary conditions. Commonly used Craig-Bampton method use a combination of dynamic modes with fixed boundary condition and static constraint modes performed by mean of Guyan static condensation, which apply a unit displacement at each one boundary node while keep all other boundary nodes fixed. Furthermore, dividing the system into components allows a combination of results from different groups or even different methods, such as FEA, SEA, or experimental results. CMS method is further used in uncertainty reanalysis (Zhang, 2005; Sellgren, 2003, Gaurav, 2011). Herran (2011) reported an improved method which orthogonalizes the constraint modes with respect to the mass matrix flowing Faucher’s method. Since the reduced mass matrix is diagonal, the computation efficiency of explicit resolution can be improved. The Automated Multi-level Synthesis (AMLS) method developed by Bennighof (2004) is widely used in current FEA computation acceleration, AMLS automatically divide the stiffness and mass matrices into tree-like structure, and the lowest level component is solved by using Craig-Bampton CMS method with fixed boundary condition. An industrial validation case of AMLS method can also be found (Ragnarsson 2011).

The other method in pushing the upper frequency limit of FEA is to improve its convergence rate. Such techniques include adaptive meshing (h-method), multi-scale technique, and using high order element (p-method). While many methods are developed for solving the mid-frequency problem, these methods are either directly target to or closely related with the p-method. Discontinuous enrich method (DEM) developed by Farhat (2003) enrich the standard polynomial field within each finite element by a non-conforming field that contains free-space solutions of the homogeneous partial differential equation to be solved. DEM method is also applied to three dimensional acoustic scattering problems (Tezaur, 2006). Similar idea enriches the finite element by harmonic functions (Housavi, 2011) can be found in crack analysis. The Partition of Unity method, which is developed by Babuška (1997), is also used in solving mid frequency vibration problem (Bel, 2005). Desmet (1998) developed a method called Wave based method (WBM), which use the exact solution of homogeneous Helmholtz equation as the approximation solution. Since the governing equation is satisfied by each of the approximation function, the final system equation is solved by only enforcing boundary and continuity conditions using a weighted residual formulation. Several research paper related with WBM and its combination with other method can be found in the literature (Bergen, 2008; Genechten, 2010; Vergeot, 2011;). Ladeveze (1999) developed a method called variational theory of complex rays (VTCR), in which the solution is decomposed into a combination of interior rays, edge rays, and corner rays that satisfy the governing equation a priori. So the final equation is also solved by enforcing the boundary and interface continuity condition by using a variational formulation. VTCR method and WBM method are closely related with each other, and both belong to the Trefftz method.

The second approach in solving the mid frequency problem is to push the lower limit of the SEA method by relaxing some of its stringent requirements, such as the coupling between systems can be strong, there can be only a few modes in some subsystems, there is only moderate uncertainty in subsystems, or the excitation can be correlated or localized (SEA assume rain-on-the-roof excitation). Most of the methods in this direction use the helpful results from FEA method. One of such method is the Mobility Power Flow Analysis, which use the mobility function at the coupling points calculated by FEA to represent the coupling between substructures and SEA concepts are used to estimate the system response (Cuschieri, 1987, 1990). Since the coupling loss factor doesn't require spatial and frequency averaging, the results can represent the model behavior at the mid frequency range. Another method called statistical model energy distribution analysis (SmEdA) method compute the model behavior of the substructures by FEA method in advance, and the coupling loss factor between individual modes of connection subsystem is used in SEA analysis (Stelzer, 2011).

The third approach in conquering the mid frequency problem is a hybrid method which combines both the FEA and SEA concepts. The Energy Finite Element Analysis (EFEA) method directly combine the element idea of FEA and energy concept of SEA. Since the field energy variable used the same rule as heat transfer law, available thermal FEA software can be directly adopted in EFEA analysis. But the natural difference between thermal problem and vibration problem make this method less attractive in real application. In fact, complex structure may have some components exhibit high-frequency behavior while others show low-frequency behavior. A hybrid deterministic-statistical method call Fuzzy Structure Theory (Soize, 1993; Shorter and Langley, 2005) was developed, in which a system is divided into master FEA structure and slave fuzzy structures described by SEA method. The coupling between the FEA and SEA components are described by a diffuse field reciprocity relation (Langley and Bremner, 1999; Langley and Cordioli, 2009). Application of hybrid FEA plus SEA concept in industry can also be found (Cotoni, etc., 2007; Chen, etc., 2011). Another similar method combing the FEA method and analytical impedance is also developed (Mace 2002)

Although plenty of new methods are proposed for mid-frequency analysis, no mature method is available to solve the mid-frequency challenge in the industry vibration analysis. This chapter will have a detailed description of Fourier Series Element Method (FSEM) method, which is more close to the first approach in solving the mid frequency problem. FSEM model of a system has smaller model size and higher convergence rate than FEM model, which make it possible to tackle higher frequency problem before encounter the computation capacity limitation. Current method is closely related with DEM, VTCR, and WBM methods. The difference is that current method doesn't only satisfy the governing equation, but also the boundary conditions in an exact sense. The final system equation is assembled by the variational formulation on both the interior and the boundary of the studied domain.

5.3 Energy equations

The expression for the total potential energy, kinetic energy of the plate and beam assembly and the external energy contribution are given, respectively, by

$$V = \sum_{i=1}^{N_p}\left(V_i^p + V_i^{p,E}\right) + \sum_{i=1}^{N_b}\left(V_i^b + V_i^{b,E}\right) + \sum_{i=1}^{N_{pp}} V_i^{pp} + \sum_{i=1}^{N_{pb}} V_i^{pb} + \sum_{i=1}^{N_{bb}} V_i^{bb} \tag{5.1}$$

$$T = \sum_{i=1}^{N_p} T_i^p + \sum_{i=1}^{N_b} T_i^b \tag{5.2}$$

$$W=\sum_{i=1}^{N_p} W_i^p + + \sum_{i=1}^{N_b} W_i^b \tag{5.3}$$

where N_p (N_b) is the total number of plates (beams) in the build-up structure; N_{pp}, N_{pb}, N_{bb} are the numbers of coupling spring among the plates, among the beams, and among the plates and beams, respectively; V_i^p (V_i^b) is the strain energy due to the vibration of the i_{th} plate (beam); $V_i^{p,E}$ ($V_i^{b,E}$) is the potential energy stored in the boundary springs of the i_{th} plate (beam); V_i^{pp}, V_i^{pb}, V_i^{bb} are the potential energies stored in the i_{th} pair of coupling spring between plate and plate, plate and beam, beam and beam, respectively; T_i^p (T_i^b) is the kinetic energy corresponding to the vibration of the i_{th} plate (beam). W_i^p and W_i^b are the energy contribution from the external force done on the i_{th} plate and beams, respectively.

5.3.1 Energy contribution from a single plate

The strain energy of a single plate is given by

$$V_i^p = \frac{1}{2}\iiint_V \sigma_{ij}\varepsilon_{ij} dV \tag{5.3}$$

For a plate with uniform thickness h, Equaiton (5.3) could be further simplified as,

$$V_i^p = \frac{1}{2}\iint_{A_i} \left(\int_{-h/2}^{h/2} \sigma_{ij}\varepsilon_{ij} dz_i\right) dA \tag{5.4}$$

where A_i is the surface area of the i_{th} plate.

The total potential energy for a classical plate can be decomposed as

$$V_i^p = V_i^{p,t} + V_i^{p,i}$$

where $V_i^{p,t}$ represents the contribution from the transverse vibration; and $V_i^{p,i}$ account for the contribution from the in-plane vibration.

For a classical plate undergoing only transverse vibration, the transverse straight lines are assumed inextensible and remain perpendicular to the deformed midsurface. The strain along the transverse direction is assumed negligible. These assumptions are equivalent to specifying

$$\varepsilon_{xz}^{i} = 0,\ \varepsilon_{yz}^{i} = 0,\ \varepsilon_{zz}^{i} = 0 \tag{5.5}$$

Then all the nonzero strains exist only in the plane parallel to the plate surface. The displacement field and associated nonzero plane strains are,

$$u_i = -z_i\,\partial w_i/\partial x_i\ ,\ v_i = -z_i\,\partial w_i/\partial y_i\ ,\ w_i = w_i(x_i, y_i)$$

$$\varepsilon_{xx}^{i} = -z_i\,\partial^2 w_i/\partial^2 x_i\ ,\ \varepsilon_{yy}^{i} = -z_i\,\partial^2 w_i/\partial^2 y_i\ ,\ \varepsilon_{xy}^{i} = -z_i\,\partial^2 w_i/\partial x_i \partial y_i \tag{5.6}$$

where x_i, y_i, z_i are the local coordinates of the i_{th} plate.

The strain energy associated with the transverse vibration is expressed as,

$$V_i^{p,t} = \frac{1}{2}\iint_{A_i}\left(\int_{-h/2}^{h/2} \boldsymbol{\sigma}_i{}^{\mathrm{T}}\boldsymbol{\varepsilon}_i dz\right) dA = \frac{1}{2}\iint_{A_i}\left(\int_{-h/2}^{h/2} \boldsymbol{\varepsilon}_i{}^{\mathrm{T}}\mathbf{C}_i\boldsymbol{\varepsilon}_i dz\right) dA \tag{5.7}$$

where $\boldsymbol{\sigma} = \begin{bmatrix}\sigma_{xx}^{i} & \sigma_{yy}^{i} & \sigma_{xy}^{i}\end{bmatrix}$, $\boldsymbol{\varepsilon} = \begin{bmatrix}\varepsilon_{xx}^{i} & \varepsilon_{yy}^{i} & 2\varepsilon_{xy}^{i}\end{bmatrix}$, $\boldsymbol{\sigma}_i = \mathbf{C}_i\boldsymbol{\varepsilon}_i$, and $\mathbf{C}_i$ is the material constitutive matrix of the i_{th} plate**.** Using the relation in Eq. (5.6), Eq. (5.7) could be further given as,

$$V_i^{p,t} = \frac{h^3}{24}\iint_{A} \ \boldsymbol{\mathfrak{D}}_\mathbf{2}\mathbf{w}_i^{\mathrm{T}}\mathbf{C}_i\boldsymbol{\mathfrak{D}}_\mathbf{2}\mathbf{w}_i\, dA \tag{5.8}$$

where $\boldsymbol{\mathfrak{D}}_\mathbf{2}\mathbf{w}_i = [\partial^2 w_i/\partial {x_i}^2 \quad \partial^2 w_i/\partial {y_i}^2 \quad 2\,\partial^2 w_i/\partial x_i \partial y_i]^{\mathrm{T}}$.

For a classical plate undergoing only in-plane vibration, the displacement field and associated strains are,

$u_i = u_i(x_i, y_i)$, $v_i = v_i(x_i, y_i)$, $w_i = 0$,

$$\varepsilon_{xx}^i = \partial u_i/\partial x_i,\ \varepsilon_{yy}^i = \partial v_i/\partial y_i,\ 2\varepsilon_{xy}^i = \partial u_i/\partial y_i + \partial v_i/\partial x_i \tag{5.9}$$

The strain energy associated with in-plane vibration is expressed as,

$$V_i^{p,i} = \frac{1}{2}\iint_{A_i}\left(\int_{-h/2}^{h/2} \boldsymbol{\varepsilon}_i{}^{\mathrm{T}}\mathbf{C}_i\boldsymbol{\varepsilon}_i dz_i\right) dA = \frac{h}{2}\iint_{A_i} \mathfrak{D}\mathbf{w}_i^{\mathrm{T}}\mathbf{C}_i\mathfrak{D}\mathbf{w}_i\, dA \tag{5.10}$$

where $\mathfrak{D}\mathbf{w}_i = [\partial u_i/\partial x_i \quad \partial v_i/\partial y_i \quad \partial u_i/\partial y_i + \partial v_i/\partial x_i]^{\mathrm{T}}$.

Eq. (5.8) and Eq. (5.10) is applicable for both isotropic and anisotropic plates.

The boundary condition of the plates and beams are all described by a set of linear and rotational springs. The strain energy stored in the boundary spring is given by,

$$V_i^{p,E} = \frac{1}{2}\int^{\Gamma_i} \mathbf{X}_i{}^T\mathbf{k}_i\mathbf{X}_i dl + \frac{1}{2}\int^{\Gamma_i} \mathbf{DX}_i{}^T\mathbf{K}_i\mathbf{DX}_i dl \tag{5.11}$$

where $\mathbf{X}_i = [u_i \quad v_i \quad w_i]^T$, $\mathbf{DX}_i = \left[\frac{\partial w_i}{\partial y_i} \quad -\frac{\partial w_i}{\partial x_i} \quad \frac{\partial v_i}{\partial x_i} - \frac{\partial u_i}{\partial y_i}\right]^T$, $\mathbf{k}_i$ and $\mathbf{K}_i$ are the coupling spring matrices in the local coordinate of the i_{th} plate, and Γ_i represents the boundary of the i_{th} plate.

The kinetic energy of the plate is simply given by

$$T_i = \frac{1}{2}\omega^2 \iint_A \rho_i h_i (u_i{}^2 + v_i{}^2 + w_i{}^2)\, dx\, dy \tag{5.12}$$

5.3.2 Energy contribution from a single beam

The potential energy of a single beam can also be obtained based on Eq. (5.3). The contribution from the flexible vibration, longitudinal vibration, and torsional vibration are assumed linearly addable and given as,

$$V_i^b = \frac{1}{2}\int_0^{l_i} E_i\left(S_i(\partial u_i/\partial x_i)^2 + I_{z,i}(\partial^2 v_i/\partial {x_i}^2)^2 + I_{y,i}(\partial^2 w_i/\partial {x_i}^2)^2\right) dx +$$

$$\frac{1}{2}\int_0^{l_i} G_i J_i (\partial \theta_i/\partial x_i)^2\, dx \tag{5.13}$$

where E_i, $I_{z,i}$, $I_{y,i}$, S_i, G_i, J_i are the Young's modulus, moment inertia about y and z axes, cross-sectional area, shear modulus, and rotatary inertia of the beam, respectively.

The kinetic energy of the beam is given by,

$$T_i = \frac{1}{2}\omega^2 \int_0^{l_i}\left[\rho_i S_i({u_i}^2 + {v_i}^2 + {w_i}^2) + \rho_i J_i {\theta_i}^2\right] dl \tag{5.14}$$

where ρ_i is the beam density.

The strain energy stored in the boundary spring is given by,

$$V_i^{b,E} = \frac{1}{2}\mathbf{X}_i{}^T\mathbf{k}_i\mathbf{X}_i + \frac{1}{2}\mathbf{DX}_i{}^T\mathbf{K}_i\mathbf{DX}_i$$

where $\mathbf{X}_i = [u_i \quad v_i \quad w_i]^T$, $\mathbf{DX}_i = \left[\theta_i \quad -\frac{\partial w_i}{\partial x_i} \quad \frac{\partial v_i}{\partial x_i}\right]^T$.

5.3.3 Energy contribution from the coupling springs

The coupling condition among the plates and beams are again described by different sets of linear coupling springs. The strain energy is first given in the global coordinates. For the k_{th} pair of coupled edge between m_{th} edge of i_{th} plate and n_{th} edge of the j_{th} plate, the strain energy stored in the spring is given as

$$V_k^{pp} = \frac{1}{2}\int_0^{l_i}\left(\overline{\mathbf{X}}_i|_m - \overline{\mathbf{X}}_j|_n\right)^T \overline{\mathbf{k}}^c\left(\overline{\mathbf{X}}_i|_m - \overline{\mathbf{X}}_j|_n\right) dl$$

$$+\frac{1}{2}\int_0^{l_i}\left(\mathbf{D}\overline{\mathbf{X}}_i|_m - \mathbf{D}\overline{\mathbf{X}}_j|_n\right)^T \overline{\mathbf{K}}^c\left(\mathbf{D}\overline{\mathbf{X}}_i|_m - \mathbf{D}\overline{\mathbf{X}}_j|_n\right) dl \tag{5.15}$$

where $\bar{x}_i$, $\bar{y}_i$, $\bar{z}_i$ represent the global coordinate, $\bar{\mathrm{X}}_i = [\bar{\mathrm{u}}_i \quad \bar{\mathrm{v}}_i \quad \bar{\mathrm{w}}_i]^{\mathrm{T}}$, $\mathbf{D}\bar{\mathbf{X}}_i = [\theta_{\bar{x},i} \quad \theta_{\bar{y},i} \quad \theta_{\bar{z},i}]^T$, and $\bar{\mathrm{u}}_{\mathrm{i}}$, $\bar{\mathrm{v}}_{\mathrm{i}}$, $\bar{\mathrm{w}}_{\mathrm{i}}$ ($\theta_{\bar{x},i}$, $\theta_{\bar{y},i}$, $\theta_{\bar{z},i}$) represent the displacement (rotation) of the i_{th} plate in the global coordinate.; $\bar{\mathbf{k}}^{\mathrm{c}}$ and $\bar{\mathbf{K}}^{\mathrm{c}}$ represents the coupling spring in the global coordinate.

For the coupling between a plate and a beam when the beam lies inside the plate surface, the coupling Eq. (5.15) also changed to

$$V_k^{pb} = \frac{1}{2}\int_0^{l_i}\left(\bar{\mathbf{X}}_i|_m - \bar{\mathbf{X}}_{b,j}\right)^T\bar{\mathbf{k}}^{\mathrm{c}}\left(\bar{\mathbf{X}}_i|_m - \bar{\mathbf{X}}_{b,j}\right)dl$$

$$+\frac{1}{2}\int_0^{l_i}\left(\mathbf{D}\bar{\mathbf{X}}_i|_m - \mathbf{D}\bar{\mathbf{X}}_{b,j}\right)^T\bar{\mathbf{K}}^{\mathrm{c}}\left(\mathbf{D}\bar{\mathbf{X}}_i|_m - \mathbf{D}\bar{\mathbf{X}}_{b,j}\right)dl \tag{5.16}$$

where $\bar{\mathbf{X}}_{b,j}$, $\mathbf{D}\bar{\mathbf{X}}_{b,j}$ represents the translation and rotation associated with the beam, respectively.

When the coupling only occurs at one point between a plate and a beam, the integration sign in Eq. (5.16) is dropped and given by

$$V_k^{pb} = \frac{1}{2}\left(\bar{\mathbf{X}}_i|_m - \bar{\mathbf{X}}_{b,j}\right)^T\bar{\mathbf{k}}^{\mathrm{c}}\left(\bar{\mathbf{X}}_i|_m - \bar{\mathbf{X}}_{b,j}\right)$$

$$+\frac{1}{2}\left(\mathbf{D}\bar{\mathbf{X}}_i|_m - \mathbf{D}\bar{\mathbf{X}}_{b,j}\right)^T\bar{\mathbf{K}}^{\mathrm{c}}\left(\mathbf{D}\bar{\mathbf{X}}_i|_m - \mathbf{D}\bar{\mathbf{X}}_{b,j}\right) \tag{5.17}$$

For two beams coupled at one point, the strain energy is given by

$$V_k^{pb} = \frac{1}{2}\left(\bar{\mathbf{X}}_{b,i} - \bar{\mathbf{X}}_{b,j}\right)^T\bar{\mathbf{k}}^{\mathrm{c}}\left(\bar{\mathbf{X}}_{b,i} - \bar{\mathbf{X}}_{b,j}\right)$$

$$+\frac{1}{2}\left(\mathbf{D}\bar{\mathbf{X}}_{b,i} - \mathbf{D}\bar{\mathbf{X}}_{b,j}\right)^T\bar{\mathbf{K}}^{\mathrm{c}}\left(\mathbf{D}\bar{\mathbf{X}}_{b,i} - \mathbf{D}\bar{\mathbf{X}}_{b,j}\right) \tag{5.18}$$

Since the condition for the fast convergence of the current method will be violated if the coupling occurs at the middle point of the beams or plate. It is suggested that the plate and beam structure be constructed such that the coupling only happen at their boundaries. However, it should be point out that the solution in the method will converge to the exact solution even the coupling exist in the middle area of the plates or beams.

The energy contribution from the external force done on the i_{th} plate and beams are

$$W_i^p = \iint_A \mathbf{F}_i \mathbf{X}_i dxdy \tag{5.42}$$

$$W_i^b = \int_l \mathbf{F}_{b,i} \mathbf{X}_{b,i} dx \tag{5.43}$$

where $\mathbf{F}_i = [f_i^u(x,y) \quad f_i^v(x,y) \quad f_i^w(x,y)]$, $\mathbf{F}_{b,i} = \left[f_{b,i}^u(x) \quad f_{b,i}^v(x) \quad f_{b,i}^w(x) \quad f_{b,i}^\theta(x)\right]$ are the external force act on the plate and beams.

5.4 Transformation from global to local coordinate

Although the displacement filed and energy equation for a single plate or beam are both described in the local coordinate, the coupling condition between two plates or beams has to be described in the global coordinate. To define the plate (or beam) local coordinates, three distinct points are needed and these points cannot stand on the same line in the space. Although the dimension of a plate contains enough information for the definition of its local coordinate, an extra point is needed for a beam to define its orientation.

5.4.1 Transformation matrix from global to local coordinates

The transformation between local and global coordinates will be described for a general triangular plate. The extra point for a rectangular point is neglected and the reference point created for a beam is used in its local coordinate definition.

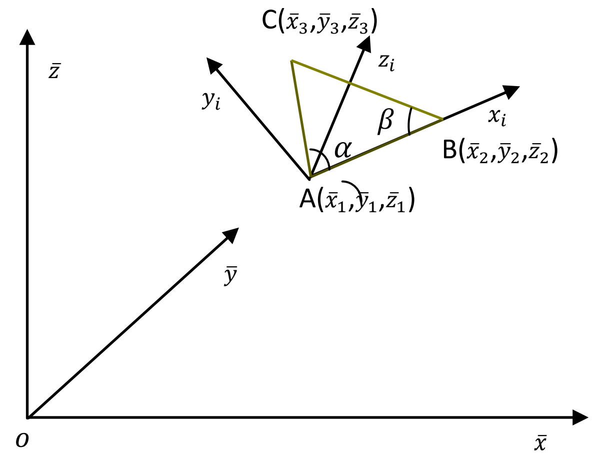

Figure 5.2 Transformation between the local and global coordinates

In Figure 5.2, the $\bar{x}$-$\bar{y}$-$\bar{z}$ coordinate represents the global coordinate, and the x_i-y_i-z_i coordinate represents the local coordinate of the i_{th} plate. A, B, C are the three apex points of the plate, and ($\bar{x}_j$,$\bar{y}_j$,$\bar{z}_j$) (j=1, 2, 3) are the global coordinates of the three points.

In the global coordinate, AB $= [(\bar{x}_2 - \bar{x}_1)^2 + (\bar{y}_2 - \bar{y}_1)^2 + (\bar{z}_2 - \bar{z}_1)^2]^{1/2}$, AC $= [(\bar{x}_3 - \bar{x}_1)^2 + (\bar{y}_3 - \bar{y}_1)^2 + (\bar{z}_3 - \bar{z}_1)^2]^{1/2}$, BC $= [(\bar{x}_3 - \bar{x}_2)^2 + (\bar{y}_3 - \bar{y}_2)^2 + (\bar{z}_3 - \bar{z}_2)^2]^{1/2}$, $\alpha = \cos^{-1}\left(\frac{AB^2+AC^2-BC^2}{2AB\cdot AC}\right)$, and $\beta = \cos^{-1}\left(\frac{AB^2+BC^2-AC^2}{2AB\cdot BC}\right)$

The coordinates in the two systems are related by a rotation matrix and a transformation vector,

$$\bar{\mathbf{X}} = \mathbf{T}_i\mathbf{X}_i + \bar{\mathbf{X}}_0 \tag{5.19}$$

where $\bar{\mathbf{X}} = [\bar{x} \quad \bar{y} \quad \bar{z}]^T$, $\mathbf{X}_i = [x \quad y \quad z]^T$, $\bar{\mathbf{X}}_0 = [\bar{x}_1 \quad \bar{y}_1 \quad \bar{z}_1]^T$, and $\mathbf{T}_i = \begin{bmatrix} T_{11} & T_{12} & T_{13} \\ T_{21} & T_{22} & T_{23} \\ T_{31} & T_{32} & T_{33} \end{bmatrix}$

The local coordinates of the three apex points are $\mathbf{A} = [0 \quad 0 \quad 0]^T$, $\mathbf{B} = [AB \quad 0 \quad 0]^T$, $\mathbf{C} = [AC\cos\alpha \quad AC\sin\alpha \quad 0]^T$, then $\mathbf{AB} = [AB \quad 0 \quad 0]^T$ and $\mathbf{AC} =$

$[AC\cos\alpha \quad AC\sin\alpha \quad 0]^T$. Since both the global and local coordinates of the three points are given and the two vectors **AB** and **AC** have zero z_i- components, the first two column of the transformation matrix $\mathbf{T}_i$ is determined by following equation,

$$\begin{bmatrix} \bar{x}_2 - \bar{x}_1 & \bar{x}_3 - \bar{x}_1 \\ \bar{y}_2 - \bar{y}_1 & \bar{y}_3 - \bar{y}_1 \\ \bar{z}_2 - \bar{z}_1 & \bar{z}_3 - \bar{z}_1 \end{bmatrix} = \begin{bmatrix} T_{11} & T_{12} \\ T_{21} & T_{22} \\ T_{31} & T_{32} \end{bmatrix} \begin{bmatrix} AB & AC\cos\alpha \\ 0 & AC\sin\alpha \end{bmatrix} \tag{5.20}$$

Since AB and AC are in the same plane but not exist in the same line, the last matrix in Eq. (5.20) is invertible and the equation could be further written as,

$$\begin{bmatrix} T_{11} & T_{12} \\ T_{21} & T_{22} \\ T_{31} & T_{32} \end{bmatrix} = \begin{bmatrix} x_2 - x_1 & x_3 - x_1 \\ y_2 - y_1 & y_3 - y_1 \\ z_2 - z_1 & z_3 - z_1 \end{bmatrix} \begin{bmatrix} AB & AC\cos\alpha \\ 0 & AC\sin\alpha \end{bmatrix}^{-1} \tag{5.21}$$

The transformation from global to local coordinate is always linear and the third column component of the transformation matrix is determined by

$$\mathbf{T}^{\langle 3\rangle} = \mathbf{T}^{\langle 1\rangle} \times \mathbf{T}^{\langle 2\rangle} \tag{5.22}$$

where $\mathbf{T}^{\langle i\rangle}$ represents the i_{th} column of the transformation matrix $\mathbf{T}$. The transformation matrix is thus calculated for a defined general plate in a three dimensional space.

5.4.2 Energy equations in the transformed local coordinates

The principal direction of the coupling or boundary spring is assumed given and have its own local coordinate system $\tilde{x}$-$\tilde{y}$-$\tilde{z}$. The spring matrix has nonzero values at its diagonal terms only in its own coordinate, and $\tilde{\mathbf{k}}_i = \mathrm{diag}[k\tilde{x}_i \quad k\tilde{y}_i \quad k\tilde{z}_i]$ ($\overline{\mathbf{K}}_i = \mathrm{diag}[K\tilde{x}_i \quad K\tilde{y}_i \quad K\tilde{z}_i]$), where diag [.] denotes the diagonal matrix formed from the listed elements $k\tilde{x}_i$, $k\tilde{y}_i$, and $k\tilde{z}_i$ ($K\tilde{x}_i$, $K\tilde{y}_i$, and $K\tilde{z}_i$). The transformation matrix between the spring local coordinate and the plate local coordinate is also assumed known as $\widetilde{\mathbf{T}}_i$. i.e. $\mathbf{X} = \widetilde{\mathbf{T}}_i\widetilde{\mathbf{X}}_i$. Then the spring matrices could be expressed in the local coordinates as,

$$\mathbf{K}_i = \widetilde{\mathbf{T}}_i\widetilde{\mathbf{K}}_i\widetilde{\mathbf{T}}_i^{\mathrm{T}}, \mathbf{k}_i = \widetilde{\mathbf{T}}_i\tilde{\mathbf{k}}_i\widetilde{\mathbf{T}}_i^{\mathrm{T}} \tag{5.23}$$

The local coordinate of the springs will be chosen to match that of the coupling edge of the first plate. Since the transformation matrix for the local coordinate of the plate is known as $\mathbf{T}_i$, The transformation matrix for the spring is obtained by times it with $\mathbf{T}_s$

$$\widetilde{\mathbf{T}}_i = \mathbf{T}_i\mathbf{T}_s \tag{5.24}$$

where $\mathbf{T}_s = \begin{bmatrix} \cos\theta_{LS} & -\sin\theta_{LS} & 0 \\ \sin\theta_{LS} & \cos\theta_{LS} & 0 \\ 0 & 0 & 1 \end{bmatrix}$. For a general triangular plate, the three edges are numbered as follow, AB as 1, BC as 2, CA as 3. Table 5.1 lists the θ_{LS} for the three triangular plate edges.

Table 5.1 transformation angles for the three edges of a general triangular plate

Edge number	1	2	3
θ_{LS}	0	$\pi - \beta$	α

For a general rectangular plate, the four edges are numbered as follow, AB as 1, BC as 2, CD as 3, and DA as 4. Table 5.2 lists the θ_{LS} for the four rectangular edges.

Table 5.2 transformation angles for the four edges of a general rectangular plate

Edge number	1	2	3	4
θ_{LS}	0	$\pi/2$	0	$\pi/2$

Based on the coordinate transformation, the energy Eq. (5.15) accounting for the contribution from the coupling springs of two plates are further expressed as,

$$V_k^{pp} = \frac{1}{2}\int_0^{l_i} \mathbf{X}_i{}^T|_m \mathbf{k}_i^c \mathbf{X}_i|_m dl + \frac{1}{2}\int_0^{l_i} \mathbf{X}_j{}^T|_n \mathbf{k}_j^c \mathbf{X}_j|_n dl - \int_0^{l_i} \mathbf{X}_i{}^T|_m \mathbf{k}_{ij}^c \mathbf{X}_j|_n dl$$

$$+\frac{1}{2}\int_0^{l_i} \mathbf{DX}_i{}^T|_m \mathbf{K}_i^c \mathbf{DX}_i|_m dl + \frac{1}{2}\int_0^{l_i} \mathbf{DX}_j{}^T|_n \mathbf{K}_j^c \mathbf{DX}_j|_n dl - \int_0^{l_i} \mathbf{DX}_i|_m{}^T \mathbf{K}_{ij}^c \mathbf{DX}_j|_n dl \tag{5.25}$$

where $\mathbf{k}_i^c = \widetilde{\mathbf{T}}_i{}^T \tilde{\mathbf{k}}_k \widetilde{\mathbf{T}}_i = \mathbf{T}_i \widetilde{\mathbf{T}}_i{}^T \bar{\mathbf{k}}_k \widetilde{\mathbf{T}}_i \mathbf{T}_i{}^T$, $\mathbf{k}_j^c = \widetilde{\mathbf{T}}_j{}^T \tilde{\mathbf{k}}_k \widetilde{\mathbf{T}}_j = \mathbf{T}_j \widetilde{\mathbf{T}}_j{}^T \bar{\mathbf{k}}_k \widetilde{\mathbf{T}}_j \mathbf{T}_j{}^T$, and $\mathbf{k}_{ij}^c = \widetilde{\mathbf{T}}_i{}^T \widetilde{\mathbf{K}}_k \widetilde{\mathbf{T}}_j = \mathbf{T}_i \widetilde{\mathbf{T}}_i{}^T \bar{\mathbf{K}}_k \widetilde{\mathbf{T}}_j \mathbf{T}_j{}^T$; $\mathbf{K}_i^c$,$\mathbf{K}_j^c$,and $\mathbf{K}_{ij}^c$ have the same format as $\mathbf{k}_i^c$,$\mathbf{k}_j^c$,and $\mathbf{k}_{ij}^c$, respectively.

The Eqs. (5.16- 5.18) follow the same pattern except that they differ Eq. (5.25) with an integration sign.

5.5 Transformation of the plate integration into a standard form

To reduce the calculation burden in solving a complex structure consists of many plates and beams, it is advantageous to have the stiffness and mass matrixes of the plates saved in advance and load them when compiling the matrix for a given structure. However, it is impossible to save the matrix of a general triangular or rectangular plate. By transforming the energy Eq. (5.8) and Eq. (5.10) into a unit right angled isosceles triangle or unit square domain, the matrices only need to be saved one time. *From now on, x', and y' will denote the original local coordinate and x and y will represents the transformed local coordinates.*

The irregular triangular domain (Figure5.3a) is mapped onto a unit right angled isosceles triangular domain (Figure5.3b) by using the following coordinate transformation,

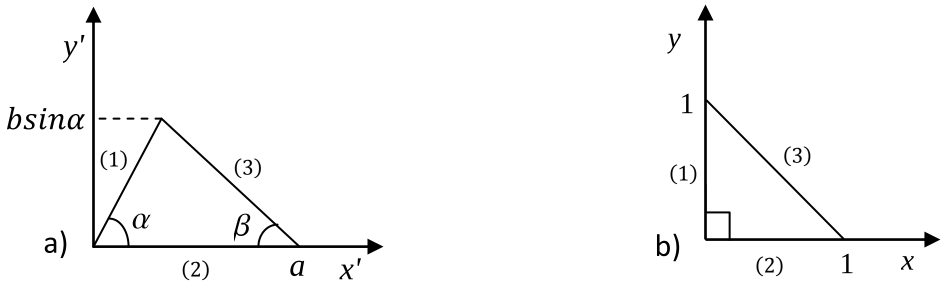

Figure 5.3 A triangular plate before (a) and after (b) coordinator transformation

$$\begin{cases} x' = ax + bycos\alpha \\ y' = bysin\alpha \end{cases} \tag{5.26}$$

Then the relation of the first and second derivatives between the original and transformed coordinates could be written as follows,

$$\begin{bmatrix} \frac{\partial w}{\partial x'} \\ \frac{\partial w}{\partial y'} \end{bmatrix} = \begin{bmatrix} 1/a & 0 \\ -\cot\alpha/a & 1/(bsin\alpha) \end{bmatrix} \begin{bmatrix} \frac{\partial w}{\partial x} \\ \frac{\partial w}{\partial y} \end{bmatrix} \tag{5.27}$$

Eq. (5.27) is further written as

$$\boldsymbol{\mathfrak{D}_1 w'} = \boldsymbol{\mathcal{T}\mathfrak{D}_1 w} \tag{5.28}$$

$$\begin{bmatrix} \frac{\partial^2 w}{\partial x'^2} \\ \frac{\partial^2 w}{\partial y'^2} \\ \frac{\partial^2 w}{\partial x' \partial y'} \end{bmatrix} = \begin{bmatrix} 1/a^2 & 0 & 0 \\ \cot^2\alpha/a^2 & 1/(bsin\alpha)^2 & -2\cot\alpha/(absin\alpha) \\ -\cot\alpha/a^2 & 0 & 1/(absin\alpha) \end{bmatrix} \begin{bmatrix} \frac{\partial^2 w}{\partial x^2} \\ \frac{\partial^2 w}{\partial y^2} \\ \frac{\partial^2 w}{\partial x \partial y} \end{bmatrix} \tag{5.29}$$

Eq. (5.29) is further written as

$$\boldsymbol{\mathfrak{D}_2 w'} = \boldsymbol{\overline{\mathcal{T}}\mathfrak{D}_2 w} \tag{5.30}$$

Eq. (5.8) and (5.10) could be further written as

$$V_i^{p,t} = \frac{h^3}{24}\iint_{\mathrm{S}} \ \boldsymbol{\mathfrak{D}}_{\mathbf{2}}\mathbf{w}_i^{\mathrm{T}}\mathbb{T}_i^{\mathrm{t}}\boldsymbol{\mathfrak{D}}_{\mathbf{2}}\mathbf{w}_i J_0 dA \tag{5.31}$$

where $\mathbb{T}_i^{\mathrm{t}} = \overline{\boldsymbol{\mathcal{T}}}^{\mathrm{T}}\mathbf{C}\overline{\boldsymbol{\mathcal{T}}}$, $\boldsymbol{\mathfrak{D}}_{\mathbf{2}}\mathbf{w}_i = [\partial^2 w_i/\partial {x_i}^2 \quad \partial^2 w_i/\partial {y_i}^2 \quad 2\,\partial^2 w_i/\partial x_i \partial y_i]^{\mathrm{T}}$, $J_0 = absin\alpha$, and S stand for a unit right angled isosceles triangular domain.

$$V_i^{p,i} = \frac{h}{2}\iint_{\mathrm{S}} \ \boldsymbol{\mathfrak{D}}\mathbf{w}_i^{\mathrm{T}}\mathbb{T}_i^{\mathrm{in}}\boldsymbol{\mathfrak{D}}\mathbf{w}_i J_0 dA \tag{5.32}$$

where $\mathbb{T}_i^{\mathrm{in}} = \widehat{\boldsymbol{\mathcal{T}}}^{\mathrm{T}}\mathbf{C}\widehat{\boldsymbol{\mathcal{T}}}$, $\boldsymbol{\mathfrak{D}}\mathbf{w}_i = [\partial u_i/\partial x_i \quad \partial u_i/\partial y_i \quad \partial v_i/\partial x_i \quad \partial v_i/\partial y_i]^{\mathrm{T}}$, $J_0 = absin\alpha$, and S stand for a unit right angled isosceles triangular domain. $\widehat{\boldsymbol{\mathcal{T}}}$ stands for the following transformation matrix

$$\widehat{\boldsymbol{\mathcal{T}}} = \begin{bmatrix} 1/a & 0 & 0 & 0 \\ 0 & 0 & -\cot\alpha/a & 1/(bsin\alpha) \\ -\cot\alpha/a & 1/(bsin\alpha) & 1/a & 0 \end{bmatrix} \tag{5.33}$$

For the energy equation of rectangular plate, the integration region is transformed into unit square domain. The transformation matrices are

$$\boldsymbol{\mathcal{T}} = \begin{bmatrix} 1/a & 0 \\ 0 & 1/b \end{bmatrix} \tag{5.34}$$

$$\overline{\boldsymbol{\mathcal{T}}} = \begin{bmatrix} 1/a^2 & 0 & 0 \\ 0 & 1/b^2 & 0 \\ 0 & 0 & 1/(ab) \end{bmatrix} \tag{5.35}$$

$$\widehat{\boldsymbol{\mathcal{T}}} = \begin{bmatrix} 1/a & 0 & 0 & 0 \\ 0 & 0 & 0 & 1/b \\ 0 & 1/b & 1/a & 0 \end{bmatrix} \tag{5.37}$$

For a general coupling edge between two plates, Eq. (5.25) is further written as

$$V_k^{pp} = \frac{1}{2}\int_0^1 \mathbf{X}^T|_m \mathbf{k}_i^{\mathrm{c}}\mathbf{X}|_m l_i dl + \frac{1}{2}\int_0^1 \mathbf{X}^T|_n \mathbf{k}_j^{\mathrm{c}}\mathbf{X}|_n l_i dl - \int_0^1 \mathbf{X}^T|_m \mathbf{k}_{ij}^{\mathrm{c}}\mathbf{X}|_n l_i dl$$

$$+\frac{1}{2}\int_0^1 \mathbf{DX}^T|_m \breve{\mathbf{K}}_i^c \mathbf{DX}|_m l_k dl + \frac{1}{2}\int_0^1 \mathbf{DX}^T|_n \breve{\mathbf{K}}_j^c \mathbf{DX}|_n l_k dl - \int_0^1 \mathbf{DX}|_m{}^T \breve{\mathbf{K}}_{ij}^c \mathbf{DX}|_n l_k dl \quad (5.25)$$

where l_i is the length of the coupling edge. $\mathbf{DX}|_m = [\mathfrak{D}\mathbf{u} \quad \mathfrak{D}\mathbf{v} \quad \mathfrak{D}\mathbf{w}]|_m$, $\mathfrak{D}\mathbf{u} = \begin{bmatrix}\frac{\partial u}{\partial x} & \frac{\partial u}{\partial y}\end{bmatrix}$, $\mathfrak{D}\mathbf{v} = \begin{bmatrix}\frac{\partial v}{\partial x} & \frac{\partial v}{\partial y}\end{bmatrix}$, and $\mathfrak{D}\mathbf{w} = \begin{bmatrix}\frac{\partial w}{\partial x} & \frac{\partial w}{\partial y}\end{bmatrix}$; $\breve{\mathbf{K}}_{ij}^c = \begin{bmatrix}\breve{\mathbf{K}}_{11} & \breve{\mathbf{K}}_{12} & \breve{\mathbf{K}}_{13} \\ \breve{\mathbf{K}}_{21} & \breve{\mathbf{K}}_{22} & \breve{\mathbf{K}}_{23} \\ \breve{\mathbf{K}}_{31} & \breve{\mathbf{K}}_{32} & \breve{\mathbf{K}}_{33}\end{bmatrix}$, in which

$\breve{\mathbf{K}}_{11} = \mathrm{K}_{33}^c \boldsymbol{\mathcal{T}}_{<2>}^{i}{}^{\mathrm{T}} \boldsymbol{\mathcal{T}}_{<2>}^{j}$, $\breve{\mathbf{K}}_{12} = -\mathrm{K}_{33}^c \boldsymbol{\mathcal{T}}_{<2>}^{i}{}^{\mathrm{T}} \boldsymbol{\mathcal{T}}_{<1>}^{j}$, $\breve{\mathbf{K}}_{13} = -\boldsymbol{\mathcal{T}}_{<2>}^{i}{}^{\mathrm{T}}\left(\mathrm{K}_{31}^c \boldsymbol{\mathcal{T}}_{<2>}^{j} - \mathrm{K}_{32}^c \boldsymbol{\mathcal{T}}_{<1>}^{j}\right)$, $\breve{\mathbf{K}}_{21} = -\mathrm{K}_{33}^c \boldsymbol{\mathcal{T}}_{<1>}^{i}{}^{\mathrm{T}} \boldsymbol{\mathcal{T}}_{<2>}^{j}$, $\breve{\mathbf{K}}_{22} = \mathrm{K}_{33}^c \boldsymbol{\mathcal{T}}_{<1>}^{i}{}^{\mathrm{T}} \boldsymbol{\mathcal{T}}_{<1>}^{j}$, $\breve{\mathbf{K}}_{23} = \boldsymbol{\mathcal{T}}_{<1>}^{i}{}^{\mathrm{T}}\left(\mathrm{K}_{31}^c \boldsymbol{\mathcal{T}}_{<2>}^{j} - \mathrm{K}_{32}^c \boldsymbol{\mathcal{T}}_{<1>}^{j}\right)$, $\breve{\mathbf{K}}_{31} = -\left(\boldsymbol{\mathcal{T}}_{<2>}^{i}{}^{\mathrm{T}} \mathrm{K}_{13}^c - \boldsymbol{\mathcal{T}}_{<1>}^{i}{}^{\mathrm{T}} \mathrm{K}_{23}^c\right) \boldsymbol{\mathcal{T}}_{<2>}^{j}$, $\breve{\mathbf{K}}_{32} = \left(\boldsymbol{\mathcal{T}}_{<2>}^{i}{}^{\mathrm{T}} \mathrm{K}_{13}^c - \boldsymbol{\mathcal{T}}_{<1>}^{i}{}^{\mathrm{T}} \mathrm{K}_{23}^c\right) \boldsymbol{\mathcal{T}}_{<1>}^{j}$, $\breve{\mathbf{K}}_{33} = \begin{bmatrix}\boldsymbol{\mathcal{T}}_{<2>}^{i} \\ -\boldsymbol{\mathcal{T}}_{<1>}^{i}\end{bmatrix}^{\mathrm{T}} \begin{bmatrix}\mathrm{K}_{11}^c & \mathrm{K}_{12}^c \\ \mathrm{K}_{21}^c & \mathrm{K}_{22}^c\end{bmatrix} \begin{bmatrix}\boldsymbol{\mathcal{T}}_{<2>}^{j} \\ -\boldsymbol{\mathcal{T}}_{<1>}^{j}\end{bmatrix}$; $\boldsymbol{\mathcal{T}}_{<k>}^{i}$ is the k_{th} row of the transformation matrix $\boldsymbol{\mathcal{T}}^i$

5.6 Approximation functions of the plate and beam displacements

The vibration of the plates and beams are assumed arbitrary and the corresponding displacements are the unknown functions to be solved. The assumed solution must able to describe the vibration shapes of the plates and beams under any condition, which requires the functional being complete in the resolved domain. The transverse and in-plane displacement functions of the plates and beams will be summarized as follow,

Rectangular plates:

$$u(x,y) = \sum_{m=0}^{\infty}\sum_{n=0}^{\infty} A_{mn}^{\mathrm{R,u}} \cos(m\pi x)\cos(n\pi y)$$

$$+\sum_{j=1}^{2} \xi_j(y) \sum_{m=0}^{\infty} c_{jm}^{\mathrm{R,u}} \cos(m\pi x) + \sum_{j=1}^{2} \xi_j(x) \sum_{n=0}^{\infty} d_{jn}^{\mathrm{R,u}} \cos(n\pi y) \quad (5.26)$$

$$v(x,y) = \sum_{m=0}^{\infty}\sum_{n=0}^{\infty} A_{mn}^{\mathrm{R,v}} \cos(m\pi x)\cos(n\pi y)$$

$$+\sum_{j=1}^{2}\xi_j(y)\sum_{m=0}^{\infty}c_{jm}^{\mathrm{R,v}}\cos(m\pi x)+\sum_{j=1}^{2}\xi_j(x)\sum_{n=0}^{\infty}d_{jn}^{\mathrm{R,v}}\cos(n\pi y) \quad (5.27)$$

$$w(x,y)=\sum_{m=0}^{\infty}\sum_{n=0}^{\infty}A_{mn}^{\mathrm{R,w}}\cos(m\pi x)\cos(n\pi y)$$

$$+\sum_{j=1}^{4}\xi_j(y)\sum_{m=0}^{\infty}c_{jm}^{\mathrm{R,w}}\cos(m\pi x)+\sum_{j=1}^{4}\xi_j(x)\sum_{n=0}^{\infty}d_{jn}^{\mathrm{R,w}}\cos(n\pi y) \quad (5.28)$$

where *u*, *v*, *w*, represent displacement in x, y, z direction, respectively; R represents rectangular plate, and $A_{mn}^{\mathrm{R,u}}$, $c_{jm}^{\mathrm{R,u}}$, $d_{jn}^{\mathrm{R,u}}$, etc. are the unknown coefficients to be determined in the vibration solution. $\xi_j(x)$ ($j=1,2,3,4$) are four special functions designed to account the boundary conditions of the plate displacement.

$$\xi_1(x)=\frac{9}{4\pi}sin\left(\frac{\pi x}{2}\right)-\frac{1}{12\pi}sin\left(\frac{3\pi x}{2}\right),\ \xi_2(x)=-\frac{9}{4\pi}cos\left(\frac{\pi x}{2}\right)-\frac{1}{12\pi}cos\left(\frac{3\pi x}{2}\right), \quad (5.29,30)$$

$$\xi_3(x)=\frac{1}{\pi^3}sin\left(\frac{\pi x}{2}\right)-\frac{1}{3\pi^3}sin\left(\frac{3\pi x}{2}\right),\ \xi_4(x)=-\frac{1}{\pi^3}cos\left(\frac{\pi x}{2}\right)-\frac{1}{3\pi^3}cos\left(\frac{3\pi x}{2}\right), \quad (5.31,32)$$

Triangular plates

$$u(x,y)=\sum_{m=0}^{\infty}\sum_{n=0}^{\infty}A_{mn}^{\mathrm{T,u}}\cos(m\pi x)\cos(n\pi y)$$

$$+\xi_1(y)\sum_{m=0}^{\infty}c_{m}^{\mathrm{T,u}}\cos(m\pi x)+\xi_1(x)\sum_{n=0}^{\infty}d_{n}^{\mathrm{T,u}}\cos(n\pi y)$$

$$+(1-x-y)\sum_{m=0}^{\infty}e_{m}^{\mathrm{T,u}}\left(\cos(m\pi x)+(-1)^m\cos(m\pi y)\right) \quad (5.33)$$

$$v(x,y)=\sum_{m=0}^{\infty}\sum_{n=0}^{\infty}A_{mn}^{\mathrm{T,v}}\cos(m\pi x)\cos(n\pi y)$$

$$+\xi_1(y)\sum_{m=0}^{\infty}c_{m}^{\mathrm{T,v}}\cos(m\pi x)+\xi_1(x)\sum_{n=0}^{\infty}d_{n}^{\mathrm{T,v}}\cos(n\pi y)$$

$$+(1-x-y)\sum_{m=0}^{\infty}e_{m}^{\mathrm{T,v}}\left(\cos(m\pi x)+(-1)^m\cos(m\pi y)\right) \quad (5.34)$$

$$w(x,y)=\sum_{m=0}^{\infty}\sum_{n=0}^{\infty}A_{mn}^{\mathrm{T,w}}\cos(m\pi x)\cos(n\pi y)$$

$$+\sum_{j=1,3}\xi_j(y)\sum_{m=0}^{\infty}c_{jm}^{\mathrm{T,w}}\cos(m\pi x)+\sum_{j=1,3}\xi_j(x)\sum_{n=0}^{\infty}d_{jn}^{\mathrm{T,w}}\cos(n\pi y)$$

$$+\sum_{j=1}^{3}(1-x-y)^j\sum_{m=0}^{\infty}e_{jm}^{\mathrm{T,w}}\left(\cos(m\pi x)+(-1)^m\cos(m\pi y)\right) \tag{5.35}$$

where T represents triangular plate, and $\xi_j(x)$ ($j=1{,}3$) are the same special functions used in approximating the rectangular plate displacements.

Beams

$$u(x)=\sum_{m=0}^{\infty}A_m^{\mathrm{B,u}}\cos(m\pi x)+\sum_{j=1}^{2}c_j^{\mathrm{B,u}}\sin(j\pi x) \tag{5.36}$$

$$v(x)=\sum_{m=0}^{\infty}A_m^{\mathrm{B,v}}\cos(m\pi x)+\sum_{j=1}^{4}c_j^{\mathrm{B,v}}\sin(j\pi x) \tag{5.37}$$

$$w(x)=\sum_{m=0}^{\infty}A_m^{\mathrm{B,w}}\cos(m\pi x)+\sum_{j=1}^{4}c_j^{\mathrm{B,w}}\sin(j\pi x) \tag{5.38}$$

$$\theta(x)=\sum_{m=0}^{\infty}A_m^{\mathrm{B,\theta}}\cos(m\pi x)+\sum_{j=1}^{2}c_j^{\mathrm{B,\theta}}\sin(j\pi x) \tag{5.39}$$

where θ represents the tortional displacement of the beam; $A_m^{\mathrm{B,u}}$, $A_m^{\mathrm{B,v}}$, $A_m^{\mathrm{B,w}}$, $A_m^{\mathrm{B,\theta}}$, $c_j^{\mathrm{B,u}}$, $c_j^{\mathrm{B,v}}$, $c_j^{\mathrm{B,w}}$, $c_j^{\mathrm{B,\theta}}$ are the unknown coefficients to be determined.

5.7 Characteristic equation of a general structure

Fourier spectrum element modal is developed by using Hamiton's principal on the weak form of the governing equation expressed in energy Eqs. (5.1)-(5.3),

$$\delta(\mathrm{T}+\mathrm{W}-\mathrm{V})=0 \tag{5.40}$$

Minimization of the Hamiltonian function will lead to the following system of equations,

$$(\mathbf{K}-\omega^2\mathbf{M})\mathbf{a}=\mathbf{F} \tag{5.40}$$

where **a** is composed by all the unknown coefficients in the plate and beam displacement functions, **K,** and **M** are the stiffness and mass matrices ,and **F** is the force vector. All the matrix elements in these matrices can be analytically derived by using the general formulation provided in the Appendix.

$$\mathbf{K}=\begin{bmatrix}
\mathbf{K}_{11}^{\mathrm{p}} & \cdots & \mathbf{K}_{1i}^{\mathrm{p}} & \cdots & \mathbf{K}_{1j}^{\mathrm{p}} & \cdots & \mathbf{K}_{1N_p}^{\mathrm{p}} & \mathbf{K}_{11}^{\mathrm{pb}} & \cdots & \mathbf{K}_{1m}^{\mathrm{pb}} & \cdots & \mathbf{K}_{1n}^{\mathrm{pb}} & \cdots & \mathbf{K}_{1N_b}^{\mathrm{pb}} \\
 & \ddots & & & & & & & & & & & & \\
 & & \mathbf{K}_{ii}^{\mathrm{p}} & & \mathbf{K}_{ij}^{\mathrm{p}} & & \mathbf{K}_{iN_p}^{\mathrm{p}} & \mathbf{K}_{i1}^{\mathrm{pb}} & & \mathbf{K}_{im}^{\mathrm{pb}} & & \mathbf{K}_{in}^{\mathrm{pb}} & & \mathbf{K}_{iN_b}^{\mathrm{pb}} \\
 & & & \ddots & & & & & & & & & & \\
 & & & & \mathbf{K}_{jj}^{\mathrm{p}} & & & \mathbf{K}_{j1}^{\mathrm{pb}} & & \mathbf{K}_{jm}^{\mathrm{pb}} & & \mathbf{K}_{jn}^{\mathrm{pb}} & & \mathbf{K}_{jN_b}^{\mathrm{pb}} \\
 & & & & & \ddots & & & & & & & & \\
 & & & & & & \mathbf{K}_{N_pN_p}^{\mathrm{p}} & \mathbf{K}_{N_p1}^{\mathrm{pb}} & & \mathbf{K}_{N_pm}^{\mathrm{pb}} & & \mathbf{K}_{N_pn}^{\mathrm{pb}} & & \mathbf{K}_{N_pN_b}^{\mathrm{pb}} \\
 & & & & & & & \mathbf{K}_{11}^{\mathrm{b}} & \cdots & \mathbf{K}_{1m}^{\mathrm{b}} & \cdots & \mathbf{K}_{1n}^{\mathrm{b}} & \cdots & \mathbf{K}_{1N_b}^{\mathrm{b}} \\
 & & & & \text{symm} & & & & \ddots & & & & & \\
 & & & & & & & & & \mathbf{K}_{mm}^{\mathrm{b}} & & \mathbf{K}_{mn}^{\mathrm{b}} & & \\
 & & & & & & & & & & \ddots & & & \\
 & & & & & & & & & & & \mathbf{K}_{nn}^{\mathrm{b}} & & \\
 & & & & & & & & & & & & \ddots & \\
 & & & & & & & & & & & & & \mathbf{K}_{N_bN_b}^{\mathrm{b}}
\end{bmatrix}$$

$$\mathbf{M}=\begin{bmatrix}
\mathbf{M}_{11}^{\mathrm{p}} & & & & & & & & & & & & & \\
 & \ddots & & & & & & & & & & & & \\
 & & \mathbf{M}_{ii}^{\mathrm{p}} & & & & & & & & & & & \\
 & & & \ddots & & & & & & & & & & \\
 & & & & \mathbf{M}_{jj}^{\mathrm{p}} & & & & & & & & & \\
 & & & & & \ddots & & & & & & & & \\
 & & & & & & \mathbf{M}_{N_pN_p}^{\mathrm{p}} & & & & & & & \\
 & & & & & & & \mathbf{M}_{11}^{\mathrm{b}} & & & & & & \\
 & & & & & & & & \ddots & & & & & \\
 & & & & & & & & & \mathbf{M}_{mm}^{\mathrm{b}} & & & & \\
 & & & & & & & & & & \ddots & & & \\
 & & & & & & & & & & & \mathbf{M}_{nn}^{\mathrm{b}} & & \\
 & & & & & & & & & & & & \ddots & \\
 & & & & & & & & & & & & & \mathbf{M}_{N_bN_b}^{\mathrm{b}}
\end{bmatrix}$$

$$\mathbf{F} = \left[\mathbf{F}_1^{\mathrm{p}} \quad \cdots \quad \mathbf{F}_i^{\mathrm{p}} \quad \cdots \quad \mathbf{F}_j^{\mathrm{p}} \quad \cdots \quad \mathbf{F}_{N_p}^{\mathrm{p}} \quad \mathbf{F}_1^{\mathrm{b}} \quad \cdots \quad \mathbf{F}_i^{\mathrm{b}} \quad \cdots \quad \mathbf{F}_j^{\mathrm{b}} \quad \cdots \quad \mathbf{F}_{N_b}^{\mathrm{b}}\right]^{\mathrm{T}}$$

Eq. (5.40) represents a standard matrix characteristic equation from which all the eigenpairs can be determined by solving a standard matrix eigenvalue problem. Once the generalized coordinates, **a**, is determined, the corresponding mode shape or displacement field can be constructed by substituting **a** into Eq. (5.26-5.39).

5.8 Results and discussion

5.8.1 Example 1: a 3-D beam frame

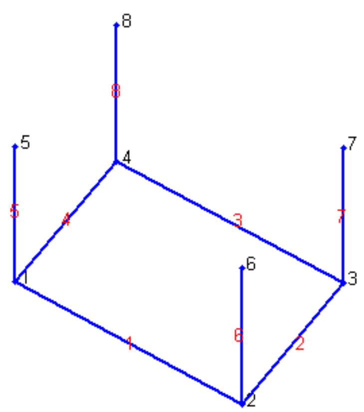

a)

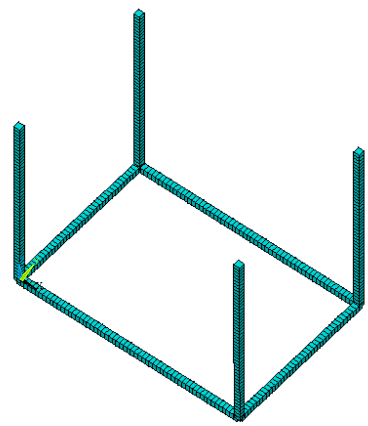

b)

c)

Figure 5.4 A rigidly connected 3-D frame. a) Setup used in current method with corner numbers at the frame corners and beam numbers in the middle of the beams. b) FEM model c) Lab setup with the same number sequence as current and FEM models.

The first testing example is a 3-D frame made of steel AISI A1018 as depicted in Figure 5.4. The frame has a length of 0.6 m (beam 1 and 3), a width of 0.4 m (beam 2 and 4), and a height of 0.5 m (beam 5, 6, 7, and 8). All the angles among the connected beams are 90 degrees. The cross sections of all the beams are 15.875 mm × 15.875 mm. The mechanical properties of the beams are: Elastic modulus $\mathrm{E} = 2.05 \times 10^{11}$ Pa, Poisson's ratio $\mu = 0.29$, material density

$\rho = 7870\ \mathrm{kg/m^3}$, and structural damping $\eta = 0.02$, which was calculated by half power method with some initial testing results.

The frame is hanged to the ceiling by a rubber band to simulate free boundary condition, the hanging point was chosen at one of the frame corner to minimize the outside influence on the frame vibration. The frame was transversely excited by an impact hammer (PCB086C01) and the response was acquired by the toolbox "Sound and vibration 6.0" of NI Labview 2009 through data acquisition hard ware NI USB-9234. The overall dimensions of the frame, the excitation and response locations in the tests are illustrated in Figure 5.5, in which F represents the excitation force and R represents response of the frame. For example, 1R (2R, 3R) and 1F (2F, 3F) constitute a set of measurement. The relative locations of the points are given in the local coordinates of the beams. For example, 0.3L7 represents the location is at 30% of beam number 7 with origin at the smaller corner number 3 as given in Figure 5.4a.

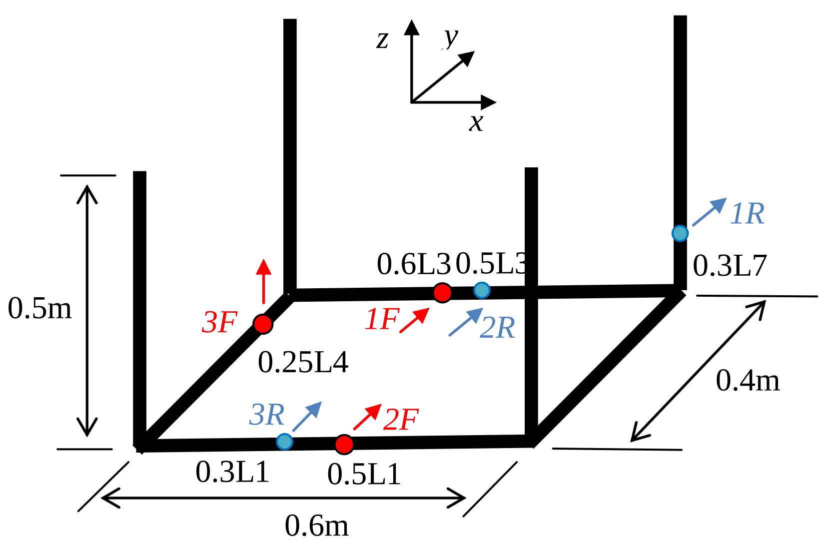

Figure 5.5 A scheme showing the input force and response locations.

The force response function (FRF) curves of the tested 3-D frame are given in Figure 5.6-5.8 for three different pair of input and output locations. The prediction from current method is very close to the FEM results with more discrepancy at high frequencies. All the theoretically predicted peaks are captured in the testing results with small shift at high frequencies and extra responses caused by experimental uncertainties, which include: the input force is not exactly on the designed location and direction; the beam joints are not as rigid as the middle potion of the beams. However, the overall agreements among the three methods are satisfactory.

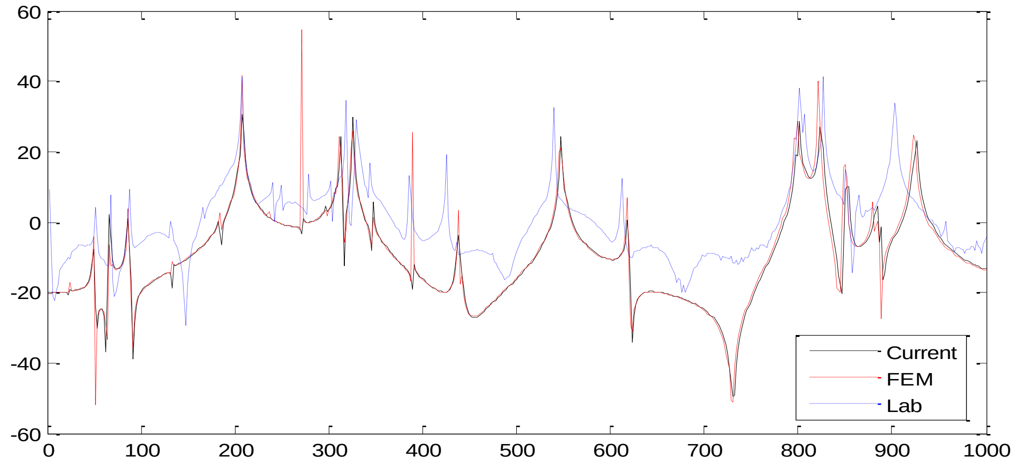

Figure 5.6 FRF curves of the 3-D frame with input force at 0.6L of beam 3 in y direction and response measured at 0.3L of beam 7 in y direction.

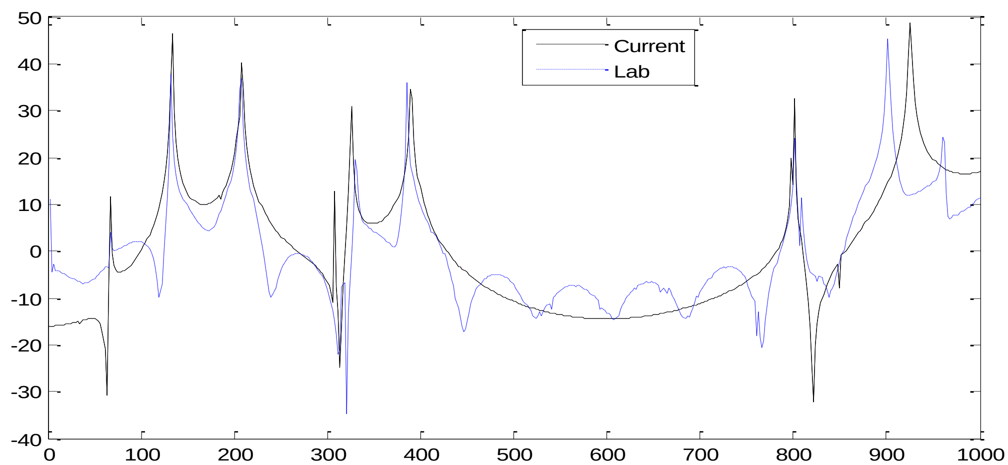

Figure 5.7 FRF curves of the 3-D frame with input force at 0.5L of beam 1 in y direction and response measured at 0.3L of beam 5 in y direction.

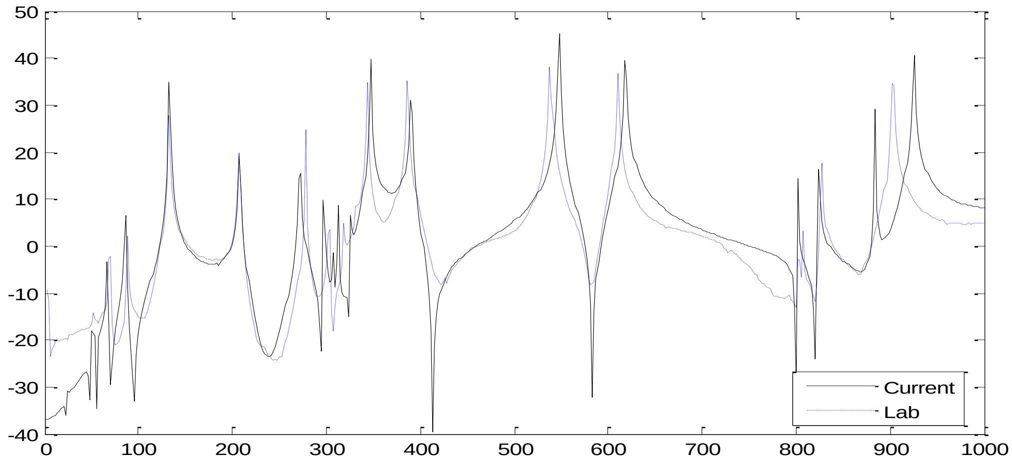

Figure 5.8 FRF curves of the 3-D frame with input force at 0.25L of beam 4 in z direction and response measured at 0.3L of beam 1 in y direction.

Table 5.3 lists the first fourteen flexible natural frequencies of the frame from the three methods. The truncation number used in current method is M=10 in Equation (5.36-5.39), which makes the size of the stiffness and mass matrices 416×416. Whereas the matrix size of FEM model with 400 elements is 2418×2418, which is about 6×6 times the size of matrix in current method. The results from FEM model match with current results pretty well with more discrepancy at high frequencies. The frequencies from the Lab results also confirmed current results.

Table 5.3 The first twelve flexible model frequencies of the tested frame from (* FSEM method with M=10; # FEA method with 400 elements; @ Lab results).

Mode	1	2	3	4	5	6	7	8	9	10	11	12
Natural frequency (Hz)	23.8*	27.7	32.1	35.5	36.3	49.7	54.9	66.7	67.8	86.5	133.3	165.5
	23.8#	27.7	32.1	35.5	36.3	49.7	54.9	66.7	67.8	86.5	133.3	165.4
	24@	27	32	34	38	52	56	66	68	88	132	166

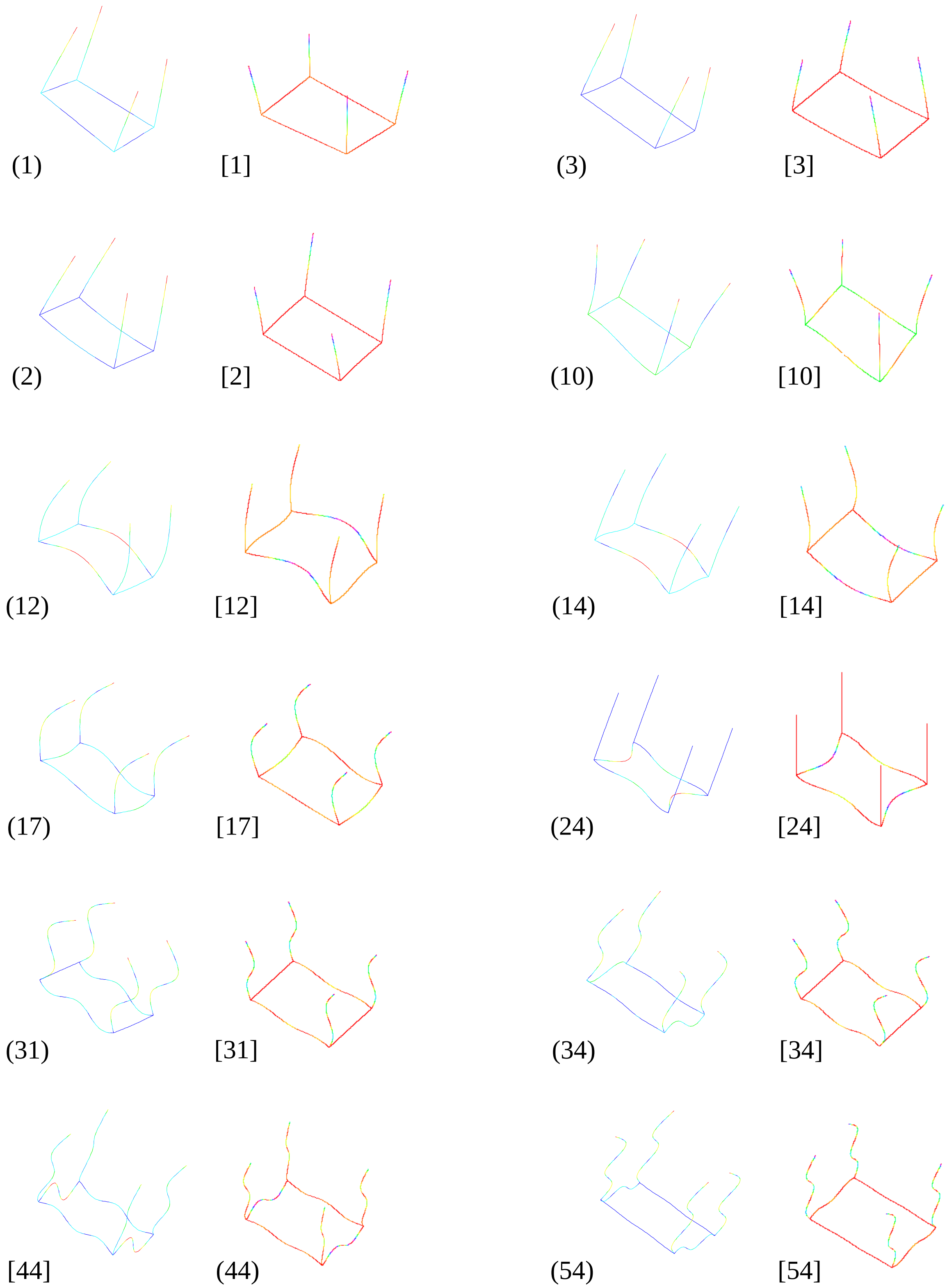

Figure 5.9 Some typical low to mid frequency mode shapes from current method (mode numbers in parentheses) and FEM method (mode numbers in brackets).

Figure 5.9 shows some randomly picked low to mid frequency mode shapes for the tested frame. The mode shapes from current method is indexed by numbers in parentheses and those from FEM method are indexed by numbers in brackets. While half of the modes from both methods look identical to each other, the rest of the modes are also the same but with opposite phase angles. This example verified that current method correctly and efficiently predicted the vibration characteristics of the simple frame. The size of the solved characteristic equation is significantly smaller than the corresponding FEM model with the same accuracy. It showed that current model might have a higher upper frequency limit than the corresponding FEM model. The applicability of current model for more complex geometry will be proven in following examples.

5.8.2 Example 2: a 3-D plate structure

The second testing example is a structure as described in Figure. 5.10, which comes from a real engineering structure with slight modification on the edges. All the plates constituting the structure have the same thickness $h = 1.219 \times 10^{-3}$m, and the same material properties with Elastic modulus $E = 2.048 \times 10^{11}$ Pa, Poisson's ratio $\mu = 0.29$, and density $\rho = 7861 \text{kg/m}^3$.

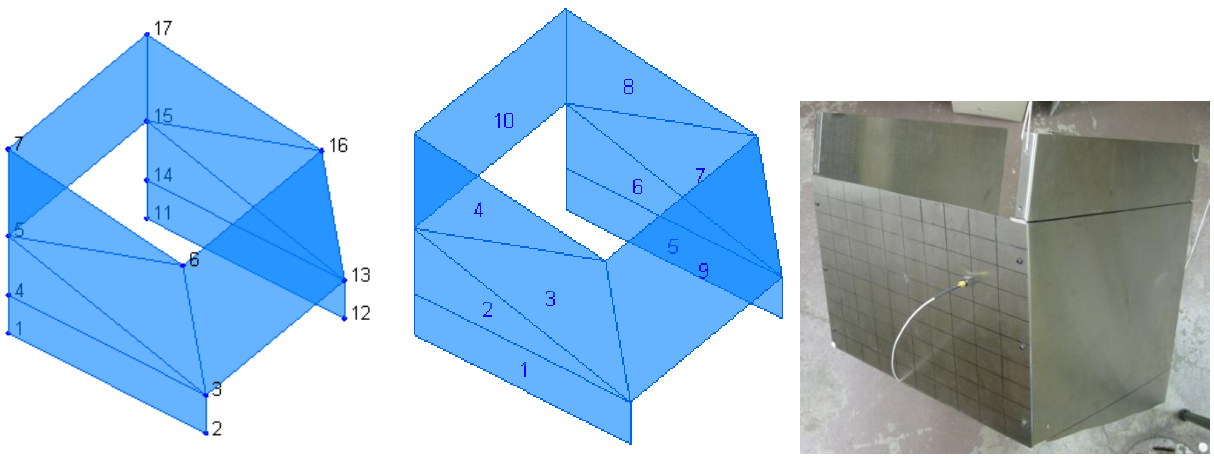

Figure 5.10 The evaluated general plate structure with a) corner numbers at the plate corners, b) plate numbers at the plate centers, and c) lab setup.

Table 5.4 The global coordinates of all the corners of the tested plate structure

Corners	1	2	3	4	5	6	7	11	12	13	14	15	16	17
x (m)	0	0.45	0.45	0	0	0.39	0	0	0.45	0.45	0	0	0.39	0
y (m)	0	0	0	0	0	0	0	0.4	0.4	0.4	0.4	0.4	0.4	0.4
z (m)	0	0	0.09	0.09	0.23	0.36	0.43	0	0	0.09	0.09	0.23	0.36	0.43

The global coordinates of all the plate corners, most of which are the structure corners, are given in Table 5.4. The plate numbers and their constituting corner numbers are given in Table 5.5. With all the plate numbers and their corresponding corners numbers given, the geometry of the structure is completely described.

Table 5.5 The plate numbers and their corresponding corner numbers of the tested plate structure

Plate Number	1	2	3	4	5	6	7	8	9	10
Point 1	1	4	5	5	11	14	15	15	6	7
Point 2	2	3	3	6	12	13	13	16	3	5
Point 3	3	5	6	7	13	15	16	17	13	15
Point 4	4				14				16	17

All the connecting plates are rigidly coupled in the plate structure. A rigidly coupled edge was simulated by setting the coupling spring stiffness to a very large value, i.e. 1.0×10^{10} in current calculation. The truncation number were set as M=N=10 for both the rectangular and triangular plates. The stiffness and mass matrices of the structure were assembled with pre-calculated matrices for a single unit square plate or a single unit right angled triangular plate. Then the frequencies and mode shapes were obtained by solving a standard eigen-value problem. An identical FEM model was also built by meshing the structure with element size around 0.01m, which make the final FEM model consists of 21,766 elements. The first fourteen flexible frequencies from the FEM model were calculated by using Lanczos method. In the lab test, the same equipment used in measuring the frame response in example 1 was used in measuring the plate structure response. Natural frequencies were identified as the distinctive peaks in the FRF curves.

Table 5.6 shows the first fourteen flexible modal frequencies of the tested plate structure. The frequencies from current methods are found very close to the FEM results. The slight differences are expected and might be caused by the difference in the matrix formulation process. The couplings of the connecting plates are also modeled differently. The experimental results also confirmed with the current results with a maximum difference of 16 %. The discrepancy was caused by following reasons: small details in the structure such as the flange were not modeled in the current and FEM model; the structure is hanged to the ceiling, which is not a completely free boundary condition, etc.

Table 5.6 The first fourteen flexible modal frequencies of the tested plate structure.

Mode	**Natural frequencies (Hz)**			**Relative error from Lab(%)**	
	Current	FEM	Lab	Current	FEM
1	8.536	8.491	9.24	7.62	8.11
2	11.952	11.805	11.2	6.71	5.40
3	13.102	13.321	15.2	13.80	12.36
4	19.809	20.084	23.6	16.06	14.90
5	22.171	22.017	25.6	13.39	14.00
6	32.25	32.176	32.6	1.07	1.30
7	35.213	35.303	34.6	1.77	2.03
8	40.289	40.123	39.4	2.26	1.84
9	41.143	41.372	44.4	7.34	6.82
10	45.016	45.597	47.5	5.23	4.01
11	51.795	51.884	53.5	3.19	3.02
12	58.021	58.138	58	0.04	0.24
13	64.846	65.867	62.4	3.92	5.56
14	67.219	67.902	70	3.97	3.00

The first eight flexible mode shapes from both current method and Finite element results are given in Figure 5.11. Although contour results were given FEM model, the accuracy of the high order identities, such as the stress level, power flow in the structure, is not assured. On the contrary, current results are presented in analytical form, then the displacement are given continuously on the whole plate domain. The corresponding high order identities are also convergent and readily available.

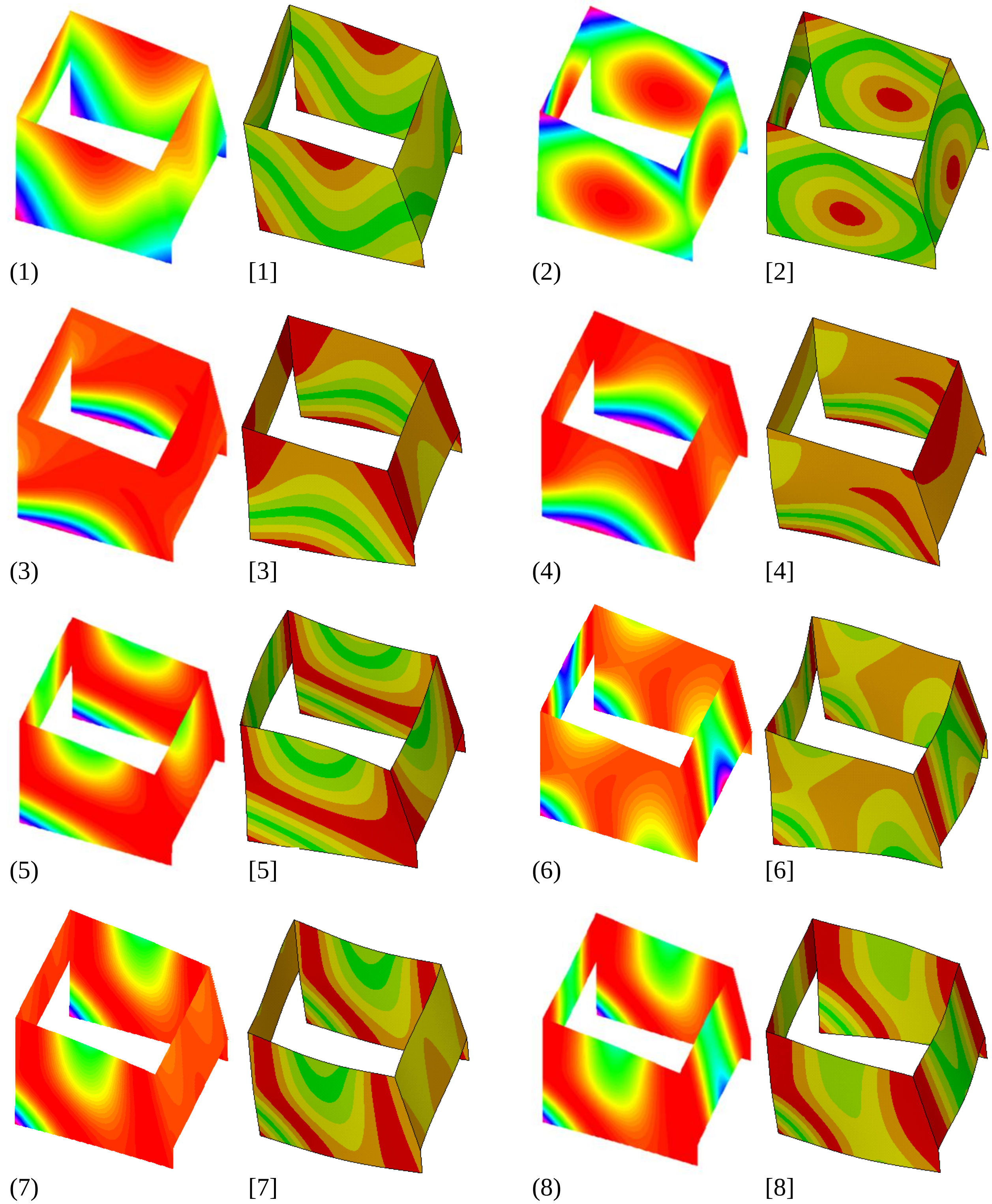

Figure 5.11 The first eight modes of the tested structure from current method (mode numbers in parentheses) and FEM method with 21,766 elements (mode numbers in brackets).

5.8.3 Example 3: a car frame structure

Figure 5.12 shows a beam frame representing the outline of a car body. The orientations and beam coupling angles are complex enough to represent all possible scenarios. The beam corner coordinates are given in Table 5.7 and also plotted in Figure 5.12a. The beam numbers with their corresponding corner numbers are given in Table 5.8 and also plotted in Figure 5.12b. The total beam number is 80, which can represent a fairly general complex beam structure. The cross sections of all the beams are solid squares with width of 0.015 meter. The orientations of all the beams are designed so that the point [1, 1, 1] lies in the beam principal planes. All the connected beams are rigidly coupled, which is simulated by a set of linear and rotational springs with sufficiently large value, i.e., 1.0×10^{10}. The mechanical properties of all the beams are: Elastic modulus $\mathrm{E} = 2.07 \times 10^{11}$ Pa, Poisson's ratio $\mu = 0.3$, material density $\rho = 7800\ \mathrm{kg/m^3}$.

Table 5.9 gives the first twenty-four flexible frequencies of the car frame from current and FEM methods. The truncation number used in current method is M=10 in Equation (5.36-5.39), then the size of the stiffness and mass matrices is 4160×4160. Whereas the matrix size of the FEM model with 2173 elements is 13038×13038, which is about 10 times the size of matrices in current method. The results from both methods are very close to each other, which confirmed the correctness of current model. It is concluded that current method works for an arbitrary beam frame model with any beam orientation and beam section. The coupling between any two beams is completely modeled with six elastic springs.

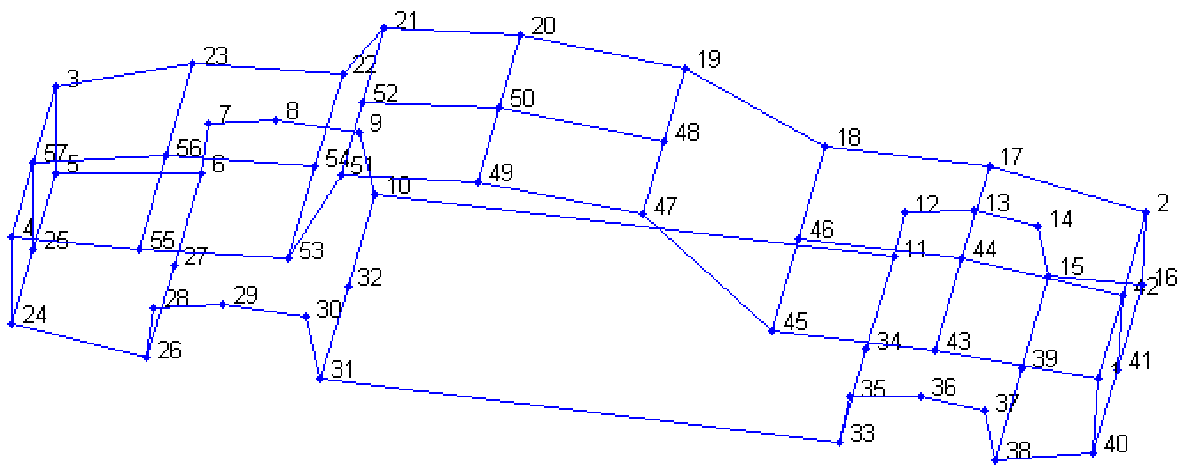

(a)

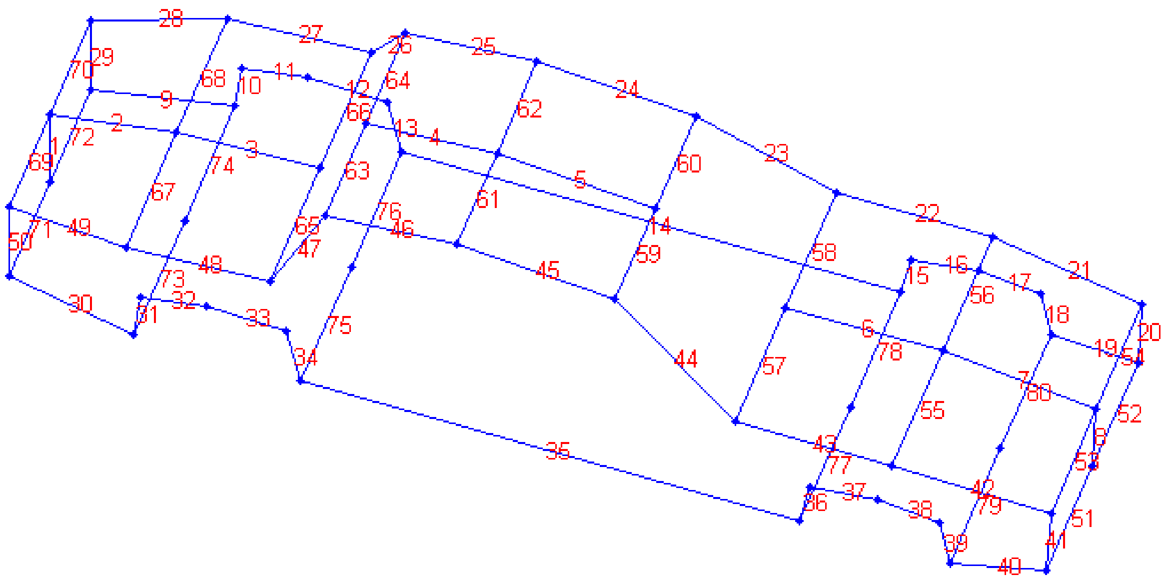

(b)

Figure 5.12 A frame structure representing the outline of a car body with a) corner numbers, and b) beam numbers.

Table 5.7 The global coordinates of all the car frame corners

Corners	x	y	z	Corners	x	y	z
1	-1.15	0.158	-0.251	**30**	-0.529	-0.0906	-0.26
2	-0.873	0.211	-0.255	**31**	0.498	-0.393	-0.279
3	-0.86	0.211	-0.131	**32**	0.498	-0.0906	-0.279
4	-0.724	0.211	-0.104	**33**	0.519	-0.393	-0.167
5	-0.559	0.211	-0.114	**34**	0.658	-0.393	-0.145
6	-0.529	0.211	-0.26	**35**	0.784	-0.393	-0.167
7	0.498	0.211	-0.279	**36**	0.805	-0.393	-0.283
8	0.519	0.211	-0.167	**37**	0.805	-0.0906	-0.283
9	0.658	0.211	-0.145	**38**	0.995	-0.365	-0.262
10	0.785	0.211	-0.167	**39**	0.995	-0.0906	-0.262
11	0.806	0.211	-0.283	**40**	1	-0.365	-0.0798
12	0.995	0.184	-0.262	**41**	1	-0.0906	-0.08
13	1	0.184	-0.0801	**42**	0.687	-0.393	-0.0288
14	0.687	0.211	-0.0291	**43**	0.687	-0.0906	-0.029
15	0.363	0.211	-0.024	**44**	0.363	-0.393	-0.0237
16	0.0967	0.149	0.178	**45**	0.363	-0.0906	-0.0239
17	-0.23	0.149	0.217	**46**	0.0966	-0.332	0.179
18	-0.501	0.148	0.197	**47**	0.0966	-0.0915	0.179
19	-0.593	0.211	0.025	**48**	-0.231	-0.331	0.217
20	-0.89	0.21	0.0116	**49**	-0.23	-0.0911	0.217
21	-1.15	0.158	-0.0393	**50**	-0.501	-0.332	0.197
22	-1.15	-0.334	-0.251	**51**	-0.501	-0.0919	0.197
23	-1.15	-0.0885	-0.251	**52**	-0.594	-0.393	0.0253
24	-0.873	-0.393	-0.255	**53**	-0.594	-0.0906	0.0251
25	-0.873	-0.0906	-0.255	**54**	-0.89	-0.394	0.0119
26	-0.86	-0.393	-0.131	**55**	-0.89	-0.0916	0.0118
27	-0.724	-0.393	-0.104	**56**	-1.15	-0.334	-0.039
28	-0.559	-0.393	-0.114	**57**	-1.15	-0.0884	-0.0392
29	-0.529	-0.393	-0.26				

Table 5.8 The corner numbers of the car frame beams

Line number	Node 1	Node 2	Line number	Node 1	Node 2	Line number	Nod e 1	Node 2
1	25	57	**28**	23	3	**55**	43	44
2	57	56	**29**	3	5	**56**	44	17
3	56	54	**30**	24	26	**57**	45	46
4	52	50	**31**	26	28	**58**	46	18
5	50	48	**32**	28	29	**59**	47	48
6	46	44	**33**	29	30	**60**	48	19
7	44	42	**34**	30	31	**61**	49	50
8	42	41	**35**	31	33	**62**	50	20
9	5	6	**36**	33	35	**63**	51	52
10	6	7	**37**	35	36	**64**	52	21
11	7	8	**38**	36	37	**65**	53	54
12	8	9	**39**	37	38	**66**	54	22
13	9	10	**40**	38	40	**67**	55	56
14	10	11	**41**	40	1	**68**	56	23
15	11	12	**42**	1	43	**69**	4	57
16	12	13	**43**	43	45	**70**	57	3
17	13	14	**44**	45	47	**71**	24	25
18	14	15	**45**	49	47	**72**	25	5
19	15	16	**46**	49	51	**73**	26	27
20	16	2	**47**	51	53	**74**	27	6
21	2	17	**48**	53	55	**75**	31	32
22	17	18	**49**	55	4	**76**	32	10
23	18	19	**50**	4	24	**77**	33	34
24	20	19	**51**	40	41	**78**	34	11
25	20	21	**52**	41	16	**79**	38	39
26	21	22	**53**	1	42	**80**	39	15
27	22	23	**54**	42	2			

Figure 5.13 gives the first few natural modes of the car frame from both current and FEM methods. While the results from current method are plotted in the left side and indexed by numbers in parentheses, the results from FEM method are plotted in the right side and indexed by numbers in square brackets. The first mode is a breathing mode, in which the frame expands in vertical direction. The second and third modes are two torsion modes. The third and fourth modes are two bending modes. The sixth mode is another torsion mode. The mode shapes from current method are almost identical to those results from FEM method.

Table 5.9 The first twenty-four flexible modal frequencies of the car frame structure from current method with truncation M=10 and FEM method with 2173 elements.

Mode	**Frequencies (Hz)**		**Mode**	**Frequencies (Hz)**		**Mode**	**Frequencies (Hz)**	
	Current	FEM		Current	FEM		Current	FEM
1	11.80	11.80	**9**	34.67	34.67	**17**	54.69	54.69
2	16.38	16.38	**10**	39.05	39.05	**18**	60.45	60.44
3	18.85	18.85	**11**	39.29	39.29	**19**	70.62	70.62
4	20.14	20.14	**12**	44.39	44.39	**20**	72.41	72.41
5	22.47	22.47	**13**	47.64	47.64	**21**	78.71	78.71
6	22.52	22.52	**14**	50.85	50.85	**22**	80.43	80.42
7	29.42	29.42	**15**	51.77	51.77	**23**	84.74	84.73
8	29.53	29.54	**16**	53.08	53.08	**24**	86.13	86.12

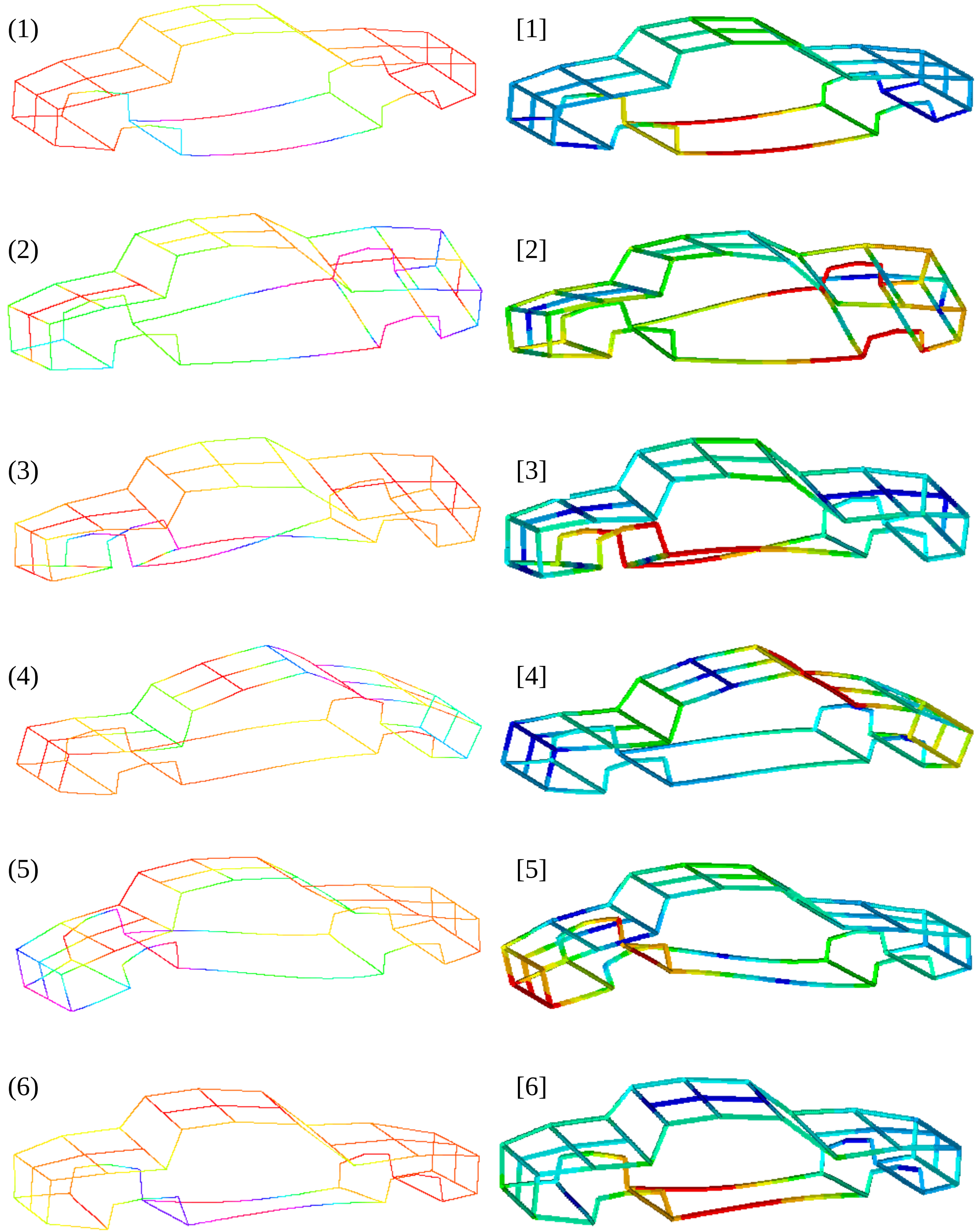

Figure 5.13 The first six mode shapes of the car frame from current method (left side and indexed in parenthesis) and FEM method with 2173 elements (right side and indexed in square bracets)

5.8.4 Example 4: a car frame structure with coupled roof side plates

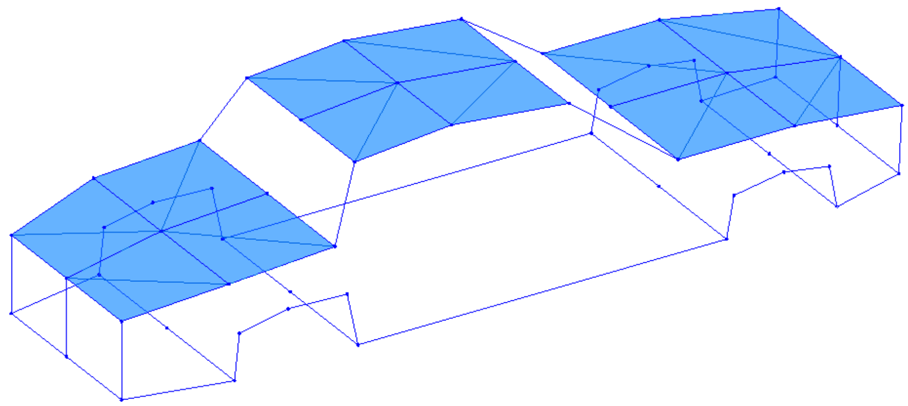

Figure 5.14 The car frame in Figure 5.12 coupled with extra plates on its roof side

Figure 5.14 shows the car frame in Example 3 coupled with extra plates on its roof. All the plates and their corresponding corner numbers are listed in Table 5.10. All the neighboring components of the sixteen triangular plates, eight rectangular plates, and eighty beams are rigidly coupled by using six elastic springs with infinite value, represented by 1.0×10^9. All the plates are assumed having the same thickness at 1 mm and the same mechanical properties with Elastic modulus $\mathrm{E} = 2.07 \times 10^{11}$ Pa, Poisson's ratio $\mu = 0.3$, material density $\rho = 7800\ \mathrm{kg/m^3}$.

Table 5.11 gives the first twenty four flexible frequencies of the car structure. The truncation number for the triangular plates and rectangular plates are set vary with their dimensions by following formula, $M = [10 \times L_i^x / L_{max}]$, $N = [10 \times L_i^y / L_{max}]$ where L_i^x (L_i^y)is the maximum length of the i^{th} plate in x (y) direction, L_{max} is the maximum length of all the plates in both x and y direction. The square bracket means rounding to the next lower integer. The matrix size of the calculated mass and stiffness matrices in current method is 5176×5176. The FEM model meshed with element size 0.01 meter has 16008 elements, which makes the mass and stiffness matrix size about $50{,}000 \times 50{,}000$, which is significantly larger than the matrices used in FSEM method.

Figure 5.15 gives the first 24 normal mode shapes of the structure. All the compared mode shapes are comparable with those modes obtained by using FEM method. Some of the mode shapes looks different because they have opposite phases. This example structure composes 16 triangular plates, 8 rectangular plates, and 80 beams. The FSEM results including model frequencies and mode shapes are all verified with FEA results calculated with fine mesh grids. It is believed that current FSEM is ready to be deployed in industry application.

5.9 Conclusions

Fourier Spectral Element Method is successfully applied to general structures composed of triangular plates, rectangular plates and beams. The connection among the plates and beams are described by six translational and rotational springs varying along the coupling edges. The vibration problem is formed in a varational formulation, and all the energy equation are transformed into a united form in the local coordinates, which enable the usage of one set of stored matrices for all the beam and plate components. The displacement fields are described by improved Fourier series functions with sufficient convergence rate to guarantee exact solution of the solved problem. Since the boundary conditions are all satisfied and the convergence speed is greatly improved, the high order derivative values including bending moments and shear forces can be calculated by directly differentiating the obtained displacement solution. The validity of the FSEM method is tested on several numerical examples ranging from a simple beam frame, a plate structure, a complex beam system, and a complex plate-beam assembly. Since the matrix size of the FSEM method is substantially smaller than the FEA method, FSEM method has the potential to reduce the calculation time, and tackle the unsolved Mid-frequency problem.

Table 5.10 The corresponding corner numbers of all the coupled plates

Plate number	**Node 1**	**Node 2**	**Node 3**	**Plate number**	**Node 1**	**Node 2**	**Node 3**	**Node4**
1	1	44	43	**13**	23	3	57	
2	1	42	44	**14**	23	57	56	
3	42	2	17	**15**	56	57	4	
4	42	17	44	**16**	56	4	55	
5	45	46	47	**17**	43	44	46	45
6	47	46	48	**18**	44	17	18	46
7	46	18	48	**19**	47	48	50	49
8	48	18	19	**20**	48	19	20	50
9	21	22	54	**21**	49	50	52	51
10	21	54	52	**22**	50	20	21	52
11	52	54	53	**23**	22	23	56	54
12	52	53	51	**24**	54	56	55	53

Table 5.11 The first twenty four flexible modal frequencies of the car structure from current FSEM method and FEM method with 16008 elements.

Mode	FSEM	FEM	Mode	FSEM	FEM	Mode	FSEM	FEM
1	11.09	11.09	**9**	33.65	33.62	**17**	57.78	57.78
2	15.90	15.73	**10**	35.39	35.19	**18**	58.20	58.12
3	17.34	17.32	**11**	37.07	36.69	**19**	60.72	60.69
4	18.69	18.58	**12**	43.53	43.52	**20**	70.44	70.40
5	21.08	21.08	**13**	46.12	45.85	**21**	72.49	72.48
6	21.91	21.89	**14**	46.15	46.14	**22**	79.26	78.58
7	27.57	27.57	**15**	52.11	51.78	**23**	83.93	83.89
8	30.10	30.03	**16**	53.08	53.08	**24**	85.10	85.06

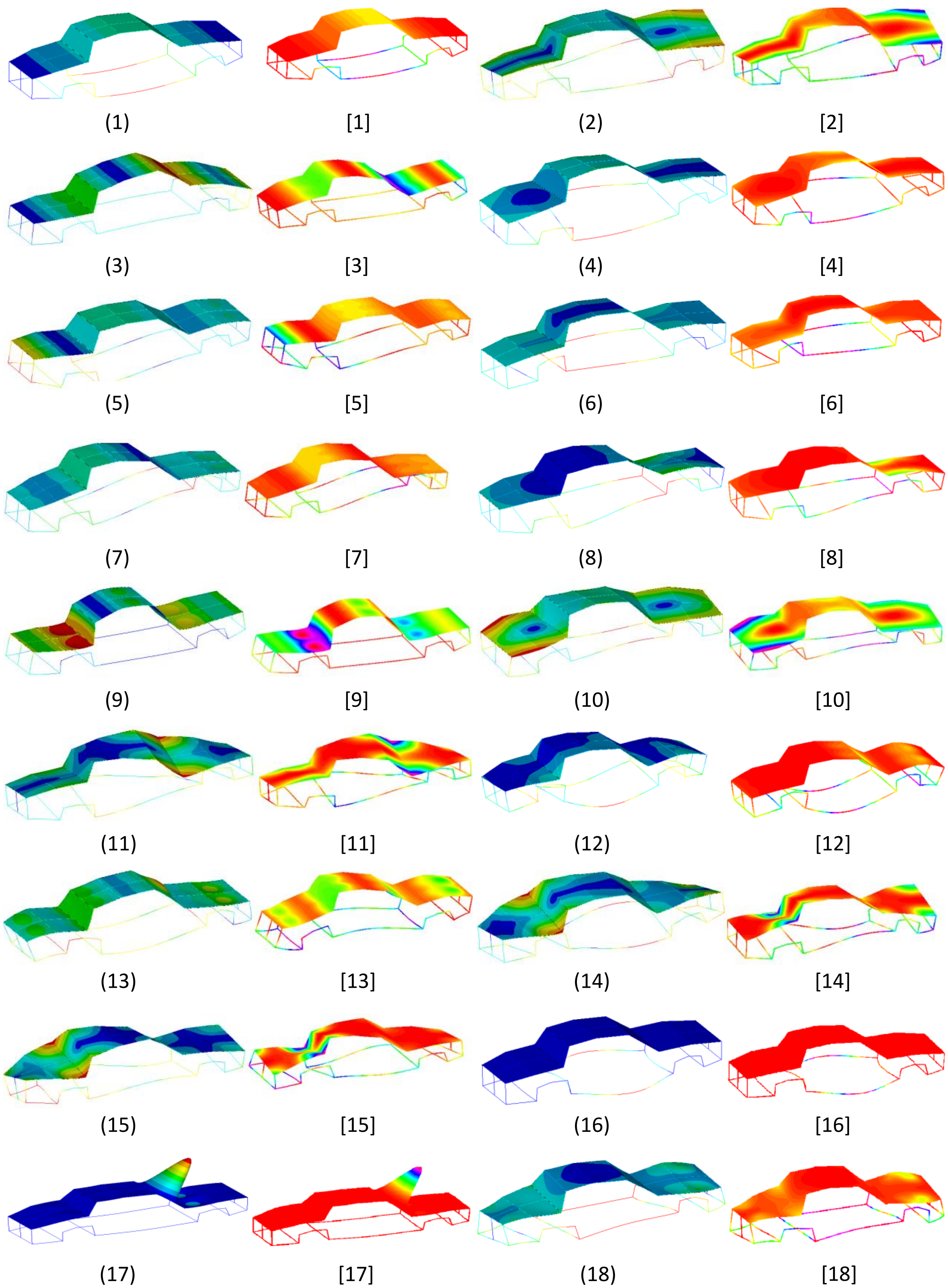
(1)
[1]
(2)
[2]
(3)
[3]
(4)
[4]
(5)
[5]
(6)
[6]
(7)
[7]
(8)
[8]
(9)
[9]
(10)
[10]
(11)
[11]
(12)
[12]
(13)
[13]
(14)
[14]
(15)
[15]
(16)
[16]
(17)
[17]
(18)
[18]

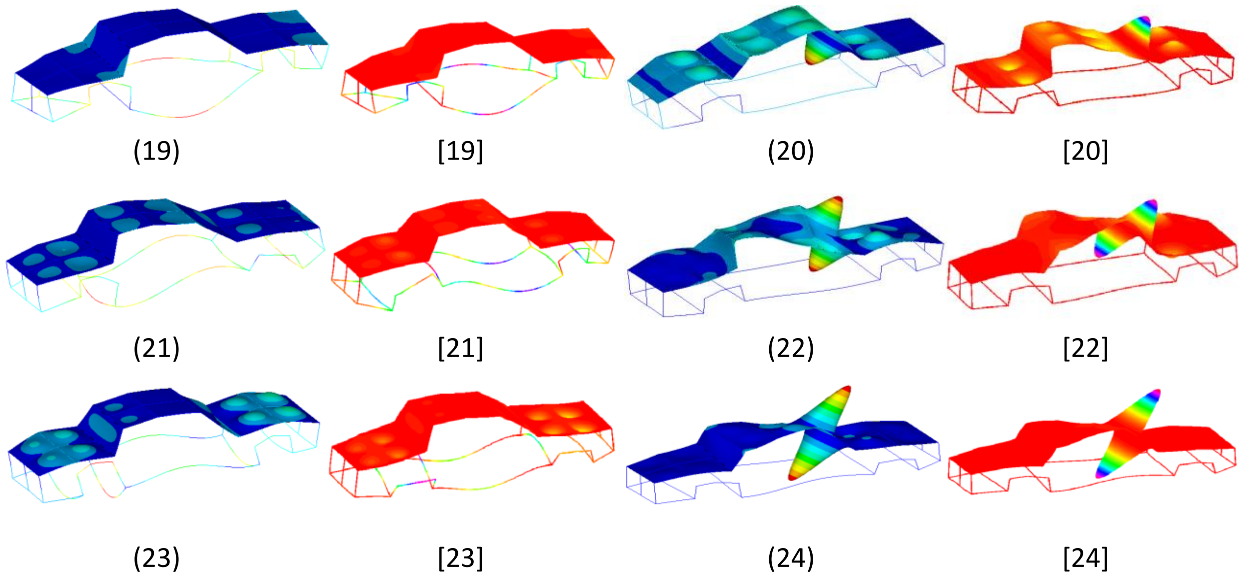

Figure 5.15 The first twenty four mode shapes of the car structure obtained by using FEM method (left side and indexed in parenthesis) and current FSEM method (right side and indexed in square brackets)

Chapter VI Concluding Remarks

6.1 Summary

The Fourier Spectral Element Method (FSEM) was initially developed about a decade ago on the vibration of beams with general boundary condition (Li, 2000). This method was further extended to the transverse vibration of rectangular plates with elastic supports (Li, 2004) and in-plane vibration of rectangular plate (Du, etc., 2007). The formulation on the plate vibration was revised to enhance convergence and alleviate the calculation burden (Li, etc., 2009; Zhang & Li, 2009). The formulation on the beam vibration was also updated and used to couple with the vibration of rectangular plates (Xu, etc., 2010; Xu, 2010). The updated formulation on the vibration of rectangular plates was also used on the vibration of coupled plate structures (Xu, 2010; Du, etc., 2010). The FSEM was further extended on the vibration of general triangular plates with arbitrary boundary conditions (Zhang & Li, 2011). Detailed formulations for a general structure composed of arbitrary number of rectangular plates, triangular plates, and beams are presented in this dissertation. The formulation on the in-plane vibration of general rectangular plates is also updated. All the energy equation are transformed into a united form in their local coordinates, which enable the usage of one set of stored matrices for all the beam and plate components, thus reducing the matrix construction time for a complex structure from hours to seconds.

The enabling feature of FSEM method is that the displacement fields of the beams or plates were subtracted by some supplementary functions, so that the remaining field is smooth enough on the boundaries to be described by standard Fourier cosine series with fast convergence rate. Although the derived quantities such as bending moment and shear force have degraded accuracy relative to the direct displacement field, they are guaranteed to converge to the exact solution. Detailed formulation on the vibration of beams, rectangular plates, triangular plates are explained in Chapter II, III, and IV, respectively. Chapter V presented the coupling formulation among all the three components, and applied the FSEM on general structures composed of arbitrary number of triangular plates, rectangular plates, and beams.

FSEM represents one of the deterministic methods in pushing the high frequency limit in vibration prediction. It is closely related with DEM, VTCR, and WBM methods, etc. The difference is that FSEM method satisfies both the governing equation and the boundary conditions in an exact sense. Since the matrix size of the FSEM method is substantially smaller than the FEA method, FSEM method has the potential to reduce the calculation time, and tackle the unsolved Mid-frequency problem.

The validity of the FSEM method has been repeatedly verified on many examples including both simple and complex structures, which can be found throughout Chapter II to Chapter V. The FEA-like assembling process makes it ready to be coupled with other methods like CMS, AMLS, SEA, etc.

6.2 Future Work

Fourier Spectral Element method has been successfully applied on general structures composed of arbitrary number of triangular plates, rectangular plates, and beams. The development on triangular plates made FSEM very versatile on analyzing structure with complex geometry. On the other hand, FSEM works more efficiently on quadrilateral shaped rectangular plates. So it is very necessary to expand the rectangular plate formulation onto general quadrilateral shaped plates, which might only need a coordinate transformation and could improve the efficiency of current FSEM method. Furthermore, there seems no barrier that prevent from extending current formulation on general 3-D solids, which could enable FSEM to predict acoustic radiation, which is a cold corner even in FEA analysis. FSEM method might find breakthrough in predicting sound pressure level correctly.

Since the FSEM matrices are less sparse than FEA matrices with the same size. Computation could be as expensive as FEA method. To speed up the calculation and shorten the reanalysis period, FSEM should find its connection with Component Modal Synthesis (CMS), especially the widely used Automated Multi-level Synthesis (AMLS) method. The computation efficiency can also able increased without sacrificing much accuracy.

Furthermore, several new analytical methods focused on mid-frequency vibration problems are proposed recently. FSEM should be carefully compared with those promising methods such as Wave Based Method (WBM), Variational Theory of Complex Ray (VTCR), Discontinuous Enrichment Method (DEM), etc. Good method will stand tall in comparison with others.

APPENDIX: General formulation used in developing the FSEM stiffness and mass matrices

Let's define

$\Pi\big(k,(i,di),(j,dj),(m_1,Tx_1),(m_2,Tx_2),(n_1,Ty_1),(n_2,Ty_2)\big)=\int_0^1\int_0^{(1-x)}(1-x-y)^k\xi_i^{(di)}(x)\xi_j^{(dj)}(y)\cos(m_1\pi x)\sin(m_2\pi x)\cos(n_1\pi y)\sin(n_2\pi y)\;dydx$ (A1)

if $Tx_1=0, Tx_2=1, Ty_1=0, Ty_2=1$

Each of the trigonometric function could either be cosine or sine function depends on $Tx_i=0$ (cosine) or $Ty_i=1$ (sine).

and

$\mathrm{I}\left(K_t,k,(i,di,l_i),\left(j,dj,l_j\right),(m_1,Tx_1),(m_2,Tx_2),(m_3,Tx_3),(m_4,Tx_4)\right)=\int_0^a K_t\left(1-\frac{y}{b}\right)^k\xi_i^{(di)}(x)\xi_j^{(dj)}(1-x))\cos(t\pi x)\cos(m_1\pi x)\sin(m_2\pi x)\cos(m_3\pi x)\sin(m_4\pi x)\,dx$

(A2)

$if\ Tx_1=0, Tx_2=1, Tx_3=0, Tx_4=1, l_i=0, l_j=1$

where $\mathrm{K}(x)=\sum_{t=0}^{L}K_t\cos(t\pi x)$ is the rotational restraint function along one of the boundaries; when $l_i=1$, the variable x in the ξ functionx is replaced by $(1-x)$.

The recurrence formulation

$\mathrm{I}(\cdots,(m_1,T_1),(m_2,T_2),\cdots)=\frac{1}{2}\big(C_1I(\cdots,(m_1+m_2,T),\cdots)+C_2I(\cdots,(m_1-m_2,T),\cdots)\big)$ (A3)

where $T=\big(1-(-1)^{(T_1+T_2)}\big)/2,\ C_1=(-1)^{\lfloor(T_1+T_2)/2\rfloor}, C_2=(-1)^{\lfloor(T_2-T_2+1)/2\rfloor}$ and $\lfloor X\rfloor$ gives the largest integer less than or equal to X.

Since all the trigonometric functions and the functions in $\xi(x)$ are of the form $\sin(m\pi x/2)$ ($\cos(m\pi x/2)$). Eq. (A3) is repeatedly used in breaking down the Π and I into following three basic integrations I_x, Π_k and Π_D, which are all evaluated analytically.

$$\mathrm{I}_x(k,m,T) = \left| \begin{array}{ll} \int_0^1 (1-x)^k \cos(m\pi x/2)dx & if\ \ T=0 \\ \int_0^1 (1-x)^k \sin(m\pi x/2)dx & if\ \ T=1 \end{array} \right. \quad \text{(A4)}$$

$$\mathrm{I}_x(k,m,0) = \left| \begin{array}{ll} 1/(k+1) & if\ m=0 \\ (2/m\pi)\sin(m\pi/2) & if\ k=0\ \&\ m\neq 0 \\ (2k/m\pi)\mathrm{I}_x(k-1,m,1) & else \end{array} \right. \quad \text{(A4.1)}$$

$$\mathrm{I}_x(k,m,1) = \left| \begin{array}{ll} 0 & if\ m=0 \\ (2/m\pi)\big(1-\cos(m\pi/2)\big) & if\ k=0\ \&\ m\neq 0 \\ 2/m\pi-(2k/m\pi)\mathrm{I}_x(k-1,m,0) & else \end{array} \right. \quad \text{(A4.2)}$$

$$\Pi_k\big(k,(m,Tx),(n,Ty)\big) =$$

$$\int_0^1 \int_0^{1-x} (1-x-y)^k \cos(m\pi x/2)\ \sin(n\pi y/2)\, dydx\ \ if\ Tx=0, Ty=1 \quad \text{(A5)}$$

Other terms when $Tx = 1\ or\ Ty = 1$ are similarly defined as those in (A1).

$$\Pi_k\big(k,(m,Tx),(n,0)\big) = \left| \begin{array}{ll} (1/(k+1))\mathrm{I}_x(k+1,m,Tx) & if\ n=0 \\ \Pi_D\big((m,Tx),(n,0)\big) & if\ k=0 \\ (2k/n\pi)\Pi_k\big(k-1,(m,Tx),(n,1)\big) & else \end{array} \right. \quad \text{(A5.1)}$$

$$\Pi_k\big(k,(m,Tx),(n,1)\big) = \left| \begin{array}{ll} 0 & if\ n=0 \\ \Pi_D\big((m,Tx),(n,1)\big) & if\ k=0 \\ (2/n\pi)\big[\mathrm{bI}_x(k,m,T)-k\Pi_k\big(k-1,(m,Tx),(n,0)\big)\big] & else \end{array} \right.$$

$$\text{(A5.2)}$$

$$\Pi_D\big((m,Tx),(n,Ty)\big) = \int_0^1 \int_0^{1-x} sin(m\pi x/2)\ \sin(n\pi y/2)\, dydx \quad if\ Tx=1, Ty=1 \quad \text{(A6)}$$

Other terms when $Tx = 0 \; or \; Ty = 0$ are similarly defined as in those in (A1).

$$\Pi_D\big((m,0),(n,0)\big) = \begin{cases} 1/2 & if\ m = 0, n = 0 \\ \sin(m\pi/2)/(m\pi) & if\ m = n \neq 0 \\ 4(\cos(m\pi/2) - \cos(n\pi/2))/\big((n^2 - m^2)\pi^2\big) & else \end{cases} \quad \text{(A6.1)}$$

$$\Pi_D\big((m,0),(n,1)\big) = \begin{cases} 0 & if\ n = 0 \\ 2(n\pi - 2\sin(n\pi/2))/(n^2\pi^2) & if\ m = 0, n \neq 0 \\ (2sin(m\pi/2) - \mathrm{m\pi}\cos(m\pi/2))/(m^2\pi^2) & if\ m = n \neq 0 \\ 4(m\sin(n\pi/2) - \mathrm{nsin}(m\pi/2))/\big((m^3 - mn^2)\pi^2\big) & else \end{cases}$$

(A6.2)

$$\Pi_D\big((m,1),(n,0)\big) = \begin{cases} 0 & if\ m = 0 \\ 2(m\pi - 2\sin(m\pi/2))/(m^2\pi^2) & if\ n = 0, m \neq 0 \\ (2sin(m\pi/2) - \mathrm{m\pi}\cos(m\pi/2))/(m^2\pi^2) & if\ m = n \neq 0 \\ 4(\mathrm{nsin}(m\pi/2) - m\sin(n\pi/2))/\big((n^3 - nm^2)\pi^2\big) & else \end{cases}$$

(A6.3)

$$\Pi_D\big((m,1),(n,1)\big) =$$

$$\begin{cases} 0 & if\ m = 0, n = 0 \\ (-4 + 4\cos(m\pi/2) + m\pi\sin(m\pi/2))/(-m^2\pi^2) & if\ m = n \neq 0 \\ 4(n^2 - m^2 - n^2\cos(m\pi/2) + m^2\cos(n\pi/2))/(mn(n^2 - m^2)\pi^2) & else \end{cases} \quad \text{(A6.4)}$$

REFERENCES

Abu-Hilal M., Forced vibration of Euler-Bernoulli beams by means of dynamic Green functions, Journal of Sound and Vibration. **267** (2003) 191-207.

Adomian G., Solving Frontier Problems of Physics: The Decomposition Method, Kluwer Academic Publishers, Dordrecht (1994)

Babuška I, Melenk J. The partition of unity method. *International Journal for Numerical Methods in Engineering* **40** (1997) 727-758.

Bardell N. S., Free vibration analysis of a flat plate using the hierarchical finite element method, *Journal of sound and vibration* **151** (1991) 263-289.

Bel1 E. D., Villon P., Bouillard P., Forced vibrations in the medium frequency range solved by a partition of unity method with local information, *International Journal for Numerical Methods in Engineering* **62 (**2005) 1105-1126

Bellman R., Differential Quadrature and long-term integration, *Journal of Mathematical Analysis and Applications* **34** (1971) 235-238.

Bellman R., Kashef B. G. and Casti J., Differential quadrature: A technique for the rapid solution of nonlinear partial differential equations, *Journal of Computational Physics* **10** (1972) 40-52.

Bennighof J. K., Lehoucq R. B., An automated multilevel substructuring method for eigenspace computation in linear elastodynamics. *SIAM Journal on Scientific Computing*, **25** (2004) 2084-2106

Bergen B., Genechten B. V., Renterghem T. V., Pluymers B., Vandepitte D., Botteldooren D., Desmet W., Comparison of numerical prediction techniques for sound propagation in complex outdoor environments, *15th International Congress on Sound and Vibration*, 2008, Daejeon, Korea.

Bert C. W., Wang X., Striz A. G., Convergence of the DQ Method in the Analysis of Anisotropic Plates, *Journal of Sound and Vibration* **170** (1994) 140-144.

Bert C.W., Malik M, Differential quadrature method in computational mechanics: A review. *Applied mechanics reviews*, **49** (1996) 1-28

Beslin O., Nicolas J., A hierarchical functions sets for very high-order plate bending modes with any boundary conditions, *Journal of Sound and Vibration* **202** (1997) 633-655.

Bhat R.B., Natural frequencies of rectangular plates using characteristic orthogonal polynomials in the Rayleigh-Ritz method, *Journal of Applied Mechanics* **102** (1985) 493-499.

Bhat R. B., Flexural vibration of polygonal plates using characteristic orthogonal polynomials in two variables. *Journal of Sound and Vibration* **114** (1987) 65-71

Boyd J. P., A proof that the discrete singular convolution (DSC)/ Lagrange-distributed approximation function (LDAF) method is inferior to high order finite differences, *Journal of Computational Physics*. **214** (2006) 538-549.

Burroughs C.B., Fischer R.W., Kern F.R., An introduction to statistical energy analysis, *Journal of the Acoustical Society of America* **101** (1997) 1779-1789.

Carmichael T. E., The vibration of a rectangular plate with edges elastically restrained against rotation, *The Quarterly Journal of Mechanics and Applied Mathematics* **12** (1959) 29-42.

Chen W., Cheung Y. K., Refined triangular discrete Kirchhoff plate element for thin plate bending, vibration and buckling analysis, *International Journal for Numerical Methods in Engineering* **41** (1998) 1507-1525

Chen S. M., Wang D. F., Zan J. M., Interior noise prediction of the automobile based on hybrid FE-SEA method, *Mathematical Problems in Engineering*. 2011, doi:10.1155/2011/327170.

Cheung M. S., Finite Strip Analysis of Structures, *Ph. D Thesis, University of Calgary* 1971.

Cheung Y. K., Zhou D., Three-dimensional vibrational analysis of cantilevered and completely free isosceles triangular plates. *International Journal of Solids and Structures* **39** (2002) 673-687

Cotoni V., Shorter P.J., Langley R.S., Numerical and experimental validation of a finite element-statistical energy analysis method, *Journal of the Acoustical Society of America* **122** (2007) 259-270.

Craig R.R., Chang C. J., A review of substructure coupling method for dynamic analysis, *13th Annual Meeting of Society for Engineering Science, Advances in Engineering Science* (1977) 393-408.

Cupial P., Calculation of the natural frequencies of composite plates by the Rayleigh-Ritz method with orthogonal polynomials, *Journal of Sound and Vibration* **201** (1997) 385-387.

Cuschier J., Power flow as a complement to statistical energy analysis and finite element analysis, Statistical Energy Analysis *ASME Publication NCA*, **3** (1987).

Cuschier J., Structural power-flow analysis using a mobility approach of an L-shaped plate. *Journal of the Acoustical Society of America,* **87** (1990) 1159-1165

Desmet W., Mid-frequency vibro-acoustic modeling: challenges and potential solutions, *ISMA, Leuven, Belgium*, **2** (2002) 835-862.

Desmet W., A wave based prediction technique for coupled vibro-acoustic analysis. *KULeuven, division PMA, PhD. thesis*, 1998.

Desmet W., D18: Assessment report on WBM, 7th FRAMEWORK PROGRAMME: CAE methodologies for Mid frequency analysis in vibration and acoustics, 2011

Dickinson S.M., Li E.K.H., On the use of simply supported plate functions in the Rayleigh-Ritz method applied to the vibration of rectangular plates, *Journal of Sound and Vibration* **80** (1982) 292-297.

Dickinson S.M., Di-Blasio A., On the use of orthogonal polynomials in the Rayleigh-Ritz method for the flexural vibration and buckling of isotropic and orthotropic rectangular plates, *Journal of Applied Mechanics* **108** (1986) 51-62.

Du J.T., Li W.L., Jin G.Y., Yang T.J., Z.G. Liu. An analytical method for the in-plane vibration analysis of rectangular plates with elastically restrained edges, *Journal of Sound and Vibration* **306** (2007) 908-927.

Egle D. M., The response of a rectangular plate with an elastic edge restraint, *ASME Journal of Engineering for Industry* **94** (1972) 517-525

Escalante M.R., Rosales M.B. and Filipich C.P., Natural frequencies of thin rectangular plates with partial intermediate supports, *Latin American Applied Research* **34** (2004) 217-224

Fahy F., Statistical energy analysis: a critical review, *Philosophical Transactions: Physical Sciences and Engineering.* **346** (1994) 431-447.

Farhat C., Harari I., Hetmaniuk U., A discontinuous Galerkin method with Lagrange multipliers for the solution of Helmholtz problems in the mid-frequency regime, *Computer Methods in Applied Mechanics.* **192** (2003) 1389-1419

Filipich C.P., Rosales M.B., Arbitrary precision frequencies of a free rectangular thin plate, *Journal of Sound and Vibration* **230** (2000) 521-539.

Foda M. A., Abduljabbar Z., A dynamic green function formulation for the response of a beam structure to a moving mass, *Journal of Sound and Vibration*. **210** (1998) 295-306.

Fries T. P., Belytschko T.The extended/generalized finite element method: an overview of the method and its applications. *International Journal for Numerical Methods in Engineering* **84** *(*2010) 253-304

Gaurav G., Efficient computational methods for uncertainty quantification of large systems, *Ph.D thesis, Oakland University, Oakland, MI*, 2011.

Genechten B. V., Vergote K., Vandepitte D., Desmet W., A multi-level wave based numerical modelling framework for the steady-state dynamic analysis of bounded Helmholtz problems with multiple inclusions, *Computer Methods in Applied Mechanics and Engineering* **199** (2010) 1881-1905

Goel R. P., Free vibration of a beam-mass system with elastically restrained ends, *Journal of Sound and Vibration*. **47** (1976) 9-14.

Gorman D.J., A comprehensive study of the free vibration of rectangular plates resting on symmetrically-distributed uniform elastic edge supports, *Journal of Applied Mechanics* **56** (1980) 893-899.

Gorman D.J., Free vibration analysis of Mindlin plates with uniform elastic edge support by the superposition method, *Journal of Sound and Vibration* **207** (1997) 335-350.

Gorman D.J., Free vibration and buckling of in-plane loaded plates with rotational elastic edge support, *Journal of Sound and Vibration* **225** (2000) 755-773.

Gorman D.J., Free vibration analysis of corner-supported rectangular plates with symmetrically distributed edge beams, *Journal of Sound and Vibration* **263** (2003) 979-1003.

Greif R. and Mittendorf S. C., Structural vibrations and Fourier Series, *Journal of Sound and Vibration*. **48** (1976) 113-122.

Grice R. M., Pinnington R. J., Analysis of the flexural vibration of a thin-plate box using a combination of finite element analysis and analytical impedances, *Journal of Sound and* V*Ibration* **249** (2002) 499-527

Gurgoze M., Erol H., Determination of the frequency response function of a cantilevered beam simply supported in-span, *Journal of Sound and Vibration*. **247** (2001) 372-378.

Haldar S., Sengupta D., free vibration analysis of composite right angle triangular plate using a shear flexible element, *Journal of Reinforced Plastics and Composites* **22** (2003) 229-255

Herran M., Nélias D, Combescure A, Chalons H, Optimal component mode synthesis for medium frequency problem. *International Journal for Numerical Methods in Engineering*, **86** (2011)301-315

Hong S. B. Wang A., Vlahopoulos N., A hybrid finite element formulation for a beam-plate system, *Journal of Sound and Vibration* **298** (2006) 233-256.

Hopkins C., Statistical energy analysis of coupled plate systems with low modal density and low modal overlap, *Journal of sound and vibration* **251** (2002), 193-214.

Hoppmann W. Greenspon H., J., An experimental device for obtaining elastic rotational constraints on the boundary of a plate, *Proceedings of the U.S. national congress of applied mechanics* (1954) 187-191

Hou Y., Wei G. W., Xiang Y., DSC-Ritz method for the free vibration analysis of Mindlin plates, *International Journal for Numerical Methods in Engineering*. **62** (2005) 262-288.

Huang M., Sakiyama T., Matsuda H., Morita C., Free vibration analysis of anisotropic right triangular plates. *Journal of Applied Mechanics* **4** (2001) 1-11

Huang C. S., Leissa A. W., M. J. Chang, Vibration of skewed cantilevered triangular, trapezoidal and parallelogram Mindlin plates with considering corner stress singularities. *International Journal for Numerical Methods in Engineering* **62** (2005) 1789-1806

Hurlebaus S., Gaul L., Wang J. T.-S., An exact solution for calculating the eigenfrequencies of orthotropic plates with completely free boundary, *Journal of Sound and Vibration* **244** (2001) 747-759

Igawa H., Komatru K., Yamaguchi I., and Kasai T., Wave propagation analysis of framestructures using the spectral element method, *Journal of Sound and Vibration*, **277** (2004) 1071-1081.

Joga-Rao C.V., Kantham C.L., Natural frequencies of rectangular plates with edges elastically restrained against rotation, *Journal of Aeronautical science* **24** (1957) 855-856

Karunasena W., Kitipornchai S., Bermani F.G., Free vibration of cantilevered arbitrary triangular Mindlin plates. International *Journal of Mechanical Science* **38** (1996) 431-442

Karunasena W., Kitipornchai S., Free vibration of shear-deformable general triangular plates, *Journal of Sound and Vibration* **199** (1997) 595-613

Kim C. G., Hong C. S., Buckling of unbalanced anisotropic sandwich plates with finite bonding stiffness, *AIAA Journal* **26** (1988) 982-988

Kim C.S., Dickinson S. M., The free flexural vibration of right triangular isotropic and orthotropic plates, *Journal of Sound and Vibration* **141** (1990) 291-311

Kim H. K. and Kim M. S., Vibration of beams with generally restrained boundary conditions using Fourier series, *Journal of Sound and Vibration.* **245** (2001) 771-784.

Kim H. K., Kim M. S., Vibration analysis of PWR fuel rod, *Journal of Sound and Vibration*. **282** (2005) 553-572.

Klerk D., Rixen D.J., Voormeeren S.N., General framework for dynamic substructuring: history, review, and classification of techniques. *AIAA Journal*, **46** (2008) 1169-1181

Ladeve`ze P., Arnaud L., Rouch P., Blanze Ć., The variational theory of complex rays for the calculation of medium-frequency vibrations, *Engineering Computations.***18** (1999) 193-214.

Lai H.Y., Hsu J.C., Chen C.K., An innovative eigenvalue problem solver for free vibration of Euler-Bernoulli beam by using the Adomian decomposition method, *Computers and Mathematics with Applications* **56** (2008) 3204-3220

Lam K. Y., Liew K. M., Chow S.T., Free vibration analysis of isotropic and orthotropic plates. *International Journal of Mechanical Science* **32** (1990) 455-464

Langley R. S., Bremner P., A hybrid method for the vibration analysis of complex structural-acoustic systems. *Journal of the Acoustical Society of America* **105** (1999) 1657-1671

Langley R.S., Response variance prediction in the statistical energy analysis of built-up systems, *Journal of the Acoustical Society of America* **115** (2004) 706-718.

Langley R.S., Cotoni V., Response variance prediction for uncertain vibro-acoustic systems using a hybrid deterministic-statistical method, *Journal of the Acoustical Society of America* **122** (2007) 3445-3463.

Langley R. S., Cordioli J. A., Hybrid deterministic-statistical analysis of vibro-acoustic systems with domain couplings on statistical components, *Journal of Sound and Vibration* **321** (2009) 893-912.

Laura P. A. Romanelli A., E., Vibration of rectangular plates elastically restrained against rotation along all edges and subjected to a biaxial state of stress, *Journal of Sound and Vibration* **37** (1974) 367-377.

Laura P. A. A., Luisoni L. E., Filipich C., A note on the determination of the fundamental frequency of vibration of thin, rectangular plates with edges possessing different rotational flexibility coefficients, *Journal of Sound and Vibration* **55** (1977) 327-333

Laura P. A. A., Luisoni L. E., Filipich C., On the effect of different edge flexibility coefficients on transverse vibration of thin rectangular plates, *Journal of Sound and Vibration* **57** (1978) 333-340

Laura P. A. A., Grossi R., Transverse vibration of a rectangular plate elastically restrained against rotation along three edges and free on the fourth edge, *Journal of Sound and Vibration* **59** (1978) 355-368

Laura P. A. A., Grossi R.O., Soni S. R., Free vibration of a rectangular plate of variable thinkness elastically restrained against rotation along three edges and free on the fourth edge, *Journal of Sound and Vibration* **62** (1979) 493-503

Laura P.A.A., Grossi R.O.G., Transverse vibration of rectangular plates with edges elastically restrained against translation and rotation, *Journal of Sound and Vibration* **75** (1981) 101-107.

Laura P. A. A. and Gutierrez R. H., Analysis of vibrating rectangular plates with nonuniform boundary conditions by using the differential quadrature method, *Journal of Sound and Vibration* **173** (1994) 702-706.

Laura P.A.A., Comments on ‘‘Natural frequencies of rectangular plates using a set of static beam functions in the Rayleigh-Ritz method’’, *Journal of Sound and Vibration* **200** (1997) 540-542.

Leissa A.W., The free vibrations of rectangular plates, *Journal of Sound and Vibration* **31 (**1973) 257-293.

Leissa A. W., Jaber N. A., Vibration of completely free triangular plates, International *Journal of Mechanical Science* **34** (1992) 605-616

Leissa A. W., Vibration of plates, *Acoustical Society of America* 1993.

Leissa A. W., P. A. A. Laura and R. H. Gutierrez, Vibration of rectangular plates with non-uniform elastic edge supports, *Journal of Applied Mechanics* **47**(1979) 891-895.

Lestari W., Hanagud S., Nonlinear vibration of buckled beams: some exact solutions, *International Journal of Solids and Structures*. **38** (2001) 4741-4757.

Li W.L. and Daniels M., A Fourier series method for the vibrations of elastically restrained plates arbitrarily loaded with springs and masses, *Journal of Sound and Vibration* **252** (2002) 768-781

Li W.L., Free vibration of beams with general boundary conditions, *Journal of Sound and Vibration* **237** (2000) 709-725.

Li W.L., Dynamic analysis of beams with arbitrary elastic supports at both ends, *Journal of Sound and Vibration* **246** (2001) 751-756.

Li W.L., Comparison of Fourier sine and cosine series expansions for beams with arbitrary boundary conditions. *Journal of Sound and Vibration* **255** (2002) 185-194.

Li W.L., Reply to: discussion on “free vibrations of beams with general boundary conditions”. *Journal of Sound and Vibration* **257** (2002) 593-595

Li W.L., Vibration analysis of rectangular plates with general elastic boundary supports, *Journal of Sound and Vibration* **273** (2004) 619-635.

Li W.L., Bonilha M. W., Xiao J., Vibration and power flows in a coupled beam system, *Journal of Vibration and Acoustics,* **129** (2007) 616-622.

Li W.L., Zhang X.F., Du J.T. and Liu Z.G., An exact series solution for the transverse vibration of rectangular plates with general elastic boundary supports, *Journal of Sound and Vibration* **321** (2009) 254-269

Liew K. M., On the use of pb-2 Rayleigh-Ritz method for vibration of triangular plates with curved internal supports, *Journal of Sound and Vibration* **165** (1993) 329-340

Liew K. M., Wang C. M., Vibration of Triangular Plates: Point Supports, Mixed Edges and Partial Internal Curved Supports, *Journal of Sound and Vibration* ***172*** (1994) 527-537

Lin H. Y., Dynamic analysis of a multi-span uniform beam carrying a number of various concentrated elements, *Journal of Sound and Vibration*. **309** (2008) 262-275.

Lin H.Y., On the natural frequencies and mode shapes of a multi-span Timoshenko beam carrying a number of various concentrated elements, *Journal of Sound and Vibration*. **319** (2009) 593-605.

Low K. H., Frequencies of beams carrying multiple masses: Rayleigh estimation versus eigenanalysis solution, *Journal of Sound and Vibration*. **268** (2003) 843-853.

Lu C.F., Zhang Z.C., Chen W.Q., Free vibration of generally supported rectangular Kirchhoff plates: State-space-based differential quadrature method. *International Journal for Numerical Methods in Engineering* **70** *(*2007) 1430-1450

Lyon R. H., Maidanik G., Power flow between linearly coupled oscillators, *Journal of the Acoustical Society of America* **34** (1962) 623-639.

Lyon R.H., DeJong R.G., Theory and application of statistical energy analysis, 2nd edition, *Butterworth-Heinemann, Boston* (1995)

Mace B., Statistical energy analysis, energy distribution models and system modes, *Journal of sound and vibration* **264** (2003) 391-409.

Maurizi M.J. and Robledo G. G., A further note on the “Dynamic analysis of generally supported beams using Fourier Series”, *Journal of Sound and Vibration*. **214** (1998) 972-973.

Maurizi M. J., A contribution on “Transverse vibration of an Euler-Bernoulli uniform beam on up to five resilient supports including ends”, *Journal of Sound and Vibration*. **272** (2004) 1071-1072.

Mousavi S. E., Grinspun E., Sukumar N., Harmonic enrichment functions: A unified treatment of multiple, intersecting and branched cracks in the extended finite element method. *International Journal for Numerical Methods in Engineering* **85** (2011) 1306-1322

Naguleswaran S., Transverse vibration of an Euler-Bernoulli uniform beam on up to five resilient supports including ends, *Journal of Sound and Vibration*. **261** (2003) 372-384.

Naguleswaran S., Author’s reply, *Journal of Sound and Vibration*. **272** (2004) 1073-1074.

Nallim L.G., Luccioni B. M., Grossi R. O., Vibration of general triangular composite plates with elastically restrained edges. *Thin-Walled Structure* **43** (2005) 1711-1745

Nassar E. E. M., On the dynamic characteristics of beams, plates, and shells, *PhD Thesis, Georgia Institute of Technology* 1973

Natarajan L., Zhang X. F., Wu S.F. and Li W. L, Vibro-acoustic analysis of an arbitrarily shaped vibrating structure. *158th meeting of the Acoustical Society of America*, San Antonio, Texas, 2009

Park W.S., Thompson D.J., Ferguson N.S., The influence of modal behaviour on the energy transmission between two coupled plates, *Journal of sound and vibration* **276** (2004) 1019-1041.

Pierre C. and Castanier M.P., Mid-frequency dynamics of complex structural systems: Assessing the state of the art and defining future research directions. *Technical Report AFRLSRARTR020444, NTIS, Springfield, VA* (2004)

Ragnarsson P., VanGaal T., Pluymers B., Donders S., Vandepitte D., Desmet W., Fast approximation of synthesized frequency response functions with automated multi-level substructuring (AMLS), *Finite Elements in Analysis and Design* **47** (2011) 195-199

Rao C. K., Mirza S., A note on vibrations of generally restrained beams, *Journal of Sound and Vibration*. **130** (1989) 453-465.

Reddy J.N., An introduction to the Finite Element Method, *3rd edition, McGraw-Hill, New York, NY*, 2006.

Rosa M. A., Maurizi M. J., On the dynamic behavior of slender beams with elastic ends carrying a concentrated mass, *Computer & Structures*. **58** (1996) 1145-1159.

Rosa M. A., Maurizi M. J., The influence of concentrated masses and Pasternak soil on the free vibrations of euler beams- exact solution, *Journal of Sound and Vibration*. **212** (1998) 573-581.

Rosales M.B., Filipich C.P., Vibration of orthotropic plates: discussion on the completeness of the solutions used in direct methods, *Journal of Sound and Vibration* **261** (2003) 751-757.

Sakiyama T., Huang M., Matsuda H., Morita C., Free vibration analysis of orthotropic right cantilever triangular plates. *Journal of Sound and Vibration* **259** (2003) 219-228

Saliba H.T., Free vibration of simply supported general triangular thin plates: an accurate simplified solution. *Journal of Sound and Vibration* **196** (1996) 45-57

Secgin A., Sarigul A. S., A novel scheme for the discrete prediction of high-frequency vibration response: Discrete singular convolution-mode superposition approach, *Journal of Sound and Vibration*. **320** (2009) 1004-1022

Sellgren U., Component Mode Synthesis - A method for efficient dynamic simulation of complex technical systems, *VISP WP5 Document Data*, Stockholm, 2003.

Shankar K., Keane A.J., Energy flow predictions in a structure of rigidly joined beams using receptance theory, *Journal of Sound and Vibration* **185** (1995) 867-890.

Shorter P.J., Langley R.S.,Vibro-acoustic analysis of complex systems, *Journal of Sound and Vibration* **288** (2005) 669-700

Shu C., A generalized approach for implementing general boundary conditions in the GDQ free vibration analysis of plates, *International Journal of Solids Structures* **34** (1997) 837-846

Shu C., Wang C.M., Treatment of mixed and nonuniform boundary conditions in GDQ vibration analysis of rectangular plates, *Engineering structure* **21** (1999) 125-134.

Shu C. , Differential Quadrature and its Application in Engineering, *Springer-Verlag London Limited* (2000).

Singh B., Chakraverty S., Transverse vibration of triangular plates using characteristic orthogonal polynomials in two variables, *International Journal of Mechanical Science* **34** (1992) 947-955

Singh B., Saxena V., Transverse vibration of triangular plates with variable thickness. *Journal of Sound and Vibration* **194** (1996) 471-496

Singh B., Hassan S.M., Transverse vibration of triangular plate with arbitrary thickness variation and various boundary conditions. *Journal of Sound and Vibration* **214** (1998) 29-55

Soize C., A model and numerical method in the medium frequency range for vibroacoustic predictions using the theory of structural fuzzy, *Journal of the Acoustical Society of America* **94** (1993) 849-865

Stelzer R. D21 Assessment report on SmEdA *7th FRAMEWORK PROGRAMME: CAE methodologies for Mid frequency analysis in vibration and acoustics*, 2011

Tezaur R., Farhat C., Three-dimensional discontinuous Galerkin elements with plane waves and Lagrange multipliers for the solution of mid-frequency Helmholtz problems, *International Journal for Numerical Methods in Engineering* **66** (2006)796-815

Troshin A.G., Sanderson M.A., Structural energy flow in a Resiliently coupled T-shapedbeam by wave intensity mobility approach, *ACUSTICA-acta acustica* **84** (1998) 860-869.

Vergote K., Genechten B. V., Vandepitte D., Desmet W., On the analysis of vibro-acoustic systems in the mid-frequency range using a hybrid deterministic-statistical approach. *Computers and Structures* **89** (2011) 868-877

Woodhouse J., An approach to the theoretical background of statistical energy analysis applied to structural vibration, *Journal of the Acoustical Society of America* **69** (1981) 1695-1709.

Wang J. T. S. and Lin C. C., Dynamic analysis of generally supported beams using Fourier series, *Journal of Sound and Vibration*. **196** (1996) 285-293.

Warburton G.B., The vibrations of rectangular plates, *Proceeding of the Institute of Mechanical Engineers, Series A* **168** (1954) 371-384.

Warburton G.B., Response using the Rayleigh-Ritz method, *Journal of Earthquake Engineering and Structural Dynamics* **7** (1979) 327-334.

Warburton G.B., Edney S.L., Vibrations of rectangular plates with elastically restrained edges, *Journal of Sound and Vibration* **95** (1984) 537-552.

Wei G. W., Discrete singular convolution for the solution of the Fokker-Planck equation, Journal of Chemical Physics. **110** (1999) 8930-8942

Wei G. W., Zhao Y. B., Xiang Y., The determination of natural frequencies of rectangular plates with mixed boundary conditions by discrete singular convolution, *International Journal of Mechanical Sciences*. **43** (2001)1731-1746.

Wei G. W., Discrete singular convolution for beam analysis, *Engineering Structures*. **23** (2001)1045-1053.

Wei G. W., Zhao Y. B., Xiang Y., Discrete singular convolution and its application to the analysis of plates with internal supports. Part 1: Theory and algorithm, *International Journal for Numerical Methods in Engineering* **55** (2002) 913-946.

Wei G. W., Zhao S., On the validity of " A proof that the discrete singular convolution (DSC)/ Lagrange-distributed approximation function (LDAF) method is inferior to high order finite differences, *Journal of Computational Physics*. **226** (2007) 2389-2392.

Xiang Y., Liew K.M., Kitipornchai S., Wang C. M., Vibration of triangular Mindlin plates subject to isotropic in-plane stresses. *Journal of Sound and Vibration* **116** (1994) 61-66

Xu H. A., The Fourier spectral element method for vibration and power flow analysis of complex dynamic systems, *Ph.D thesis, Wayne State University, Detroit, MI*, 2010.

Xu, H. A., Li, W. L. and Du, J. T., Vibrations of rectangular plates reinforced by any number of beams of arbitrary lengths and placement angles, *Journal of Sound and Vibration* , **329** (2010) 3759-3779.

Xu H. A., Li W. L., Dynamic behavior of multi-span bridges under moving loads with focusing on the effect of the coupling conditions between spans. *Journal of Sound and Vibration* **312** (2008) 736-753.

Yagci B., Filiz S., Romero L.L., Ozdogantar O. B., A spectral-Tchebychev technique for solving linear and nonlinear beam equations, *Journal of Sound and Vibration*. **321** (2009) 375-404

Yan H., Parrett A., Nack W., Statistical energy analysis by finite elements for middle frequency vibration, *Finite elements in analysis and design* **35** (2000) 297-304.

Zhang X. F., Li W. L., Vibration of general triangular plates with elastically restrained edges, *Journal of Sound and Vibration.* To be submitted, 2011.

Zhang X. F., Li W. L., A unified approach for predicting sound radiation from baffled rectangular plates with arbitrary boundary conditions, *Journal of Sound and Vibration*. **329** (2010)5307-5320

Zhang X. F., Li W. L., Vibrations of rectangular plates with arbitrary non-uniform elastic edge restraints, *Journal of Sound and Vibration,* **326** (2009) 221-234

Zhang X.F., Li W. L., Reducing Sound Radiation from a Plate through Tuning/Modifying Boundary Supports, *IMAC XXVII*, Orlando, Florida, 2009

Zhang X. F., Wang P. and Li W. L., Reduction of panel sound radiation through topology design, *INTER-NOISE 2006*, Honolulu, Hawaii, 2006

Zhang G., Component-based and parametric reduced-order modeling methods for vibration analysis of complex structures, *Ph.D thesis, The University of Michigan, Ann Arbor, MI*, 2005.

Zhao Y. B., Wei G. W., DSC analysis of rectangular plates with non-uniform boundary conditions, *Journal of Sound and Vibration* **255** (2002) 203-228.

Zhao X., Vlahopoulos N., A basic hybrid finite element formulation for mid-frequencyanalysis of beams connected at an arbitrary angle, *Journal of Sound and Vibration*, **269** (2004) 135-164

Zhao Y. B. and Wei G. W., DSC analysis of rectangular plates with non-uniform boundary conditions, *Journal of Sound and Vibration*. **255** (2002) 203-228.

Zhao S., Wei G. W., Xiang Y., DSC analysis of free-edged beams by an iteratively matched boundary method, *Journal of Sound and Vibration*. **284** (2005) 487-493.

Zhou D., Natural frequencies of elastically restrained rectangular plates using a set of static beam functions in the Rayleigh-Ritz method, *Computers & Structures* **57** (1995) 731-735.

Zhou D., Natural frequencies of rectangular plates using a set of static beam functions in the Rayleigh-Ritz method, *Journal of Sound and Vibration* **189** (1996) 81-88.

Zhu D. C., Development of hierarchal finite element methods at BIAA, *Proceedings of the international conference on computational mechanics*, 1985, Tokyo.

Zienkiewicz O. C., Achievements and some unsolved problems of the Finite element method, *International Journal for Numerical Methods in Engineering*. **47** (2000) 9-28

ABSTRACT

THE FOURIER SPECTRAL ELEMENT METHOD FOR VIBRATION ANALYSIS OF GENERAL DYNAMIC STRUCTURES

by

XUEFENG ZHANG

May 2012

Advisor: Dr. Wen Li

Major: Mechanical Engineering

Degree: Doctor of Philosophy

The Fourier Spectral Element Method (FSEM) was proposed by Wen Li on the vibration of simple beams (Li, 2000), and was extended to the vibration of rectangular plates (Li, 2004). This dissertation proposes a revised formulation on the vibration of rectangular plates with general boundary conditions, and extends the FSEM on the vibration of general triangular plates with elastic boundary supports. 3-D coupling formulation among the plates and beams is further developed. A general dynamic structure is then analyzed by dividing the structure into coupled triangular plates, rectangular plates, and beams. The accuracy and fast convergence of FSEM method is repeatedly benchmarked by analytical, experimental, and numerical results from the literature, laboratory tests, and commercial software.

The enabling feature of FSEM method is that the approximation solution satisfies both the governing equation and the boundary conditions of the beam (plates) vibration in an exact sense. The displacement function composes a standard Fourier cosine series plus several supplementary functions to ensure the convergence to the exact solution including displacement, bending moment, and shear forces, etc. All the formulation is transformed into standard forms and a set of stored matrices ensure fast assembly of the studied structure matrix. Since the matrix

size of the FSEM method is substantially smaller than the FEA method, FSEM method has the potential to reduce the calculation time, and tackle the unsolved Mid-frequency problem.

AUTOBIOGRAPHICAL STATEMENT

Xuefeng Zhang was born on March 1, 1979 (Chinese calendar) in a small village named Xiao Zhang Jia Po Cun, which is located in Linxian County, Shanxi, China. He earned his B. S. degree on Engineering Mechanics at Taiyuan University of Technology in July, 2002, and then he continued his M.S. study on Biomechanics in the same University. After he earned his M.S degree in July, 2005, he worked as a faculty in Taiyuan University of Technology for two semesters. Then he joined Dr. Wen Li's research group as a PhD student at Mississippi State University in January, 2006. He became a PhD student in Mechanical Engineering Department at Wayne State University in September, 2007 followed Dr. Wen Li's group. Then he continued his PhD study till present.